POLYETHYLENE TEREPHTHALATE: FACTORS AFFECTING THE IMPACT BEHAVIOUR

by

K. J. STAFFORD

A Doctoral Thesis submitted in partial fulfilment of the requirements for the award of Ph.D. of Loughborough University of Technology

Supervisors: Prof. R. J. Reynolds

Dr. J. B. Jackson

ACKNOWLEDGEMENT

I wish to thank the members of the Materials Science and Polymer techniques groups of the P and P laboratory of I.C.I. for their help and criticism during my time spent there. In particular I would like to express my appreciation of the help given by Dr. R. T. Murray with the electron microscopy, and Mr. D. Bye for his advice in the preparation of my samples.
Last, but not least, I would thank my supervisors Dr. J. B. Jackson and Prof. R. J. Reynolds for their help and patience during the course of the work.

SUMMARY

The following study forms part of a programme of work designed to produce a commercial moulding material based upon Polyethylene terephthalate. The work described relates specifically to the investigation of the impact characteristics of PET, and improvements that may be obtained in the impact strength by incorporation of the rubbery phase into the glassy PET matrix. The two phase systems studied in greatest detail were PET/Ionomer (Surlyn A) blends. A grafting reaction that was found to occur in the melt between these two polymers has been investigated in some detail using a Weissenberg Rheogoniometer.

Also reported are studies of the crazing properties and nature of the craze structures produced in amorphous PET, together with a study of the crack velocity profiles obtained during the high velocity impact fracture of PET mouldings. This latter work led to a correlation of the topographical features observed on the fracture surface with the crack velocity. As a result a stick-slip mechanism of crack propagation was proposed, involving crazing formation and fracture.

C O N T E N T S

CONTENTS (Continued)

CONTENTS (Continued)

CONTENTS (Continued)

CHAPTER ONE

1. POLY(ETHYLENE TEREPHTHALATE)

Following the work of Carothers[1] who prepared high molecular weight fibre-forming aliphatic polyesters, Whinfield & Dixon[2] in 1940 showed that fibre forming polyesters could also be made from symmetrical aromatic dicarboxylic acids (notably terephthalic acid). These were also highly crystalline and had the advantage of a considerably higher melting point, due to the greater rigidity of the chain structure. Poly(ethylene terephthalate) forms the most important of these series of polyesters and has been developed commercially as a synthetic fibre. Like the polyamides Nylon 66 and 6, this polymer can be melt spun and oriented by drawing, and subsequently the material was shown to have potential as a moulding material.

1.1. Comparison of the Physical Properties of PET with other Commercial Moulding Thermoplastics. *

The properties of a high molecular weight, crystalline PET have been compared with other engineering polymers and composites in order to assess the advantages and disadvantages of this material. The values quoted for PET are those of "ARNITE", a commercially available moulding material based upon PET. Analysis has shown that "ARNITE" is a high molecular weight PET of I.V. 0.85 (cf 0.65 for ICI fibre spinning grade PET), polymerised in the presence of manganese and germanium catalysts. A nucleating agent (talc) is present in order to give high crystallinity (35 - 40%) injection mouldings when a hot mould is used.

1.1.1. Abrasion Resistance

PET has an excellent abrasion resistance, similar to that of Nylon 6 which is known for its wearing properties. Table 1-1 compares the abrasion resistance of PET with other leading moulding materials.

*Data abstracted from trade literature

Table 1-1. Abrasion Resistance ASTM D 1044

Polymer	Volume loss/1000 revs in mm^3
Crystalline PET	2.5
Nylon 6	4.0
PTFE	4.5
Nylon 6 30% glass fibre	9.0
Polyacetal	11.5
Polycarbonate	12.5
Polyphenylene oxide	13.0
Polypropylene	32.0
ABS	33.5

1.1.2. Flexural Modulus

PET has an exceptionally high flexural modulus for a thermoplastic. All other common unreinforced thermoplastics are less rigid. Table 1-2 compares the flexural modulus of crystalline PET with other common thermoplastics.

Table 1-2. Flexural Modulus

Polymer	Flexural Modulus in $Kgf/cm^2 \times 10^{-4}$
Nylon 6 30% glass fibre	3.5
PET	2.8
Polyphenylene oxide	2.5
Polyacetal	2.5
Polycarbonate	2.5
ABS	2.4
Polypropylene	1.5
Nylon 6	0.7

1.1.3. Coefficient of Friction Against Mild Steel

PET exhibits a very low coefficient of friction (0.19), a property that may find use in many engineering applications such as bearing bushes and gear wheels. PET is superior in this property to the majority of thermoplastics.

1.1.4. Other Properties

Allied to these properties the high melting point (255°C), hardness (84 shore) and chemical resistance, low creep below its Tg and moisture absorption (0.6% at 70°C) give PET a unique spectrum of properties that are useful to the design engineer.

1.2. Disadvantages

PET has properties which militate against its use as an engineering material. The most important of these are described below.

1.2.1. Crystallisation Rate

Many of the important characteristics of PET mouldings are dependent upon using a highly crystalline product. However, because of a relatively slow crystallisation rate (i.e. compared with polyethylene for example), the melt is quenched on entering the cold mould tool and an amorphous, or semi-amorphous product is produced, particularly in the case of the high molecular weight polymer. In order to obtain mouldings of adequate crystallinity a hot mould must be used (held at 140°C, (the temperature for maximum crystallisation rate) and a nucleating agent (talc) must be present if economically short cycle times are to be obtained.

1.2.2. Hydrolytic Degradation in the Melt

At melttemperature (265°C) in the presence of water PET suffers chain scission reactions due to hydrolysis and consequent reduction in molecular weight produces very brittle mouldings. It is, therefore, necessary to dry the polymer chip under vacuum prior to use and it is advisable to use heated, closed hoppers to avoid moisture absorption from the air. Also after any pauses in production the cylinder of the extruder must be purged with fresh material. These requirements obviously increase the cost of production moulding and may tend to high technical service costs.

1.2.3. Low Melt Viscosity

Due to the low viscosity of the melt, the extruder nozzle must be heated and provided with a valve to prevent 'drooling'.

1.2.4. Impact Strength

The impact strength of crystalline PET may be considered inadequate for many applications, particularly in mouldings containing sharp corners. The Izod impact strength is 0.8 ft lbs/inch of notch (ASTM D256) and any variation from ideal moulding conditions will reduce this figure markedly.

1.3. Required Improvements

It was thus considered that although PET displays many useful properties for the design engineer, its use as a general moulding material is likely to be restricted due to the sensitivity to processing conditions and low impact strength.

Before ICI were willing to commercialise a moulding grade PET, it was decided that theprocessing characteristics and impact strength would need to be improved, and whilst other members of the laboratory, in which the work was being carried out, were involved with problems such as nucleation and hydrolytic degradation, the purpose of the study reported here was to obtain a better understanding of the fracture process in PET

and to find methods of increasing the impact strength to a value compatible with its use as a moulding material.

1.4. Possible Methods of Improving Impact Strength of PET

According to Vincent[3] the mechanical behaviour of polymers can be considered in terms of the two phenomenological parameters, yield stress σ_y, and brittle stress σ_b. A polymer is brittle if σ_b is less than σ_y (in practice for toughness σ_y should be well below σ_b).

The values of these two parameters can be influenced in several ways, the most obvious possibilities being as discussed below:

1.4.1. Control of Crystalline Morphology

Amorphous PET can be obtained by rapid quenching of the polymer melt to below the Tg (69°C). In practice this is a difficult process and only relatively thin sections can be obtained in the amorphous state. The amorphous material has σ_y below σ_b at room temperature and exhibits typical tough characteristics at moderate strain rates. However, strain rate and temperature have a greater effect on σ_y than σ_b. Amorphous PET undergoes a tough/brittle transition on increasing the strain rate or decreasing the temperature. Amorphous PET is, therefore, a reasonably tough thermoplastic at room temperature, similar in many respects to unplasticised P.V.C.

By reduction in crystallinity the toughness has been increased at the expense of many of the desirable physical properties of the semi-crystalline material. The modulus and yield stress are reduced drastically and important quantities such as abrasion resistance and creep are adversely affected. Amorphous PET also loses its mechanical strength on raising the temperature above Tg (69°C) and is only useful as a moulded material below 65°C. The semi-crystalline material on the other hand retains much of its usefulness above the glass transition temperature of its amorphous regions and as a consequence of the high melting point of the crystalline zones ($\sim$265°C) can be considered to be a useful material up to 150°C.

On increasing the crystallinity by heat treatment σ_y increases and progressively approaches σ_b. As a consequence the material becomes more brittle as the crystallinity increases. The degree of embrittlement has been found to be dependent on the crystalline texture and the degree of crystallinity. The characteristic mode of crystallisation in PET is spherulitic in which crystallites are ordered radially from a nucleus. The average spherulite size depends upon the number of nuclei per unit volume, which in turn is a function of the crystallisation temperature and thermal history. Excessively large spherulites can lead to the formation of inter-spherulitic voiding which act as stress concentrating centres producing a drastic reduction in the mechanical strength of the system. In order to obtain a high modulus moulding of PET with maximum toughness it is therefore essential to achieve the optimum level of crystallinity together with small spherulitic size. This may be achieved by artificially increasing the nucleation density by inclusion of a finely divided substance in the polymer to act as heterogeneous nucleation sites. These substances are usually referred to as nucleating agents. A successful nucleating agent for PET is talc.

The reason for the high nucleation activity of talc is not understood, though it is thought to be partly due to a matching of the inter-atomic spacings on the surface of talc with spacings in the PET unit cell. The talc surface may then act as a former on which the PET molecules can lock in an ordered way.

By control of the crystalline morphology one can improve impact characteristics, either by eliminating the crystallinity thus producing the amorphous material, or by optimising the texture of the semi-crystalline polymer. However, in both types of product the toughness is not adequate to make them competitive moulding materials at their price.

1.4.2. Molecular Weight

The molecular weight of PET has been found to have an important influence on its toughness, the impact strength decreasing as molecular weight decreases. Below a viscosity average molecular weight of 10,000 (IV 0.4) a very sudden drop in impact strength is observed[4], presumably indicating the molecular weight at which chain entanglements in the amorphous polymer decrease rapidly in number.

The fibre grade PET produced in commercial quantities has a number average molecular weight of 20,000 (IV 0·65) and by increasing molecular weight the impact strength of the polymer may be improved. However, in the melt polymerisation of PET, the molecular weight obtained depends upon the equilibrium obtained between polymerisation rate governed by glycol removal rate and the rate of thermal degradation. The highest feasible molecular weight obtainable from the melt polymerisation on a commercial scale is 25,000 (IV 0.75). To obtain PET of higher molecular weight two techniques may be used; i) Solid State Polymerisation ii) Chain Extension.

Solid State Polymerisation

In this process the polymer produced by normal melt polymerisation is crushed into fine granules or powder and then heated at 200 - 240°C in a high vacuum. Under these conditions the thermal degradation reactions are reduced and the equilibrium shifted towards the production of high polymer. By this technique PET of IV (1.2) can easily be obtained, corresponding to a number average molecular weight of 45,000.

Chain Extension

By linking chain ends with difunctional compounds e.g. a diisocyanate, the average molecular weight of polyesters may be increased. This reaction of PET has been investigated as part of the general study by the author's laboratory into PET as a moulding material. The diisocyanate chosen was methylene diphenyl diisocyanate (MDI) which reacts with the hydroxyl chain ends of PET in the melt.

The reaction is sufficiently rapid to take place during the processing of moulded articles.

The use of a high molecular weight PET as a moulding material is not without complications. The increased molecular weight reduces the crystallisation rate, resulting in the necessity for using longer moulding cycles and nucleating agents. The associated viscosity increase can also produce poor mouldings with excessively large amounts of orientation. By increasing the molecular weight (IV 1•1) the impact strength may be doubled and this can give a feasible moulding material when combined with optimised crystalline texture. A high molecular weight product is at present being marketed under the trade name of 'Arnite'.

1.4.3. Copolymerisation

The lowering of $\mathcal{G}_y$ below ambient temperature can be expected to improve the impact characteristics of semi-crystalline polymers. This may be achieved by incorporation of a suitable co-unit in the chain.

An example of a copolymer of PET possessing a low Tg is a terephthalate-sebacate copolymer containing 30 mole % of the sebacate co-unit. This polymer has a glass transition temperature of 5°C when measured by DTA and a degree of crystallinity of 18%.[5] It is tougher than PET of similar crystallinity but the improvement in impact strength is obtained only at the expense of reducing other desirable properties, i.e. modulus, yield strength and melting temperature.

1.4.4. Blending with Minor Amounts of Rubbers

Many inherently brittle but strong glassy polymers have been modified to give tougher compositions by inclusion of a minor rubbery phase. This is the area of study to which the major part of the present work has been devoted. The aims were to modify PET by using minor amounts of rubber,

thus increasing toughness by a mechanism similar to that successfully operating in, for example, the rubber modified polystyrenes (HIPS and ABS)[6]. The mechanism of the toughening action and the parameters thought to be important to the impact strength are discussed at greater length below.

1.5. Rubber Modification of Polystyrene

A commercially successful rubber modified polymer system is the High Impact Polystyrene series (HIPS). The range of applications for polystyrene based polymers was increased dramatically when it was found that incorporation of minor amounts of a rubber, usually a butadiene copolymer, increased the impact strength considerably with only a minor effect on the stiffness characteristics. Because of the commercial importance of HIPS and ABS, the majority of research into the mechanism of reinforcement of the rubber has been carried out on the polymers and it is important in studying other rubber filled systems to have an understanding of the types of energy absorbing mechanisms present in these rubber blends.

1.5.1. Manufacture of HIPS and ABS

There are three main methods of manufacture of rubber filled polystyrenes[7].

a. Physical Blending

The matrix and rubber are mixed together at a temperature above the softening point of the matrix in suitable compounding equipment e.g. a Banbury Mixer or in the hot rolls of a mill.

An alternative blending method is to mix a suitable rubber latex with a latex of the matrix, coagulate the mixture and dry the coagulum.

b. Bulk Interpolymerisation

The rubber is dissolved in the monomer from which the matrix is made and the solution then polymerised. As the matrix polymer is formed, the rubber is precipitated as a swollen phase, owing to the incompatibility of the polymers. The mixture is stirred, and this causes the rubber phase to take

the form of minute spheres. Polymerisation of the monomer is completed; during the process grafting of the matrix molecules to the rubber molecules and cross-linking of rubber molecules may occur. In this way polymers which have a wide variety of microstructures are obtained.

c. Latex Interpolymerisation

This process combines features of both the blending process and the bulk interpolymerisation process. The rubber is grafted with matrix molecules by emulsion polymerisation of the matrix monomer in a rubber latex. This grafted rubber is then mixed with a latex of the matrix polymer and the mixture is coagulated and dried. The ABS polymers are examples of a polymer made by this process.

1.5.2. Two Phase Characterisation of Rubber Modified Styrene Polymers

The two phase nature of rubber modified polystyrene was first suggested by Buchdahl & Nielsen[8,9] on the basis of dynamic mechanical properties obtained with a torsion pendulum. The existence of the separate rubber and polystyrene damping peaks led them to this conclusion. Microscopy provided the positive proof of the existence of the rubber phase as a discrete phase in HIPS. Claver and Merz[10] showed the different rubber particle morphologies resulting from mechanical blending of rubber and polystyrene and from solution grafting of rubber in the presence of polymerising styrene. More recently, excellent resolution has been achieved by using osmium tetroxide staining [11].

1.5.3. Role of Rubber in Reinforcement

Merz, Claver and Baer[12] first suggested in 1956 that the rubber phase in a HIPS is dispersed in the form of small rubber particles and the energy absorption occurs through the stretching of the rubber phase. This theory was replaced in 1965 by the theory of Newman & Strella[13] who proposed that high elongation and toughness of rubber modified polystyrene can be explained by cold drawing of the polystyrene phase as a result of dilation, induced by the disperse phase. Subsequently Bucknall & Smith[14] have ascribed the ductile deformation and stress whitening to the formation of a large number

of crazes which had been initiated at the rubber particles. Bucknall & Smith further demonstrated that the influence of temperature can be explained by such a mechanism and showed that the theory is in agreement with practical experience.

In 1967 Rosen[15] reviewed the general field of two phase polymers and covered the several mechanisms of reinforcement which had been published in the literature. In addition he drew some conclusions of his own. He suggested that the minimum particle size capable of reinforcement is about 0.01μ (100Å). Based upon the crazing theory he concluded that the greater the number of particles above this critical size, the greater the number of sites of initiation of crazes, and hence, the higher the impact strength.

Boyer[16] reviewed the mechanisms in connection with a discussion of the function of the rubber loss process in HIPS.

He suggests that the rubber particles tend to trigger off a secondary loss process in polystyrene, and this initiates crazing. The suggestion was in part based upon the observation that similar activation energies ($\sim$30 to 36 kcal) are found for the three associated processes, i.e. the main loss process at Tg, and the secondary (β) loss process and crazing.

1.5.4. Craze Structure and Properties

Since it is now generally accepted that crazing is the major energy absorbing mechanism in rubber modified systems a brief discussion follows on their structure and properties.

Craze structures in glassy polymers were originally thought to be cracks. However, in the early sixties it was shown that they are sharply bounded regions of the polymer which contain polymeric material i.e. they are not voids. This material interconnects the bulk polymer on each side of the craze[17]. The filled nature of crazes is concluded from the observations that samples containing crazes over their entire cross-section are still

capable of supporting a load. Also Kambour has shown that the refractive index of a craze is substantially greater than unity[18] supporting the filled craze theory. From these determinations he was able to estimate the void content of crazes by application of the Lorentz-Lorentz equation. He concluded that in several glassy polymers the crazes were 40 - 60% void[19]. This void content was independant of the crazing agent used.

Kambour in these studies assumed that the craze behaved homogeneously to light and that therefore, the substructures were of an order less than the wavelength of light. This assumption was supported by X-ray studies which indicated that the void diameter of crazes in polycarbonate was of the order of 100Å. Crazes were also seen to be birefringent indicating orientation of the crazed material perpendicular to the length of the craze bands. A model of a craze was therefore proposed in which the craze material was made up of fibrils of oriented polymer distributed within the craze band so as to produce a system of interconnecting voids whose magnitudes were of the order of 100Å in diameter.

This model has been supported recently by electron micrographs of polycarbonate crazes that were obtained by Kambour by sectioning crazes that had been supported by impregnation with sulphur prior to sectioning[20].

The role of crazing in amorphous PET will be discussed in the following chapter.

REFERENCES

Chapter One

1. Carothers W.H. and Hill J.N., J. Am. Chem. Soc. 54, 1577 (1932)
2. Whinfield and Dickson, Nature, 158, 930 No. 4026 (1946)
3. Vincent P.I., ICI Information Service Note, No. 916 (1964)
4. Private Communication, Dr. R. Turner, P and P Laboratory
5. Jackson J.B., Polymer 10 No. 3, p. 159 - 65 (March 1969)
6. Composite Materials, L. Holliday, Elsevier Publishing Co. (1966) p 228
7. Ibid pp 235 - 246
8. Buchdahl R., Nielsen L.E., J. Polymer Sci., 15, 9 (1955)
9. Nielsen L.E., J. Amer. Chem. Soc., 75, 1435 (1953)
10. Claver, G.C., Merz, F.J., Official Digest, Federation Paint Varnish Prod. Clubs. 28, 858, (1956)
11. Kato, K., Polymer Eng. Sci. 7, 38 (1967)
12. Merz, E.A., Claver, G.C., Baer, M., J. Poly. Sci., 22, 325 (1956)
13. Newman S., Strella S., J. Appl. Polym. Sci., 9, 2297 (1965)
14. Bucknall C.B., Smith R.R., Polymer, 6, 437 (1965)
15. Rosen S.L., Polymer Eng. and Sci., 7, 115 (1967)
16. Boyer R.F., Polymer Eng. and Sci., 8, 161 (1968)
17. Spurr O.K., Niegisch W.D., J. Appl. Polymer Soc. 6, 585 (1962)
18. Kambour R.P., Polymer 5, 107 (1964)
19. Kambour R.P., J. Polymer Sci. Pt. A, 2, 4159 (1964)
20. Kambour R.P., Russell R.R., Polymer 12, 4, p. 237 (1971)

CHAPTER TWO

2. CRAZING IN POLY(ETHYLENE TEREPHTHALATE)

The accepted toughening mechanism in HIPS and ABS systems is dependant upon the formation of crazes in the matrix as the principal energy absorbing mechanism.

For a rubber modified PET system to absorb impact energy using a similar mechanism to that proposed for the rubber-toughened polystyrenes, it is a necessary condition that the PET be able to craze. Crazing has been shown to occur in many glassy polymers including polystyrene, polymethyl methacrylate, polycarbonate, polyvinylchloride. However, formation of craze structures in PET has not been reported.

2.1. Experimental

2.1.1. Preparation of Amorphous PET Samples

Tensile samples were prepared using a 2 oz. Stübbe reciprocating screw injection moulding machine. The polymer melt was injected into a mould maintained at 20°C so as to quench the polymer into the amorphous state. The dimensions of the dumbell samples so produced are shown in Fig. 2/1a. Samples for controlled solvent crazing in flexure (Fig. 2/1b) were fabricated in a similar fashion.

Uniaxially drawn film for constant load tests was obtained from ICI., Plastics Division. The strip samples were razor cut from the film at various angles to the draw direction using a parallel sided former giving samples 1 cm in width. The film thickness was 0.03 cm.

2.1.2. Tensile and Flexural Tests on Injection Moulded Samples

Dynamic and constant load tests were carried out using a Hounsfield E Type Tensometer fitted with a specially designed tensile rig mounted in a flask to enable the samples to be stressed whilst immersed in liquid, see Fig. 2/2. The stress was calculated from the measured load and the initial cross section area of the sample.

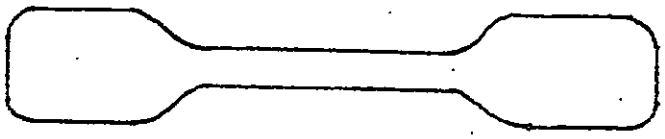

Tensile sample.(Actual size)

FIG.2/1a

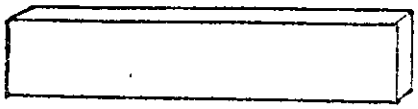

Flexural sample (Actual size)

FIG.2/1b

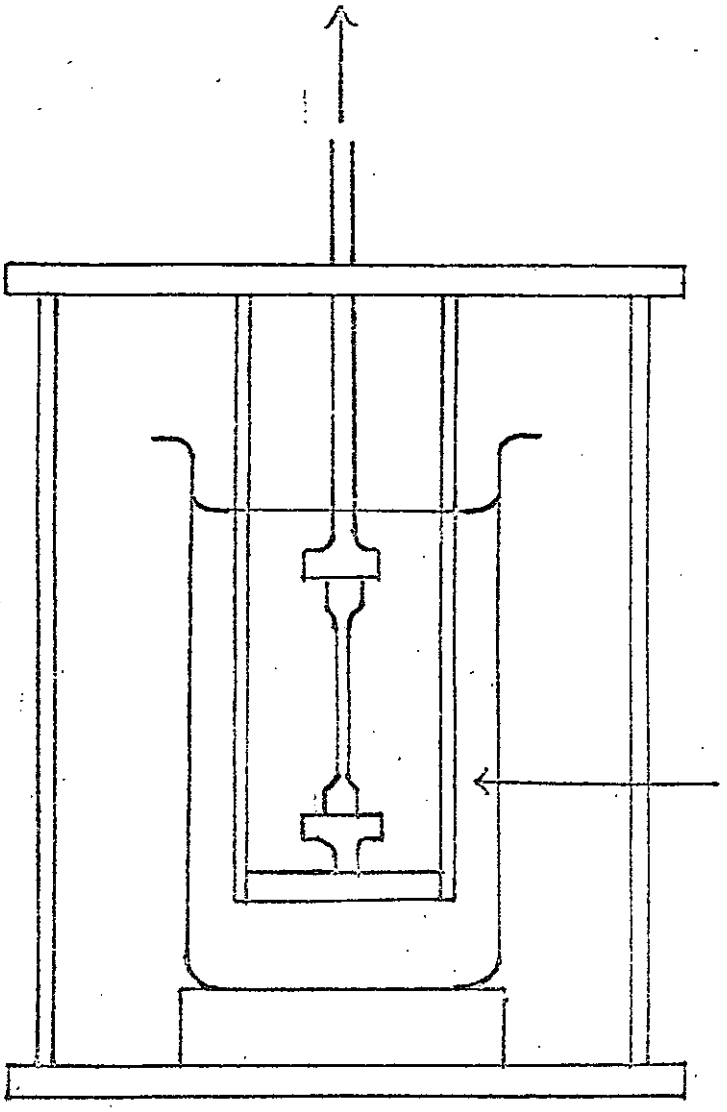

Tensile crazing apparatus

FIG 2/2

$$\text{Stress} = \frac{\text{Applied load}}{\text{Initial cross section area.}}$$

2.1.3. Void Content Measurement of Crazes

Craze refractive indices were determined by measurement of the critical angle after a technique described by Kambour[1]. This technique assumes the craze to behave as a homogeneous entity which requires that the voids in the craze material are small compared with the wavelength of the light. The method of refractive index determination involves the measurement of the critical incident angle of a parallel monochromatic light beam at the crazed polymer specimen surface for which total internal reflection occurs at the interface between the craze and bulk polymer (Fig. 2/3).

The beam upon entering the specimen is refracted to a new angle, the portion of the beam that then strikes the craze interface is either transmitted and passes on out of the rear side of the specimen (Fig. 2/3a), or suffers total internal reflection, when a shadow of the craze appears on the translucent screen (Fig. 2/3b).

For the case of total internal reflection it can be seen from Snell's Law that:

$$\frac{\sin a}{\sin b} = \mu_P \qquad \text{and}$$

$$\frac{\sin c}{\sin 90} = \frac{\mu_c}{\mu_P}$$

where μ_c and μ_P are the refractive indices of the craze and bulk polymer respectively.

Since from the geometry $\hat{c} = 90 - b$

$$\sin c = \cos b$$

It follows that $\mu_c = \mu_P \cos b$ and $\sin b = \frac{\sin a}{\mu_P}$

Therefore, from a knowledge of the critical angle for total internal reflection (a) and the refractive index of the bulk polymer (μ_P), the craze refractive index may be calculated.

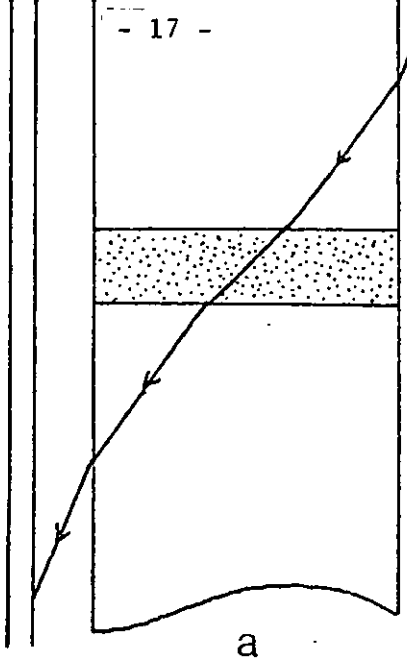

a

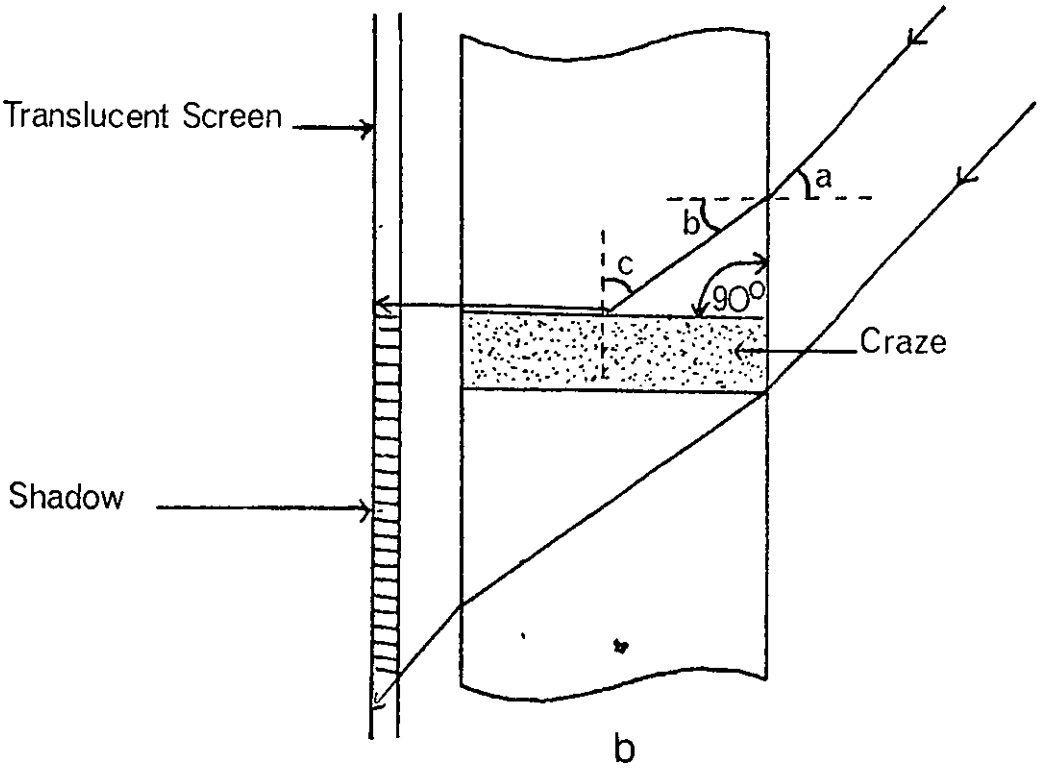
Translucent Screen
a
b
c
90°
Craze
Shadow

b

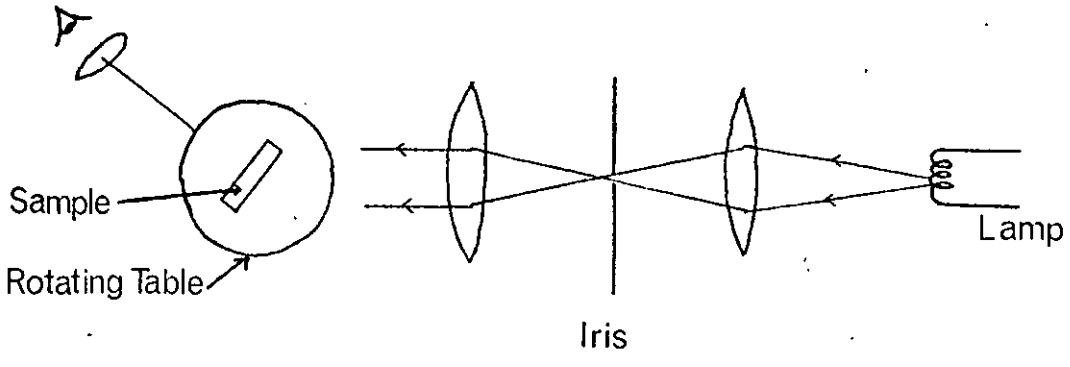
Sample
Rotating Table
Lamp
Iris

c

FIG 2/3

For specimens containing well formed widely spaced crazes, the critical incident angle can, after some practice, be determined to $\frac{1}{2}^{o}$.

Knowing the refractive index of the craze, the density may be calculated using the Lorentz-Lorentz equation.

$$\rho = (\mu_c^2 - 1)/(\mu_c^2 + 2)d_c)$$

where ρ = the specific refraction of the bulk polymer

d_c = density of the craze.

The use of this equation assumes that the specific refraction of the polymer is independent of orientation since the polymer in the craze is known to be orientated in the direction perpendicular to the craze.

The void content of the craze is then given by

$$\text{void content} = \frac{(1 - d_c)}{d_p} \times 100 \text{ vol\%}$$

where d_p = density of the polymer

Again the polymer density is assumed independent of orientation.

2.1.4. Measurement of the Refractive Index of the Bulk Polymer

The refractive index of amorphous PET was determined using the "Becke method"[2]. If a transparent isotropic substance is immersed in a colourless fluid, both having the same refractive index, the substance will become invisible owing to the disappearance of refraction and reflection effects at the interface of the two substances. If the refractive indices are different, the relief or strength of the border between the two substances depends upon the magnitude of the difference. Practical use of this fact is made by immersing substances in different fluids of known refractive index, until the border phenomena disappear. In practice, when the border phenomena appears, it is necessary to know whether the refractive index of the fluid is higher or lower than that of the substance under investigation. Under certain conditions of illumination a bright line (or "becke line" as it is commonly called) is seen. If the image is thrown slightly out of focus by raising the objective the bright line will move towards the substance having the higher refractive index.

The method requires a high powered objective to be used because of the small depth of focus. The technique used for PET was to cut some thin slivers off a sample and immerse in fluids of known refractive index until the Becke line disappeared when the refractive index was then the same as that of the immersion media.

2.1.5. Microscopy of Crazes

The crazes used for the study were obtained by straining samples in tension or in flexure in a crazing agent, usually methanol. The crazes were studied using optical and electron microscopes. Detailed notes on the type of equipment and techniques used are described elsewhere (Chapter 4 p102).

2.2. Results

2.2.1. Non Solvent Crazing

Crazing is not normally observed in tensile tests on amorphous PET. The common mode of failure in low strain rate tensile tests is for the material to yield with neck formation and subsequent cold drawing to failure. However, if the sample is stressed to just below its yield point (580 kg/cm^2) and the load maintained, crazes are observed to propagate in from the specimen surface to a depth of approximately 50μ. No evidence for internal craze formation was observed.

In polystyrene, crazing has been found to occur preferentially in materials oriented normal to the direction of the applied stress[3,4]. This effect was investigated in PET using uniaxially drawn film stressed by static loading using a rig designed for creep testing.

For samples stressed at 0° and 30° to the draw direction no crazes were observed before fracture occurred.

For specimens stressed at 60° to the draw direction, craze structures were observed in samples held at stresses greater than 450 kg/cm^2 i.e. 75% of the yield stress.

In specimens stressed at 90° to the draw direction craze structures were formed at stress levels greater than 300 kg/cm^2 i.e. 55% of the yield stress. In this case the crazes propagated well into the centre of the specimen and a few were observed to have formed across the entire cross section.

2.2.2. Solvent Crazing

For detailed study of craze structure, large, well separated crazes are required. Stressing in air produces few poorly formed surface crazes in isotropic injection moulded samples. Large crazes have been produced in other polymers by using "crazing agents" and it was envisaged that by suitable selection of a crazing environment the type of crazes required for further study could be obtained.

Many organic liquids have been found to be crazing agents for amorphous polymers. Bernier and Kambour[5] found that the critical strain for craze formation in polymers when stressed in an organic liquid decreases as the solubility parameter of the liquid approached that of the polymer. It is also found that the type of crazing changes from few widely spaced crazes to many closely spaced crazes, as the solubility parameter of the liquid approaches that of the polymer.

The solubility parameter of amorphous PET when calculated by Small's[6] method is 10.7. The lower alcohols were therefore, chosen as possible crazing agents since their solubility parameters range from 14.5 for methanol to 10.6 for n-heptanol.

As hoped, specimens immersed in methanol produced well formed, widely separated crazes when strained to 0.08% strain (150 kg/cm^2). On straining in the higher alcohols large numbers of closely spaced crazes were produced at similar strains.

Fig. 2/4 shows the effect of a methanol environment in the shape of the tensile stress/strain curve for amorphous PET.

FIG 2/4

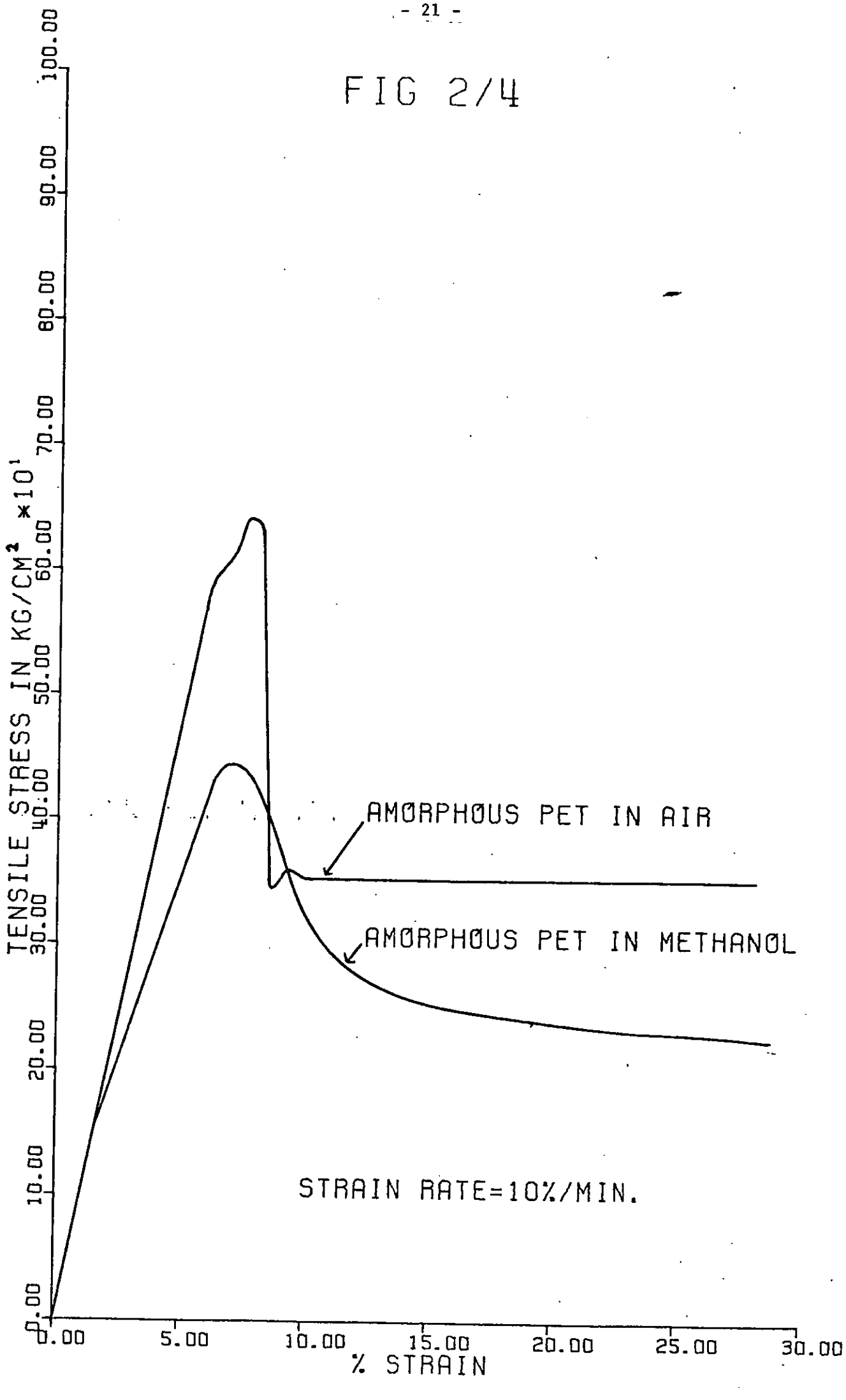
TENSILE STRESS IN KG/CM² *10¹
100.00
90.00
80.00
70.00
60.00
50.00
40.00
30.00
20.00
10.00
0.00
0.00
5.00
10.00
15.00
20.00
25.00
30.00
% STRAIN
AMORPHOUS PET IN AIR
AMORPHOUS PET IN METHANOL
STRAIN RATE=10%/MIN.

When strained in air, a well defined yield point is observed. This point is associated with shear deformation involving little or no change in density.

When the specimen was strained in methanol, crazes were seen to form at low stresses. They grew rapidly, each tending to cover the entire cross section. Craze formation accelerated with stress increase and it was apparent that the yield stress observed (440 kg/cm^2) was the stress at which plastic deformation by craze formation equalled the rate of crosshead extension. At no time was there evidence of deformation other than 90^o to the tensile stress direction; thus shear deformation did not contribute significantly to the strain.

2.2.3. Investigation of Single Craze Bands

The following detailed examination of single crazes was carried out using crazes produced in specimens that had been stressed in a methanol environment to slightly above the craze initiation stress, such that only one or two well formed crazes were obtained.

2.2.4. Refractive Index of Methanol grown Crazes in PET

A powerful way of demonstrating that the reflecting bands observed in amorphous polymers are crazes and not microcracks, is to measure their refractive index. Crazes in PET would be expected to have a refractive index between that of air 1.0, and that of the polymer, 1.60. Microcracks on the other hand will have a refractive index of 1.0.

The crazes used in the determinations were grown in a methanol environment. In order to allow the crazing agent to evaporate out of the crazes after formation, the specimens were kept under load for 3 - 4 hours in a well ventilated room, after removal of the crazing environment.

The refractive indices were measured by the critical angle method as described in the experimental section.

In order to calculate the craze density and void content, the refractive index and density of amorphous PET were required. A value of 1.60 was obtained for the refractive index as measured by the "Becke method". A value of 1.348 was obtained for the density by using a density gradient column with calcium nitrate solution as the gradient liquid.

Table 2/1 shows the values obtained for refractive index and void content for crazes grown in five different specimens.

Table 2/1

Critical Angle (a)	Refractive Index μ_c	Density d_c	Void Content vol %
50.5°	1.40	0.955	29%
50°	1.40	0.955	29%
51°	1.40	0.955	29%
49.5°	1.41	0.976	28%
52°	1.39	0.934	31%

Clearly the structures seen are not cracks but must contain significant amounts of polymer (70%). A value of 30% void content is low when compared with polystyrene (40%) styrene acrylonitrile copolymer (60%) polymethyl methacrylate (40%) and polycarbonate (45%)[7].

However, there was some evidence that if crazes were produced by stressing some way above the critical craze stress, crazes of higher void content were formed. In these cases it was difficult to make measurements due to the close proximity of crazes in the sample.

2.2.5. Craze Healing

It is known that crazes can be "healed" by raising the temperature above Tg, or application of a compressive stress. In the latter case there is evidence that on subsequent tensile loading the crazes will reform at their old sites. However, it was noted in the amorphous PET specimens, that a natural healing process appears to occur on removal of the applied stress and methanol environment. This process manifests itself as a rise in the craze refractive index with time (Fig. 2/5). Over the first half of the healing process the rate is approximately linear with log time suggesting the occurence of a disorientation process.

The crazes are, however, visually evident for a considerable period of time, indicating that the rate slows considerably in the latter stages. The polymer never reverts to a completely uncrazed state unless the temperature is raised above the Tg.

2.2.6. Microscopy of Crazes

a. Optical Microscopy

Fig. 2/6 is an optical micrograph of a crazed film taken in transmitted light. The crazes can be seen to be short and form perpendicular to the direction of the applied stress. The craze thickness is seen to be of the order of 2μ, though this figure must of necessity be only an estimate due to the effects of refraction around crazes under the optical microscope.

Crazes produced in an injection moulded dumbell specimen (Fig. 2/7) are much longer and are seen to have propagated across the entire cross section of the specimen in places.

Optical microscopy does not reveal any internal detail of crazes. It is, therefore, necessary to use the electron microscope in further studies of craze structure.

FIG 2/5

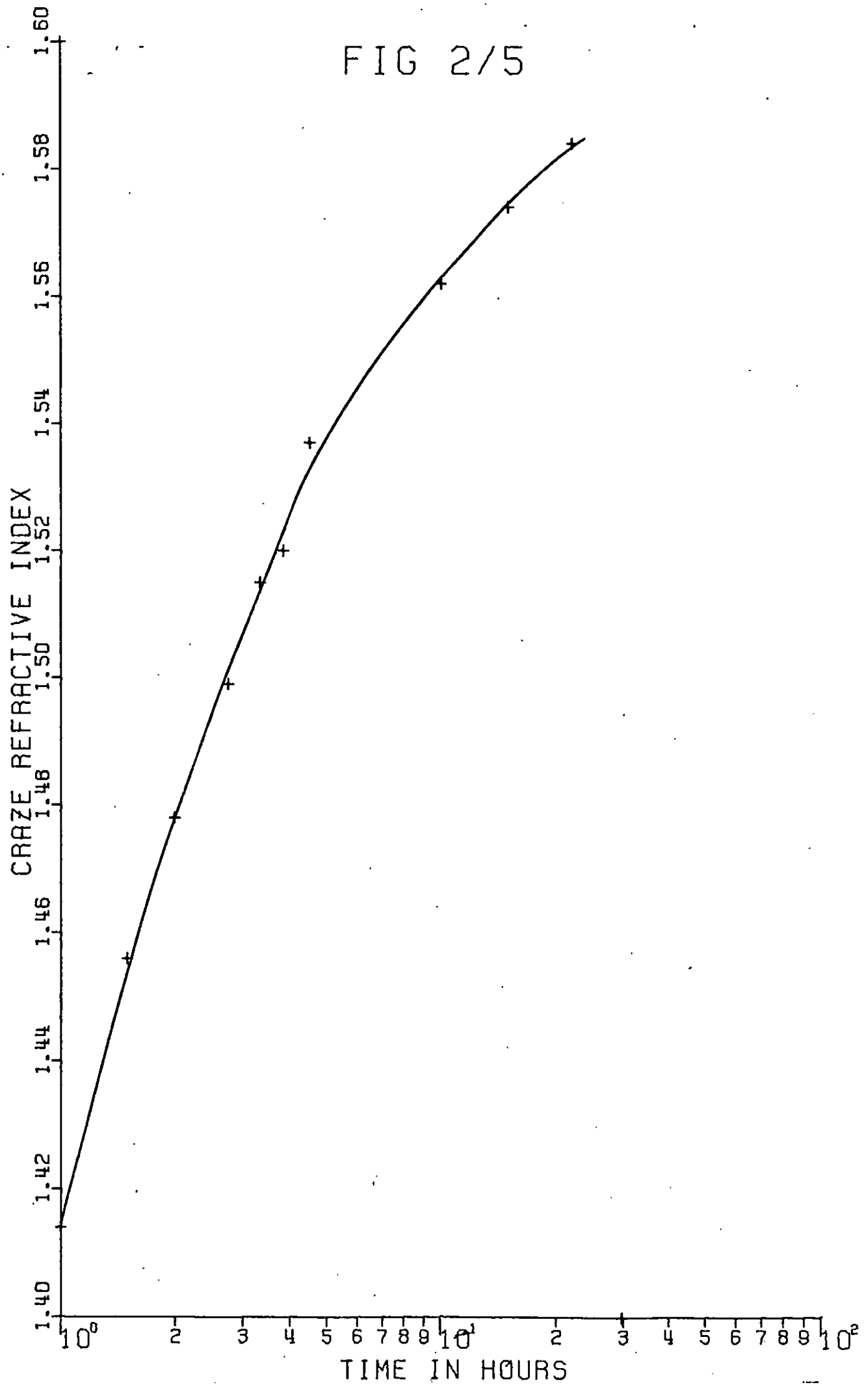
CRAZE REFRACTIVE INDEX
1.60
1.58
1.56
1.54
1.52
1.50
1.48
1.46
1.44
1.42
1.40
10⁰
2
3
4
5
6
7
8
9
10¹
2
3
4
5
6
7
8
9
10²
TIME IN HOURS

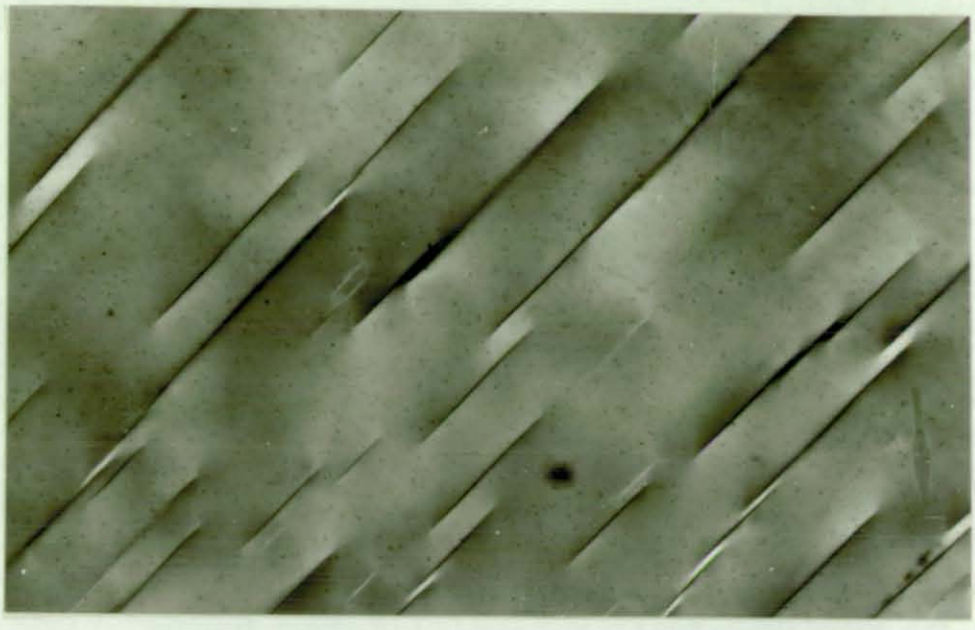

FIG 2-6 mag. 250x

FIG 2-7 mag. 15x

b. Electron Microscopy of Sections

The commonly used method for the visual examination of the internal craze structure is to produce thin sections using an ultramicrotone with subsequent examination in a transmission electron microscope. Previous investigators have found that the crazed structure must be supported during microtoming by filling up the voids in the craze with a suitable material. Kambour[8] obtained a degree of success by photodeposition of silver from impregnating silver nitrate solution, whilst it has been shown by Bucknall that in HIPS systems photodeposition of osmium from impregnated osmic acid leads to an indication of craze structure being obtained. The most successful photographs to date were obtained by Kambour[10] by impregnation of the crazes with liquid sulphur or iodine/sulphur mixtures with subsequent removal by sublimation after sectioning. Crazes in PET were filled with silver and also with osmium prior to microtoming. Attempts at microtoming were unsuccessful, the sections tending to fracture at the crazes during sectioning.

In using the technique developed by Kambour it was found necessary to use the iodine/sulphur mixture since the melting point of sulphur (119°C) is above the glass transition temperature of PET; the iodine/sulphur mixture melts at 65°C, which made it a suitable impregnating medium.

On immersing the crazed specimen in this mixture, the iodine was found to be soluble to some extent in the polymer, and upon subsequent sectioning the crazes again fractured.

Unfortunately, therefore, sections of crazes were not obtained from PET samples.

c. Electron Microscopy of Crazes at the Specimen Surface

By observation of the craze structure at the surface of a specimen, it is possible to obtain information concerning its structure without carrying out any physical operation such as sectioning. In this way the possibility of producing artifacts during sample preparation is minimised. The freshly methanol-crazed specimen was coated in an evaporator with aluminium, to give a continuous coating $\sim$1000 Å thick and the sample then studied in a Cambridge Stereoscan Mark II scanning electron microscope. Figure 2/8 shows the craze appearance when the specimen surface is at 45° to the electron beam. It is obvious from the photograph that bundles of polymer bridge the gap between the craze boundaries. These bundles, $\sim$3000 Å thick, are interleaved and it would appear from this photograph that the craze is made up of fibrils of polymer aligned perpendicularly to the craze direction and not a semi-oriented mass of polymer filled with holes.

By increasing the angle of the specimen to the incident beam to 80° a clearer representation of the craze is seen (Fig. 2/9). It must be remembered that the craze observed is in a semi-relaxed state and that one sees loops that have been formed when the originally taut craze fibrils have been relieved of stress on relaxation of the specimen.

Fig. 2/10 is a micrograph at high magnification and low tilt angle (30°). It shows visual evidence that the loops are made up of bundles of smaller fibrils of diameter $\sim$500 Å. It is possible that the formation of the fibrils into larger units is a structure associated with the craze at the surface only, and that the internal craze structure is composed of a network of the fine fibrils.

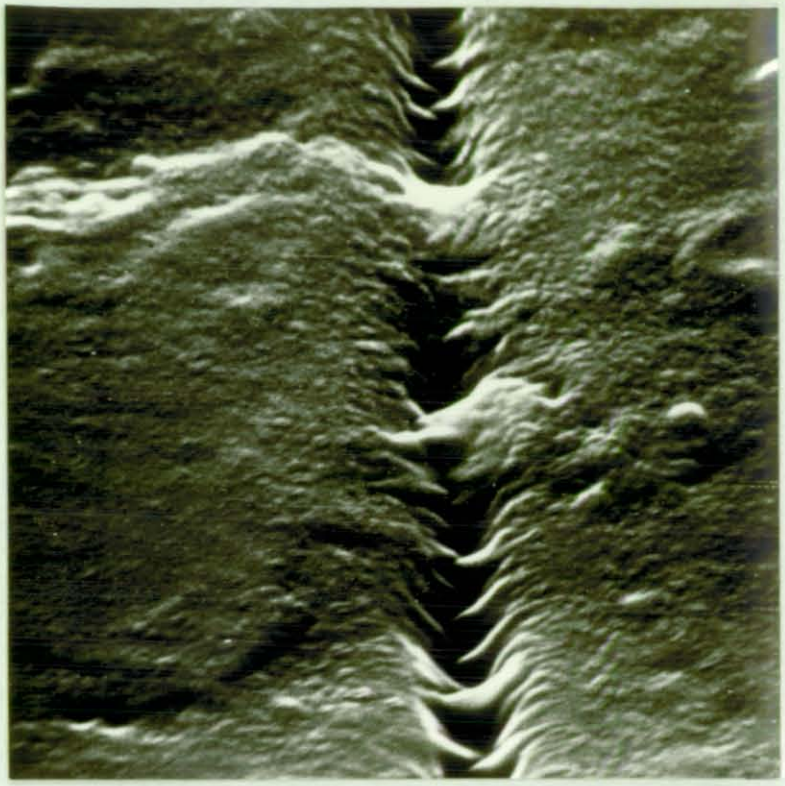

FIG 2-8 tilt angle 45° mag. 7·5 K

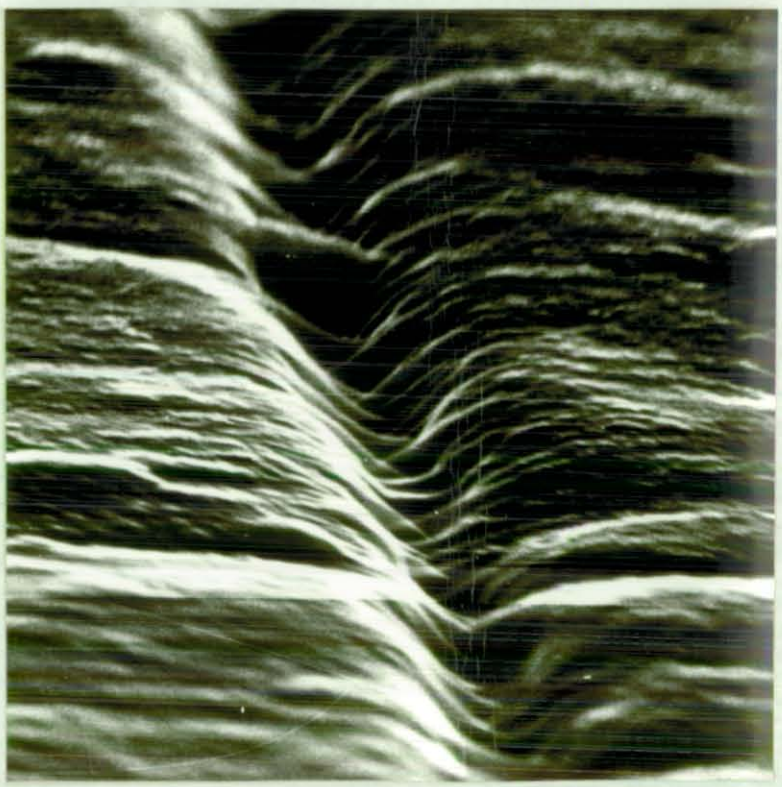

FIG 2-9 tilt angle 80° mag. 15K

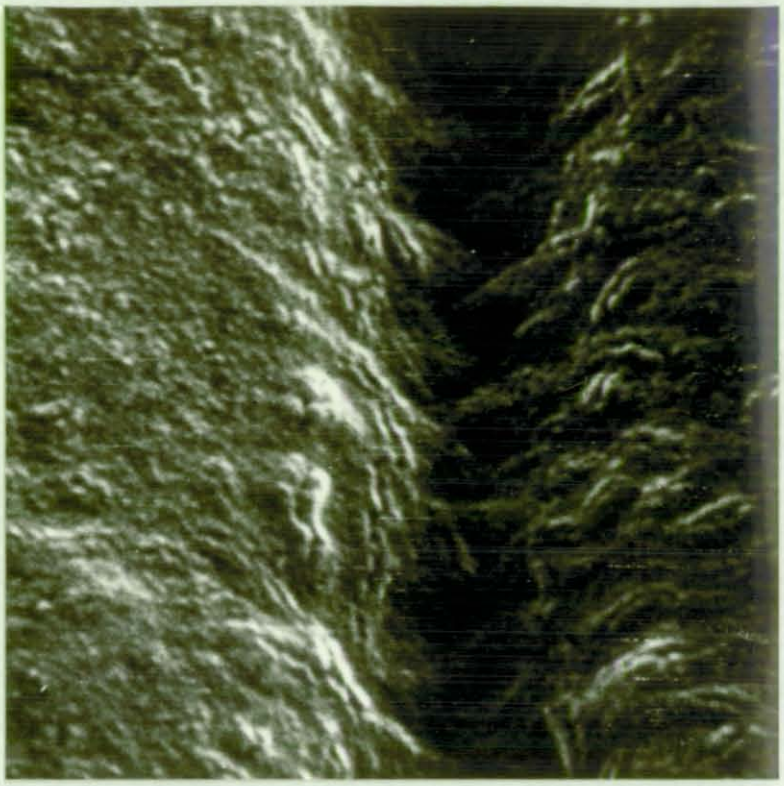

FIG 2-10 tilt angle 30° mag. 30 K

d. Surface Appearance of Fractured Crazes

Figures 2 - 11 and 2 - 12 are transmission electron micrographs of carbon replicas of the fracture surface of a craze. These fracture surfaces were prepared as follows. An injection moulded bar of amorphous PET was stressed in an environment of methanol at just above the craze initiation stress such that large well spaced crazes were produced. The craze was then dried out at room temperature, whilst being held under stress for four hours. The sample was then immersed in liquid nitrogen and fractured.

A crack was seen to propagate through the craze and the surface of the specimen was highly reflecting. Upon viewing the specimen using an optical microscope irregular markings were observed.

The higher magnification using a replication technique and transmission electron microscopy gave the photograph shown in Fig. 2-11.

The micrograph shows that the surface consisted of islands of craze material. From the shadowing detail, the thickness of the craze on the surface can be estimated. It is found that the thickness is of the order of 1.3μ. If as it appears, the crack has propagated preferentially along the interface between the craze and the bulk polymer this thickness of 1.3μ represents the original craze depth. It would be more correct to say that the original craze was probably greater than 1.3μ thick since upon fracture the craze can have relaxed to some extent.

Because of this relaxation one cannot expect to be able to see much evidence of the original craze structure from the fracture surfaces. However, as can be seen from Fig. 2-12, the surface does exhibit fine detail that could be envisaged as being the result of fracturing a honeycomb-like structure. The finest detail shown could result from a void filled structure of void diameter 100 to 1000 Å.

FIG 2-11 mag 2·5K

FIG 2-12 mag 20K

2.3. Conclusions

It has been demonstrated that craze structures can be obtained in amorphous PET. These structures form most easily in oriented specimens or by the use of suitable 'crazing agents'.

The crazes that are formed in the presence of methanol have a void content of ~30% and exhibit a craze healing phenomenon at room temperature (i.e. below the Tg of the bulk polymer).

Whilst electron micrographs of craze sections were not obtained it was found possible to investigate the internal structure by observation of the craze bands at the surface of the specimen, and by the general appearance of low temperature fracture crazes. From this evidence the crazes are most probably made up of oriented fibrils stretching across the craze band, with similar structure as that observed by Kambour in polycarbonate and polystyrene.

It is clear from the experiments that PET is able to craze under favourable conditions in a similar fashion to polystyrene, and it is therefore, feasible that a rubber modified PET would be able to absorb energy by craze formation and deformation as postulated for the high impact polystyrenes.

REFERENCES

1. Kambour, R.P., Nature, p. 1299 (1962).
2. Hartshorn and Stuart, Crystals and the Polarising Microscope, Edward Arnold, London 1960, p. 253.
3. Maxwell, B. and L.F. Rahm, Ind. Eng. Chem., 41, No. 9, p. 1989 (1949).
4. White, E.F.T., B.M. Murphy and R.N. Haward, Polymer Letters, 7, 157 (1969).
5. Bernier, G.A. and R.P. Kambour, Macromolecules 1, 393, 1968.
6. Small, P.A., J. Appl. Chem. 3, p. 71, (1953).
7. Kambour, R.P., J. Polym. Sci. A2, P. 4159 (1964).
8. Kambour, R.P., J. Polym. Sci., A2, 7, p. 1393 (1969).
9. Bucknall, C., Personal Communication.
10. Kambour, R.P., Unpublished Work.

CHAPTER THREE

3. BLENDING OF PET WITH MINOR AMOUNTS OF A "RUBBER"

For the purpose of this study a rubber was defined as a material with a Tg (from DTA) below $0^{\circ}C$ and a shear modulus of less than 5×10^{3} kg/cm^{2}.

3.1. Selection of Suitable Rubbers

The factors considered when selecting suitable rubbers to use as a minor phase in potential high impact PET compositions were:

i. The polymer must be chemically and thermally stable under the conditions employed for fabricating PET.

ii. It must be incompatible with PET, i.e. the resulting blend must be a two phase system.

iii. Suitable chemical sites must be present to provide adhesion between the phases either by a grafting reaction, or by selective compatibility with the PET.

iv. The polymer must have good low temperature impact properties.

v. The cost of the rubber should be less than or equal to that of PET.

Application of these criteria resulted in the choice of ethylene copolymers containing, as co-monomer, a unit which could take part in esterification (graft) reactions with PET and/or have a solubility parameter close to that of PET to promote adhesion by allowing a limited amount of compatibility at the phase boundaries. Two ethylene copolymers were chosen for detailed study, ethylene/vinylacetate copolymer and "Surlyn A" ionomers. Some feasibility studies were also carried out on the use of high rubber content ABS and a number of experimental elastomeric polyesters. Parallel investigations carried out by other workers in the laboratory studied blends containing ethylene copolymers of methyl methacrylate, ethyl acrylate, hydroxyethylene methacrylate.

3.2. Experimental

3.2.1. Drying

Due to the susceptibility of PET to hydrolytic degradation in the melt, the polymer was thoroughly dried prior to any processing step. Theprocedure adopted was to heat the material in chip form to 140°C under a vacuum (10^{-1}mm, Hg), for a period of not less than four hours. The material was then cooled whilst still under vacuum and the subsequent processing step completed as quickly as possible to minimise water uptake of the dried chip.

3.2.2. Blending Techniques

a. Extrusion Blending

Blending was carried out by extrusion of mixtures of tumble blended chip. An Iddon 1½" extruder fitted with a nylon type screw was used, operating at barrel temperatures of 250° - 270°C, at a screw speed of 80 r.p.m. Where required, improved dispersions were obtained by subjecting the blend to a second extrusion. However, since each processing step degrades the PET, the number of steps was kept to a minimum consistant with reasonable dispersion.

b. Static Mixer

A recent technique for mixing molten polymers is use of a 'static mixer'. The nearest analogy to the mixing action is that of "shuffling" a pack of cards, where randomisation is achieved by repeated splitting and rejoining of the "feedstock". The mixer used was manufactured in P. & P. Laboratory and was similar in design to the mixer manufactured by the Kenics Corporation[1,2].

The mixer (Fig. 3-1) consists of alternate clockwise twisted strips of metal fixed into a tube. The pitch of each twist is arranged to be 1.5 times the I.D. of the tube. Each element contains half a twist and is arranged with its leading edge at right angles to the trailing edge of the preceding one. This gives two mixing actions, a radial and longitudinal mixing. Radial mixing is caused by material on the outside of the tube slowly moving into the centre and then out again, longitudinal mixing is caused by the larger path length down the outside of the tube, so that this material in effect flows more slowly than down the centre. In theory if an n element mixer is used the material is sub-divided 2^n times; in this case n is 20.

The polymer melt was fed to the static mixer by a conventional screw extruder, the total residence time being in the region of 6 - 7 mins.

3.2.3. Sample Preparation

All tests were carried out on specimens produced by injection moulding. A 2 oz. capacity Stübbe reciprocating screw injection moulding machine was used operating at barrel temperatures of 265°C to 275°C and cycle times of 5 sec injection, 5 sec interval and 5 sec cool.

Amorphous specimens were obtained by use of a water cooled mould tool to quench the melt into the amorphous state. Crystalline specimens were prepared in one of two ways.

i. The amorphous specimens were heated to 140°C for 2 - 3 hours.

ii. A mould tool maintained at 140°C was used during injection moulding using a 'cooling' time of 30 secs.

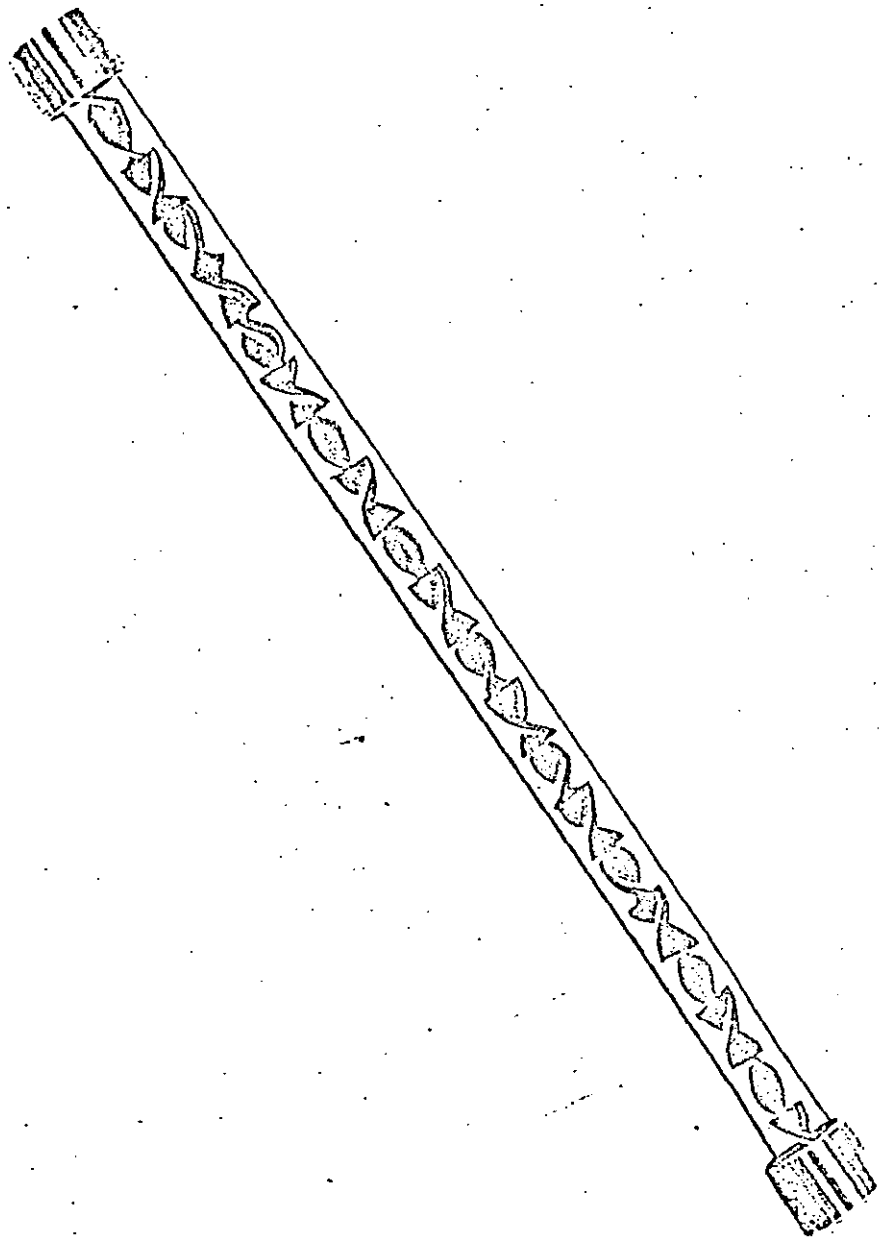

FIG 3-1

3.2.4. Mechanical Testing Procedures

a. Tensile Testing

Dumbell samples of dimensions shown in Fig. 3/2a were tested on a Hounsfield type E tensometer using a strain rate of 100%/min. From the load elongation curve yield stress, breaking stress and elongation to break were determined (Fig. 3/2b).

Initial modulus determinations were made using an extensometer to measure the strain, in this test a strain rate of 10%/min was used and the slope of the load/extension curve taken over the first 0.5% strain.

b. Flexural Testing

Injection moulded specimens of dimensions 4.1 cm x 0.64 cm x 0.32 cm were tested in three point bending using a span of 3.8 cm.

The modulus, yield or breaking stress and the extension to break were calculated from the load/extension curve (Fig. 3/2b) using equations obtained from simple beam theory.

Flexural Modulus = $(l^3/4bd^3)$ x (FSD/(b-a) x (chart speed/Xhead speed)

Yield or breaking stress = $3/2 \times W/bd^2 \times l$

Extension to break = $6d/l^2$ x Xhead speed x (c-a)/chart speed.

where l = span in cm

b = specimen width in cm

d = specimen depth in cm

FSD = full scale of deflection on the chart, in Kg.

c. Impact Testing

Testing was conducted on a Hounsfield Charpy Impact testing machine. The specimens, were notched prior to testing with a Hounsfield notching machine. The dimensions of the notch used throughout were 0.28 cm deep, 45° angle, 0.025 cm tip radius.

The impact strength for notched samples was calculated using the formula:

Impact strength = Energy absorbed/Cross section area kgcm./cm^2

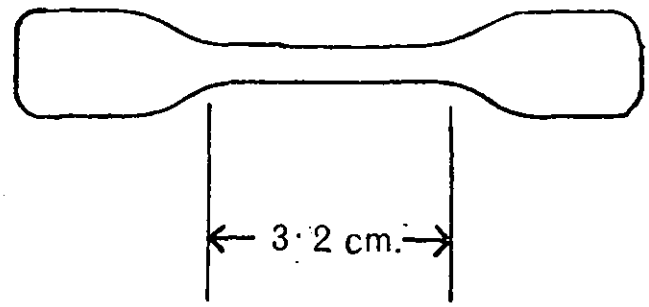

(a) dumbell sample

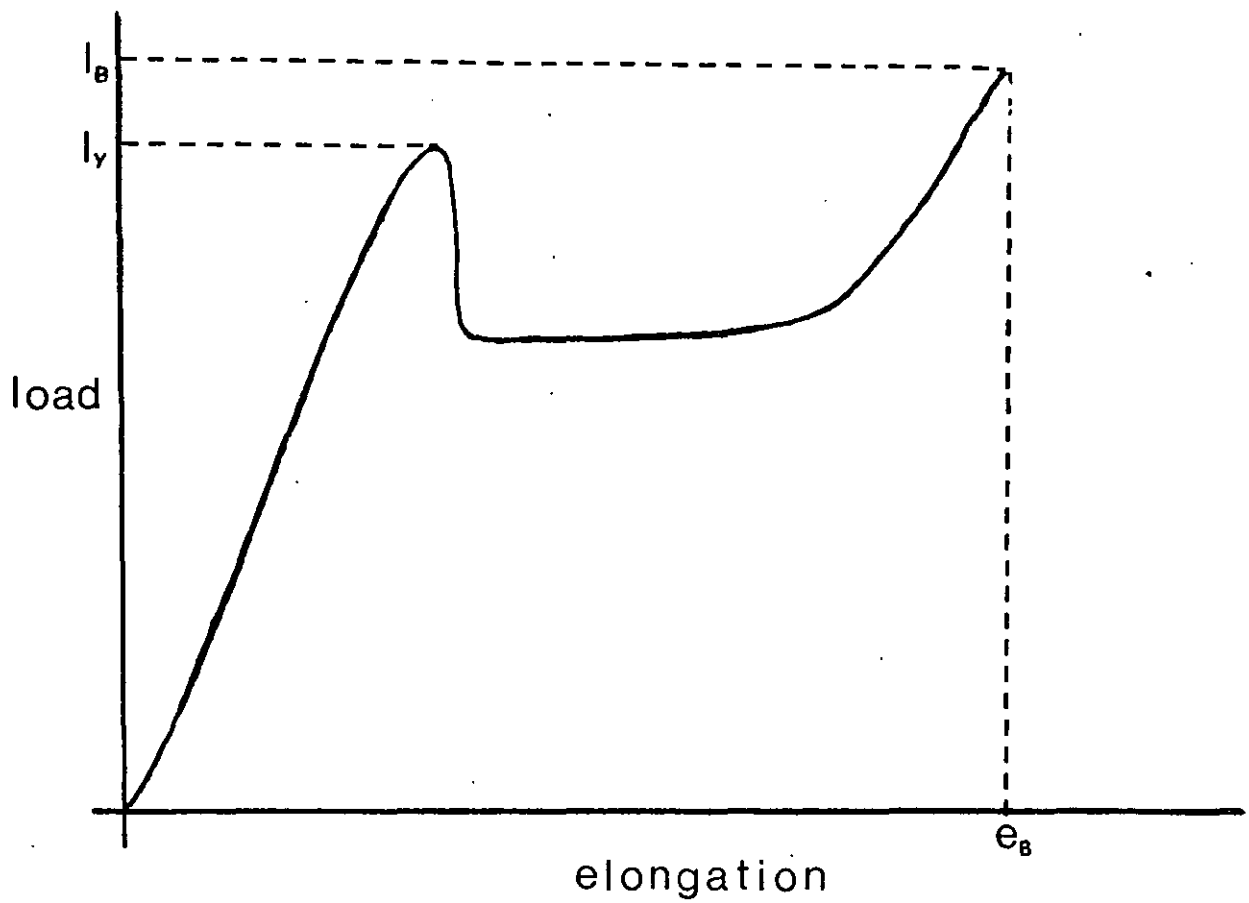

FIG 3-2

All testing was carried out at room temperature, samples being kept dry in a desiccator prior to testing since moisture has been found to have a detrimental effect on impact strength in PET[3].

3.2.5. Melt Rheology of Blends

The melt rheology characteristics of the blends were investigated using a Weissenberg Rheogoniometer, operating in a forced oscillation mode. Suitable disc specimens were prepared by pressing the polymer between aluminium foil on a hot plate, and after quenching the foil was stripped off. A description of the parameters measured is given later in the section on results (p. 62)

3.2.6. Nature of Dispersions

Information on the physical nature of the dispersions was obtained by optical and electron microscopy. Two modes of sample preparation were used for optical microscopy:

i. Observation of thin films prepared by pressing small quantities of blend between glass coverslips heated to 280 - 300°C on a hot plate and quenching to room temperature.

ii. Microtomy to prepare thin sections ($\sim 10\mu$) which were viewed immersed in a liquid medium of the same refractive index as the major phase (oil of Cassia R.I. 1.60 was used for PET).

In certain cases a more detailed study of dispersions was carried out using electron microscopy.

Samples were sectioned using an ultra-microtome and examined in a transmission electron microscope (Phillips E.M. 300).

Injection moulded specimens were subjected to fracture at liquid nitrogen temperature and the fracture surfaces examined with a scanning electron microscope (Cambridge Stereoscan Mark II).

3.3. Results:- Ethylene-vinylacetate/PET Blends

3.3.1. Ethylene-vinylacetate Copolymers (E-VA)

E-VA copolymers are produced commercially using a free radical high pressure polymerisation process similar to that used in the production of low density polyethylene. The radical polymerisation of ethylene with vinyl acetate represents the rare incidence of ideal copolymerisation, i.e. the rate constants K, of the four possible growth steps of the copolymer are approximately equal. This means that during copolymerisation the ratio between monomer ethylene and monomer vinyl acetate is equal throughout the reaction, and equal to that existing in the copolymer in the process of formation. This ideal case permits the production of uniform synthesised copolymers throughout the entire ethylene/vinyl acetate and associated melt index ranges.

The effect of including vinyl acetate in the polyethylene chain is to reduce molecular order and E-VA copolymers, therefore, become progressively less crystalline as the vinyl acetate content increases. In many respects their properties are those that would be expected of very low crystallinity polyethylenes.

a. Characterisation of E-VA copolymers

E-VA copolymers were obtained from ICI Plastics Division, and the range extended by three grades obtained from Du Pont UK. Table 3-1 lists the serial numbers, nominal VA contents and MFI of the range of copolymers used.

Serial Number	wt-% VA	MFI	Manufacturer
VJG 501	7.5	2.0	ICI
A9839	17.5	2.0	ICI
A13389	24.0	3.0	ICI
A13351	28.0	5.0	ICI
Elvax 150	32.0	25.0	Du Pont
Elvax 260	26.0	20.0	Du Pont
Elvax 40	40.0	55.0	Du Pont

Table 3-1

b. Determination of Vinyl acetate Content

Before blend production the vinyl acetate content of the various grades of E-VA copolymers was determined.

A 10 lb batch of each E-VA was obtained and all work carried out using the same batch. Prior to characterisation a portion of the polymer was milled at 100°C to obtain an homogeneous sample from which specimens for infrared investigation were then prepared by compression moulding plaques between Melinex film. Using a Grubb Parsons spectrometer with a lithium fluoride prism, the optical density per m.m. of the carbonyl overtone band at 2.2$\mu$was obtained for each grade of E-VA. The infrared spectrometer does not give absolute concentrations directly; a calibration must be performed by another method. This was achieved by calculating the comonomer content, in weight per cent, from the carbon analyses of samples for which the optical density of the 2.2μ band was known. The comonomer content was then plotted against the optical density to give a calibration curve (Fig. 3/4).

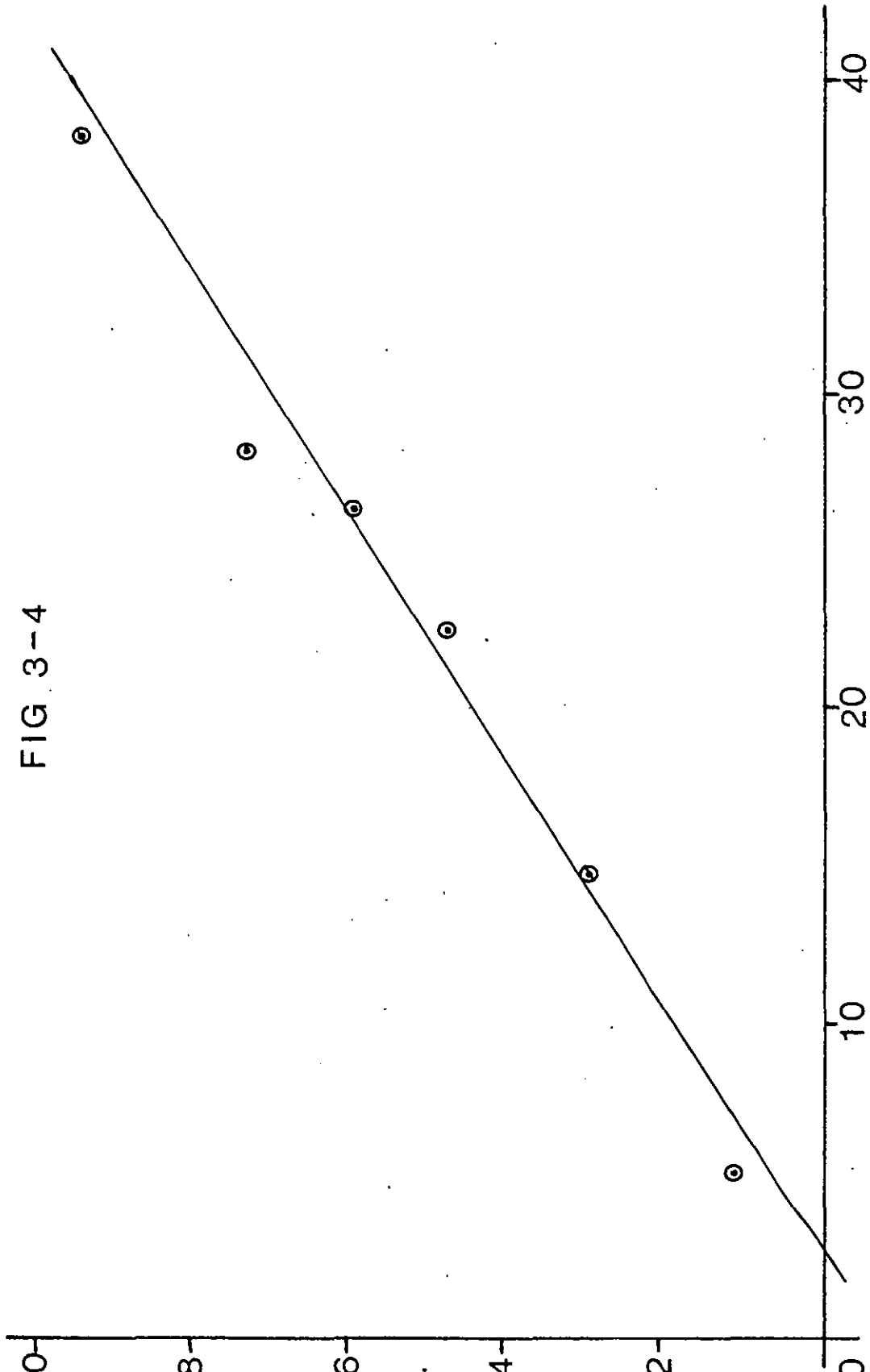

FIG 3-4

From this curve the vinyl acetate content of the particular batches of E-VA used in the ensuing experiments were obtained (Table 3-2).

Batch	VJG 501	A9839	A13389	A13351	Elvax 260	Elvax 40
wt% Vinyl Acetate	6	14	22	31	26	41

Table 3-2

c. Physical Properties of E-VA Copolymers

The effect of comonomer content on the properties of E-VA copolymers has been well studied[4,5]. Increasing vinyl acetate content reduced the crystallinity progressively until at loadings of 20 wt% and above the copolymer is completely amorphous. The decrease in crystallinity is reflected in a drop in breaking stress, yield stress and modulus. E-VA copolymers become 'tougher' as their vinyl acetate loading increases and the low temperature impact properties are outstanding at loadings of greater than 15 wt%. An important property of value when using E-VA copolymers in PET blends is the thermal stability at elevated temperatures. This has been shown to be adequate for a copolymer of 26 wt% vinyl acetate[6]. After 20 mins. heating under nitrogen at 270°C, 50g of "Elvax 260" gave 0.115g. of volatiles, which when titrated contained an equivalent of 0.031g. of acetic acid, i.e. less than 0.5% of the available acetic acid had been liberated.

3.3.2. Morphology of PET/E-VA Blends

Blends containing 5, 10 and 20 wt-% of E-VA in PET were prepared using a range of copolymers of vinyl acetate contents from 6 to 30 wt%. Blends containing 10 wt% and above showed evidence of delamination at the surface of injection moulded specimens for all the grades of E-VA used. Optical examination of thin sections of the mouldings showed that the rubber particles near the surface were elongated to form an almost continuous rubbery phase although, on hot pressing the section above 180°C between cover slips, the rubber phase relaxed the distortion and good spherical shaped particles were in the range of 1 to 20 μ in diameter.

3.3.3. Impact Strength of PET/E-VA Blends

Injection moulded impact specimens prepared from blends containing between 10 and 30 wt% of E-VA showed delamination at the surface. Crystalline specimens, prepared by using a mould held at 140°C, gave problems of 'flashing' i.e overfilling, interspersed with occasional underfilling, this latter phenomenon being characterised by sink marks in the mouldings. These problems were minimised by using a cold mould, when amorphous specimens were obtained. On subsequent crystallisation of the amorphous specimens by heating to 140°C, the surfaces tended to 'blister' and the sample distorted due to delamination at the specimen surface. Because of these problems encountered in obtaining impact specimens, the impact strengths of blends in the 10 to 30 wt% E-VA concentrations were extremely scattered. However, blends containing 5 wt% of E-VA produced much better mouldings and a plot of notched impact strength versus vinyl acetate concentration for crystalline samples is shown

in Fig. 3/3. Each point represents the arithmetic mean of 20 determinations, and though the increase in impact strength is undramatic it can be seen that an increase in the vinyl acetate concentration in the copolymer gives some improvement.

3.3.4. Phase Separation

Phase separation of the blends was carried out by extracting the granulated extrudates with cold o-chlorophenol. The E-VA was insoluble in this solvent and could be filtered from the PET solution. The polyester was then recovered by precipitation into hot, stirred toluene and further purified by repeated extractions with hot toluene to ensure complete removal of the ethylene copolymer. Infrared examination confirmed that this treatment removed all the ethylene copolymer, and that no reaction (e.g. ester interchange) between the two phases has occurred during the blending process. Solution viscosities carried out on phase-separated PET showed that the copolymer had little effect on the PET during processing; only the normal fall in I.V. (0.62 - 0.55) occurred, a fall which invariably accompanies melt processing of PET.

3.3.5. Bulk Polymer Modification by Grafting

a. Endcapping PET with Stearic Anhydride

From the results obtained it is obvious that no ester interchange (graft) reaction had occurred between the dispersed rubber and the PET matrix. In an effort to improve the adhesion between the two phases, a third component was added to the mix which could possibly provide a tie molecule between the rubber particles and the matrix.

Stearic anhydride was used to react with the hydroxyl ends of the PET chains. It was hoped that the long chain fatty acid portion that had been attached to the PET chain would be compatible with the E-VA and act as a link molecule between the two phases in the blend. The end capping of PET with stearic anhydride may be represented as:

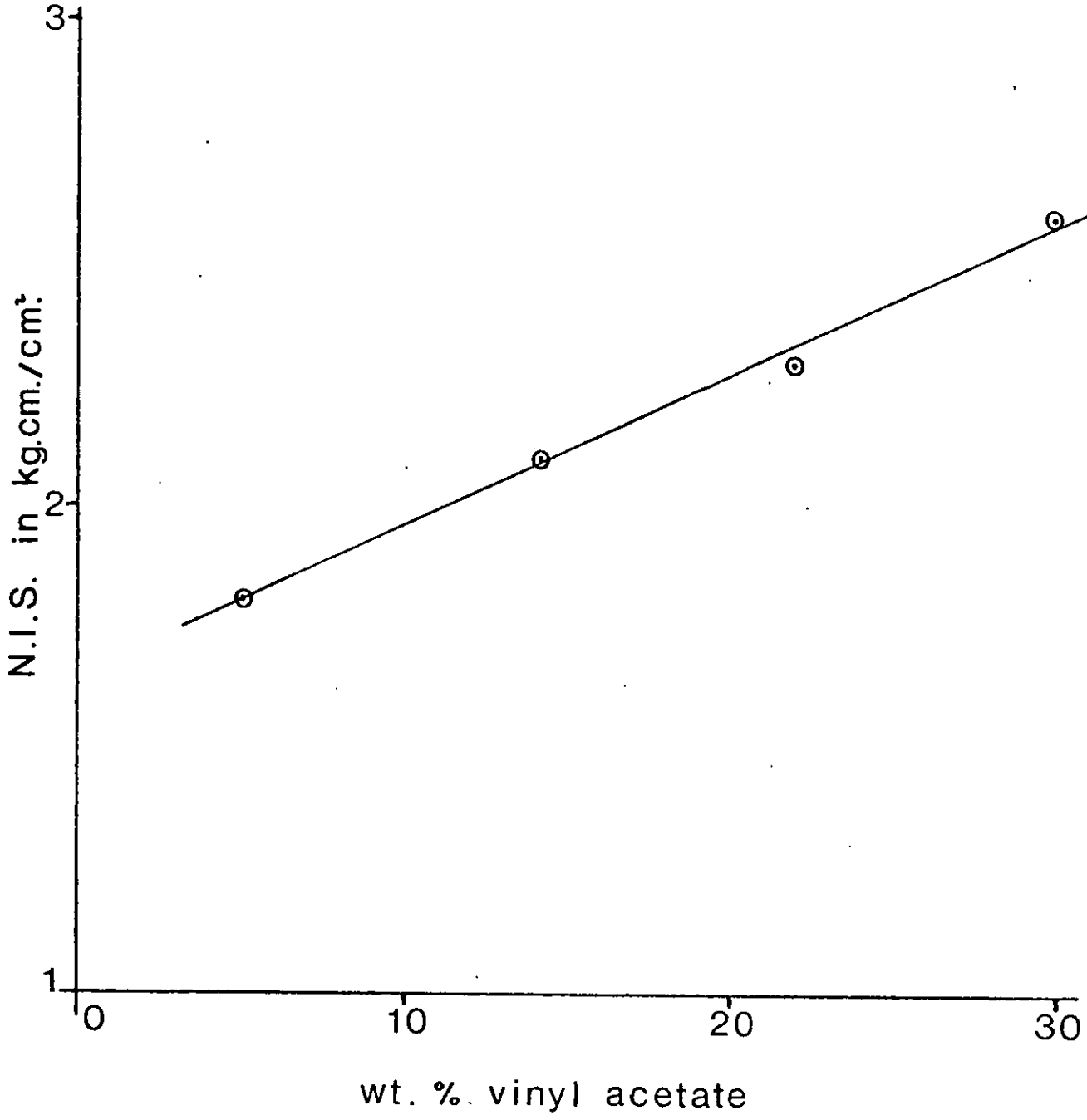

FIG 3-3

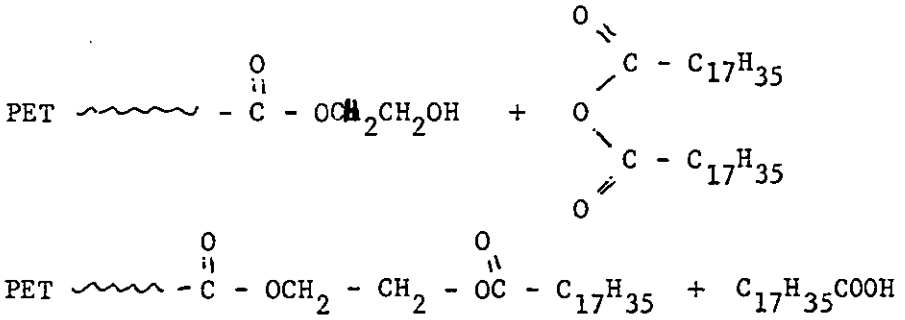

The reaction was effected in themelt during extrusion of PET chip which had been tumble blended with 3 wt% of stearic anhydride. A portion of the extrudate was dissolved in o-chlorophenol and the PET recovered by precipitation into a stirred ethanol/water mixture, and further purified by repeated extraction with ethanol to ensure complete romoval of the stearic acid.

A small amount of the extruded PET was dissolved in arsenic trichloride prior to investigation using a 'Varian 220' NMR machine. In addition to proton resonances associated with PET there was a small band at 8.77γ which is the chemical shift with reference to tetramethyl silane consistent with long chain methylene protons of the stearic residue ($-C_{17}H_{35}$), and also a small line at 7.7γ consistent with $CH_3(CH_2)_{15}\ \underline{CH_2}C{=}O$. This evidence would suggest that the PET had reacted with the stearic anhydride during the extrusion.

Blends were therefore produced containing 5 wt% E-VA, 90 wt% PET and 5 wt% stearic anhydride. All specimens made from these blends were found to be brittle, their impact strengths being lower than fibre grade PET although solution viscometry showed that the I.V. of the PET had not dropped more than normal in the processing, the mouldings were found to contain numerous small voids, presumably caused by the excess stearic anhydride or liberated stearic acid during injection moulding.

b. Addition of a Surface Active Agent

A slightly different approach adopted to improve the adhesion between the two phases was to add a surface active agent. A known surfactant for PET is

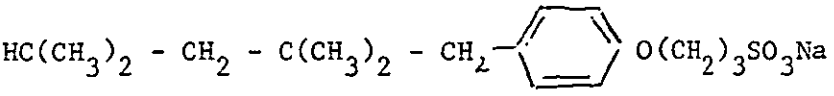

It was possible that the non polar end of the molecule would be compatible with the E-VA and the polar end would be compatible with the PET. The surfactant would in this case form a coating around the dispersed E-VA that would be compatible with the PET. Blends were produced containing 5 wt% E-VA, 90 wt% PET and 5 wt% surfactant. The mouldings were again found to be very brittle and solution viscometry on a PET extract showed that in this case there had been a large drop in I.V. during processing (from 0.65 to 0.4). The surfactant appears to have increased the degradation of the PET during the melt processing.

To overcome the effects of degradation a masterbatch technique was employed in the production of the blends. A blend of composition 30 wt% E-VA, 60 wt% PET and 10 wt% of surfactant was prepared by melt extrusion. The extrudate was granulated, dried, and tumble mixed with more PET such that the final mixture contained 5 wt% E-VA.

The mixture was then re-extruded to produce the final blend. The I.V. of the PET matrix after these processing steps was found to be 0.55.

Using this technique to blend in 5 wt% of an E-VA copolymer containing 30 wt% of vinyl acetate (Elvax 150), a crystalline blend with a notched impact strength of 2.7 Kgcm/cm^2 was obtained. Thus, use of the surfactant did not produce blends of greater impact strength than these made by blending only E-VA into PET.

3.3.6. Discussion

From the results obtained it is apparent that melt blending PET with minor amounts of E-VA copolymers does not produce any marked improvement in impact strength. For blends of 5 wt% of copolymer it is possible to demonstrate that the slight improvement obtained in the impact strength is dependent on the vinyl acetate loading[4,5] in the copolymer, and is probably due to the increased impact strength of the rubbery phase.

It had been hoped that the pendant ester groups in the E-VA would provide sites where ester interchange (graft) reactions between the rubber and the PET might occur. In the event, conditions required to promote the reaction were not found.

Since the desired grafting could not be achieved by direct reaction of these rubbery copolymers with PET, alternative approaches were made involving tie molecules produced by endcapping PET with stearic anhydride, and also by use of a PET surfactant. In both these cases no improvement in the impact strength was obtained. The stearic anhydride successfully endcapped the PET, but a by-product of the reaction i.e. stearic acid, caused excessive voiding in the final mouldings. These voids act as efficient stress concentration centres during the impact tests with consequent reduction in impact strength of these blends. Extraction of the stearic acid residue may have solved the problem. However, at all times in this work attention was paid to the commercial feasibility of processes involved. It was considered that an extraction step in the process could not be financially justified, therefore, further investigations into this line of approach were not carried out.

Addition of a surfactant did not cause voiding problems, but brought about the thermal degradation of the PET matrix to such an extent that the blend became extremely brittle. Whilst by using a masterbatch technique it was possible to obtain a blend which contained surfactant, and had an I.V. of 0.55. This showed no improvement over the equivalent blend without surfactant.

At loadings of greater than 10 wt% of E-VA, the injection mouldings showed severe delamination at the surface. This was shown to be due to distortion of the rubber particles in the shear stress fields set up during moulding.

In no cases did the fracture surfaces of blends reveal that there had been large scale crazing. The samples did not craze, and no evidence of crazing was seen in thin sections of samples that had been stressed below yield.

Since the results with E-VA copolymers were not encouraging, it was decided to investigate incorporation of Surlyn A ionomer since elastomeric copolymers of this type contain free carboxylate ions in the melt and should be more likely to undergo interchange reactions with the PET under processing conditions.

3.4. Results:- Surlyn A/PET Blends (PET Major Phase)

3.4.1. Surlyn A Ionomer

a. Structure

Surlyn A is a commercial polymer manufactured by Du Pont. It is the most common example of the class of polymers known as "Ionomers".

The ionomers are ionically cross-linked copolymers, Surlyn A being an ionomer salt of an ethylene/methacrylic acid copolymer.

The unique spectrum of characteristics of ionomers is associated with the use of ionic forces as interchain links. These links strengthen, stiffen and toughen the polymer when compared with the equivalent ethylene/methacrylic acid copolymer, without destroying its melt processability. This is the most important distinction when compared with conventional cross-linked systems. The conventional covalent cross-links set up a permanent three dimensional polymer network which prevents melt flow. The ionic linkages on the other hand disassociate and become more diffuse as the temperature is raised, permitting processing by conventional thermoplastic techniques.

The preparation of ionically cross-linked copolymers is essentially a two stage process. In the manufacture, the first stage is to produce a copolymer of ethylene and methacrylic acid by conventional free radical copolymerisation, followed by conversion of the copolymer into an ionically cross-linked system. Introduction of ionic cross links is in principle simple. A calculated quantity of the ionising species, in this case the sodium ion, is added to the matrix by addition of sodium hydroxide (or sodium methoxide) to the copolymer melt with removal of the by-product, water (or methanol). Only a limited number of ionic cross-links may be built into the macromolecular chains before brittleness, reduction in melt processibility, and water sensitivity increase beyond acceptable limits.

The physical structure of ionomers has been investigated in detail[7,8,9]. Studies based mainly on X-ray diffraction and dynamic mechanical properties suggest that in the ionomers crystalline polyethylene regions are interspersed with complex amorphous areas. These consist of polyolefine branches, hydrogen bonded carboxyl groups, and ionised carboxyl units grouped in the vicinity of regularly spaced clusters of metal

ions approximately 100 Å in diameter. Different polymeric chains may share common ionic domains in which, except for different spacing arrangement, two monovalent ions may give rise to configurations similar to one divalent ion. The metal ions are not permanently associated with any particular carboxyl group and can be redistributed by heat and shear. The effect of addition of water is to solvate the ions and to increase their miscibility, leading to the disappearance of the ordered ionic domains at high water concentrations. Schematic structures of the parent copolymer and the dry and wet ionomers are shown in Fig. 3/5.

The proposed model suggests that factors such as the COO^- to COOH ratio and/or the spacing of the ionised carboxyl groups relative to metallic ions are primarily responsible for the special features of the ionomers[8].

Surlyn A was chosen as a possible modifying rubber for PET for the following reasons:

i. It is thermally stable at PET processing temperatures.

ii. It is tough at very low temperatures and high strain rates.

iii. It has a melt viscosity similar to PET at 270°C a feature which aids dispersion.

iv. It has available active pendant COO^- groups which may graft into the PET chain by interchange, or provide adhesion by being partially soluble in the PET melt.

v. It is commercially available at moderate cost.

b. Characterisation of Surlyn A

A grade of Surlyn A suitable for moulding MFI 10.0 was obtained from Du Pont (UK) Ltd. The same batch was used in all the investigations. Prior to use the ionomer was characterised with respect to its co-unit concentration and sodium ion concentration.

FIG 3-5

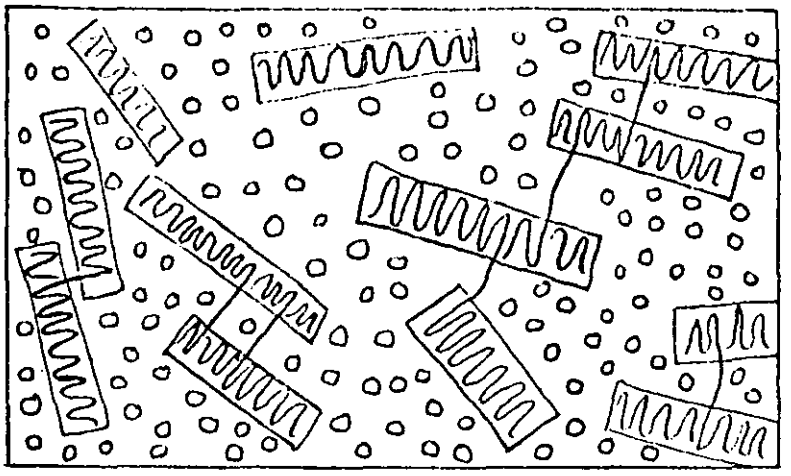

(a) E/MAA copolymer

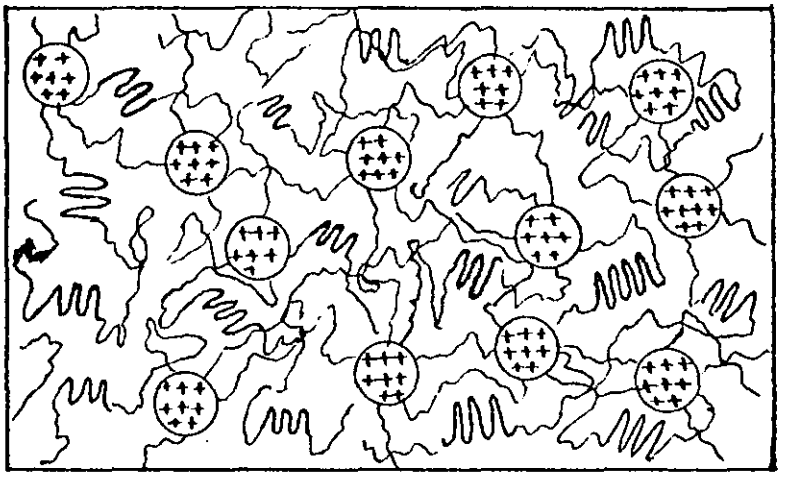

(b) dry ionomer

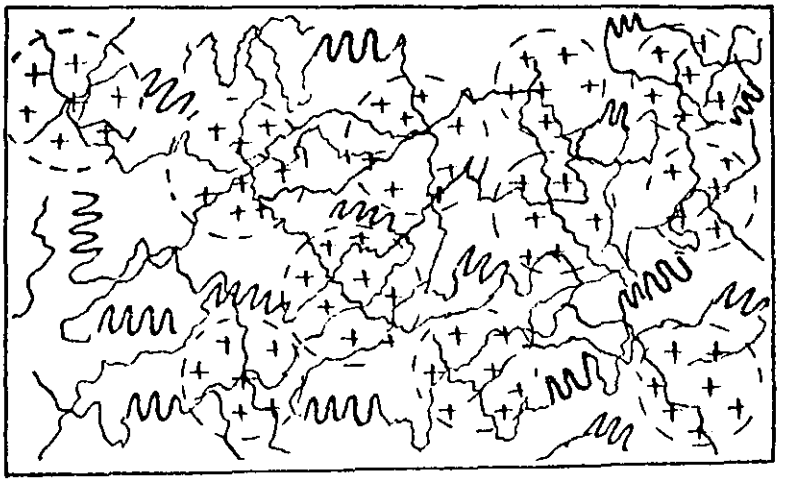

(c) wet ionomer

c. Infrared Analysis of Surlyn A

Infrared spectroscopy was used for the determination of the comonomer content and the percentage ionisation of the Surlyn A. The ratio of the optical densities of the tail of the acid -OH stretch band at 2500 cm^{-1} to the $-CH_2$ combination band at 2020 cm^{-1} was used in the analysis.

A calibration was carried out by calculating from the carbon analyses the methacrylic acid content of a range of ethylene/methacrylic acid copolymers for which the optical density ratios had been previously measured. The comonomer concentration in wt% was then plotted against the band ratios to give a calibration curve Fig. 3/6.

A sample of the Surlyn A was then converted to its parent acid (see p. 67) and the IR spectrum of a pressed film run. The optical densities of the bands at 2500 cm^{-1} and 2020 cm^{-1} were 0.531 and 0.077 respectively, giving a ratio of 6.90. From the calibration curve this ratio corresponds to a comonomer concentration of 9.25 wt%.

The IR spectrum of the Surlyn A was then run. The 2500/2020 band ratio was found to be 2.97 corresponding to a methacrylic acid content of 4 wt%. The remainder i.e. 5.25 wt% being the ionised species. The Surlyn A was then shown to be an ethylene-methacrylic acid copolymer containing 9 wt% methacrylic acid, ~58% of which had been neutralised to the sodium salt.

3.4.2. Moulding Behaviour of Blends

Blends containing 5, 10, 20 and 30 wt% of Surlyn A in PET were prepared by melt extrusion, and amorphous injection moulded specimens produced. It was clear that the blends containing Surlyn A showed much less delamination in the mouldings than in the equivalent E-VA blends.

FIG 3-6

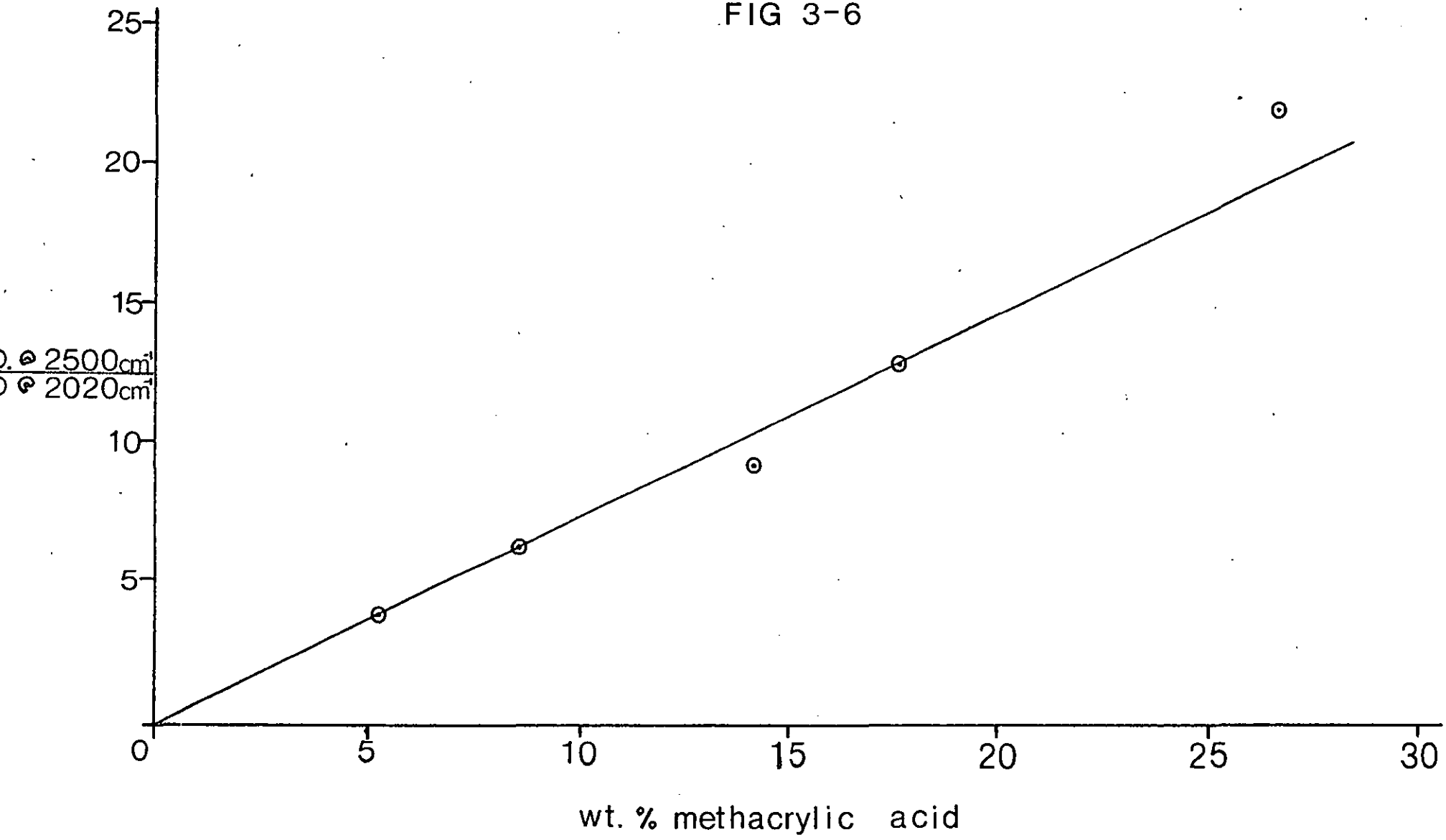

At loadings of 5 wt% and 10 wt% good moulded specimens were produced with an excellent surface, whilst the 20 and 30 wt% loadings showed some signs of delamination, though not as severe as with the E-VA blends of equivalent rubber contents.

3.4.3. Nature of Dispersions

The particle size and distribution of the Surlyn A in a 10 wt% blend were studied using electron microscopy. The electron densities of the two phases were sufficiently different to enable them to be seen without using selective staining techniques. From Fig. 3/7 a transmission electron micrograph of the blend, the Surlyn A particles are seen to be in the range 0.1 - 2 μ in diameter, and are oval in shape after having been distorted during the moulding. The dispersion was thought to be adequate for blended systems.

3.4.4. Physical Testing

a. Tensile Tests

Plots of the initial modulus and yield stress for both crystalline and amorphous blends as a function of rubber content and reproduced in Figure 3/8. As expected the modulus and yield stress decrease with increasing rubber content.

b. Impact Strength

A plot of impact strength versus Surlyn A content for crystalline and amorphous blends is reproduced in Fig. 3/9. There is a noticeable increase in the notched impact strength with increasing rubber content, though little advantage is gained by using loadings of greater than 10 wt%. This may well be due to the inferior mouldings obtained at high rubber contents associated with surface delamination. Solution viscometry on extracted PET showed that the I.V. was in the vicinity of 0.55 i.e. the Surlyn A had not adversely affected the PET during thermal processing.

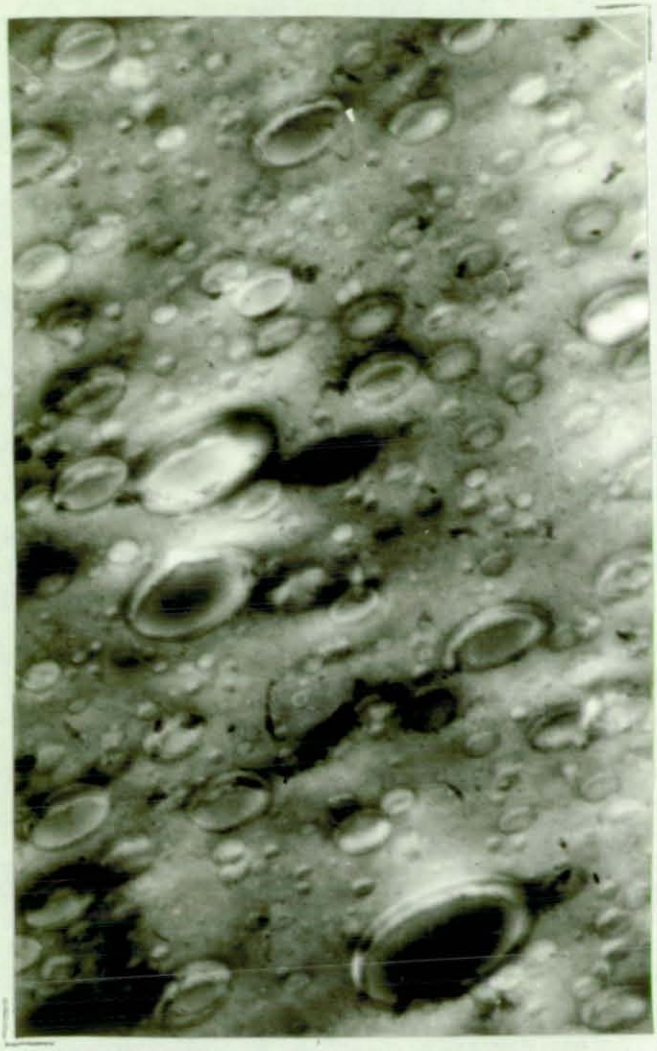

20% SA in PET Mag. 7K

FIG. 3-7

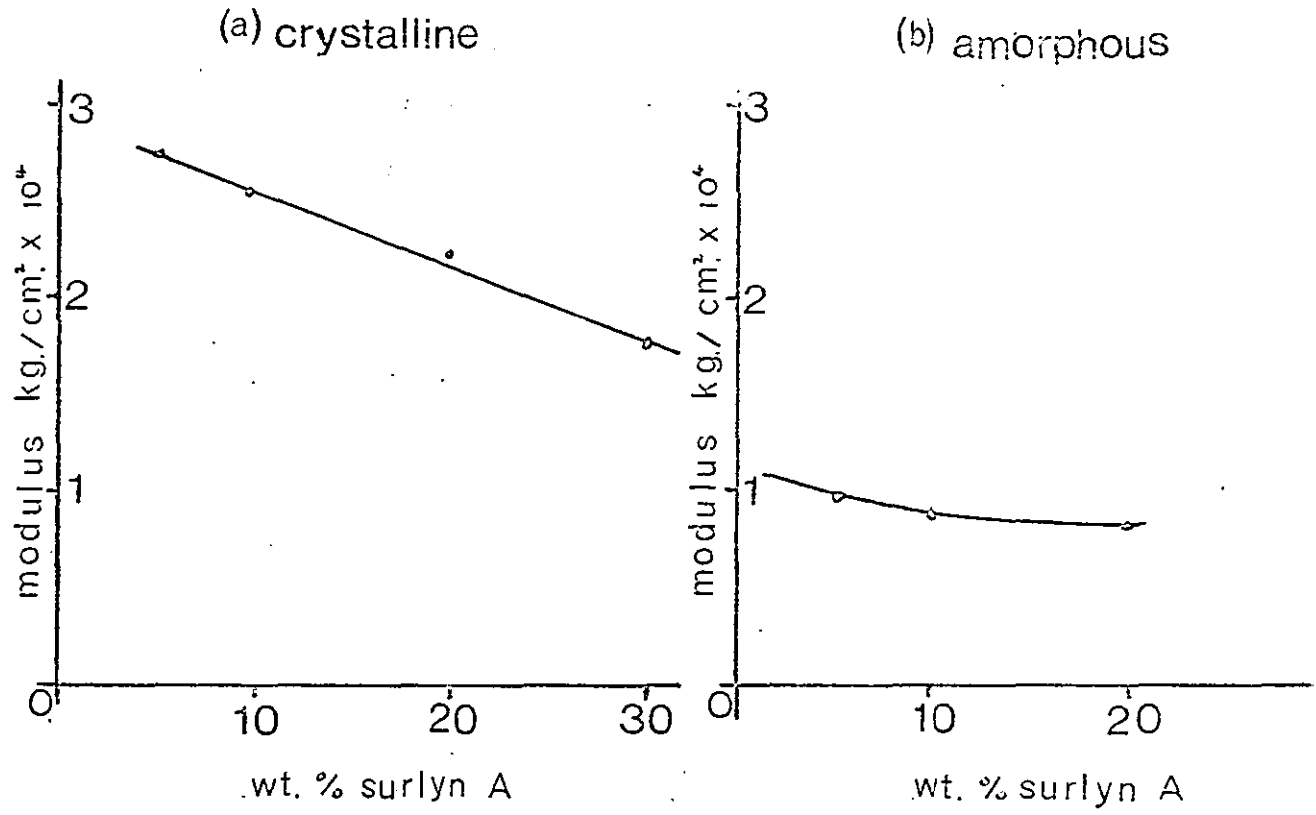
(a) crystalline
modulus kg./cm². x 10⁴
3
2
1
0
10
20
30
wt. % surlyn A
(b) amorphous
modulus kg./ cm². x 10⁴
3
2
1
0
10
20
wt. % surlyn A

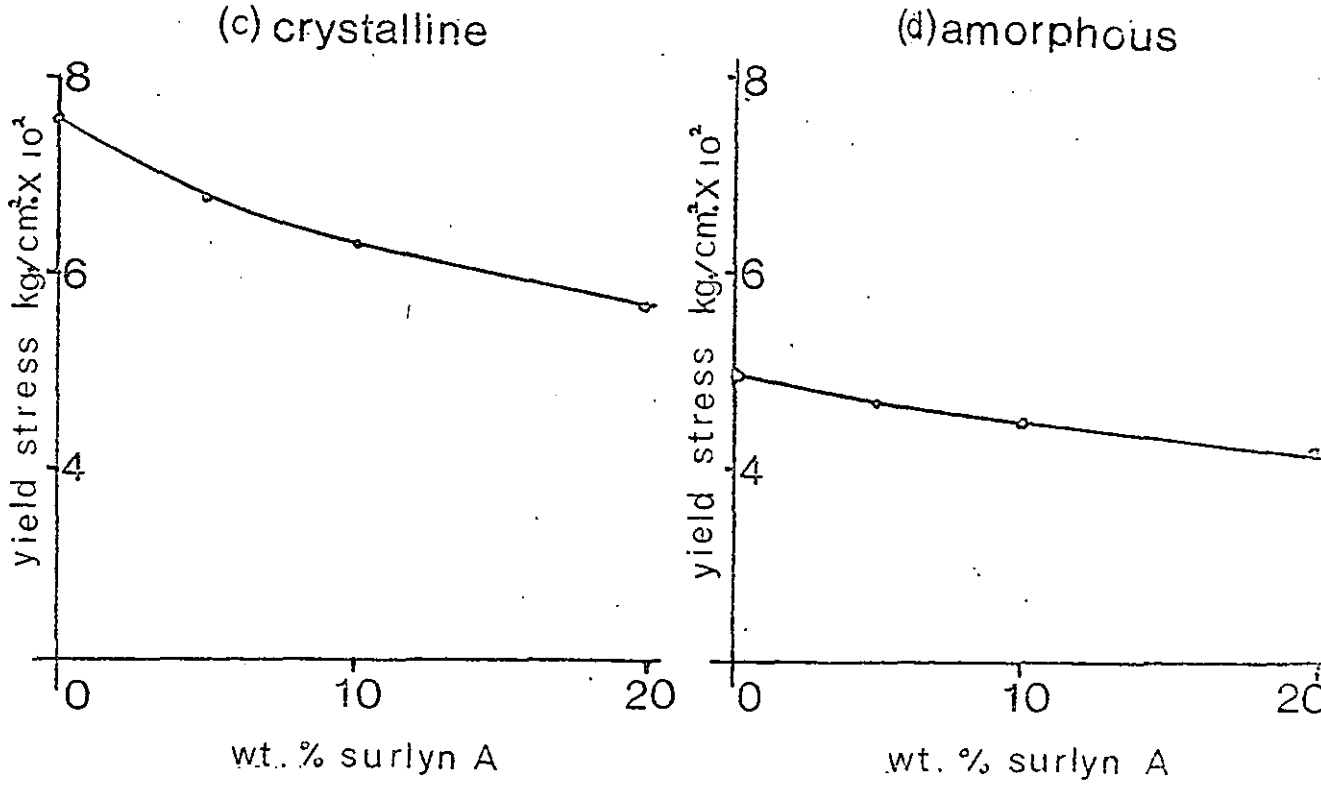
(c) crystalline
yield stress kg/cm².X 10²
8
6
4
0
10
20
wt. % surlyn A
(d)amorphous
yield stress kg/cm².X 10²
8
6
4
0
10
20
wt. % surlyn A

FIG 3-8

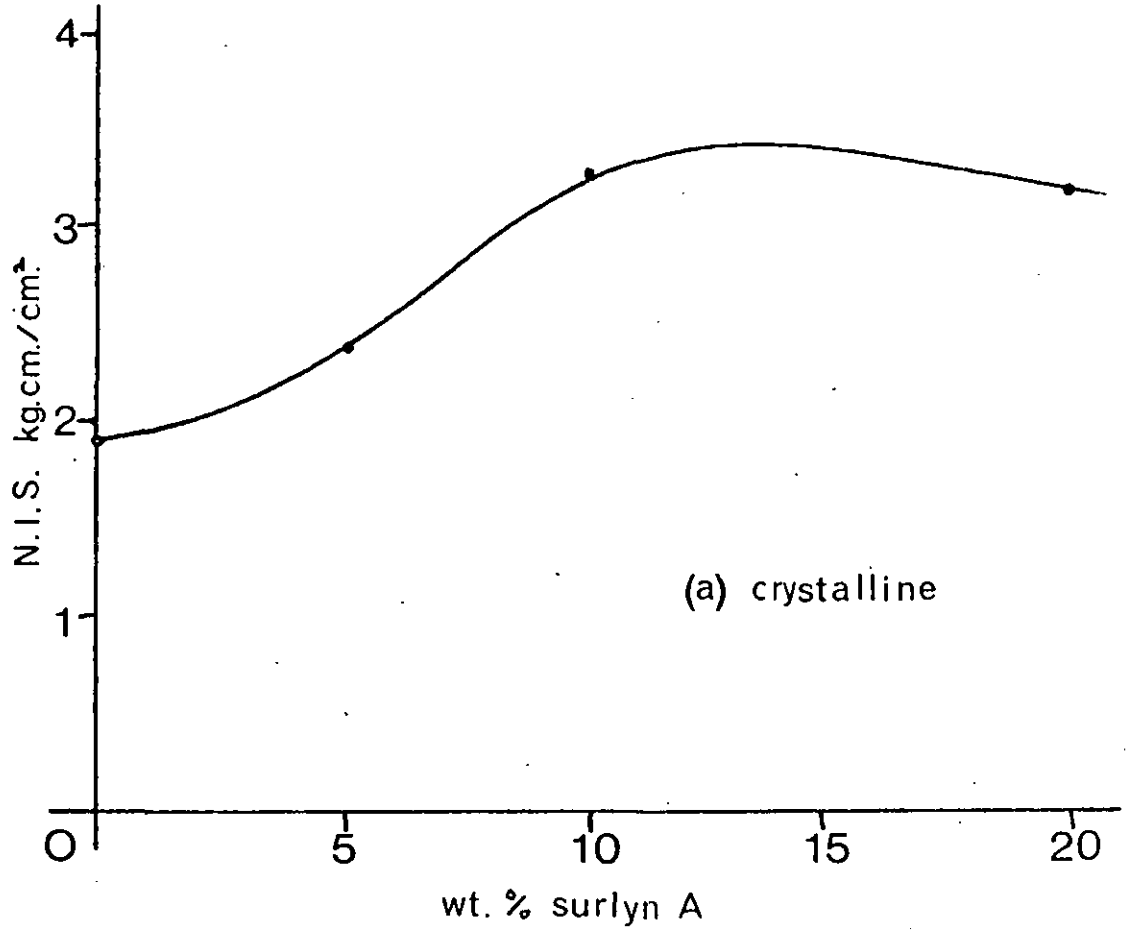
4
3
2
1
N.I.S. kg.cm./cm²
(a) crystalline
0
5
10
15
20
wt. % surlyn A

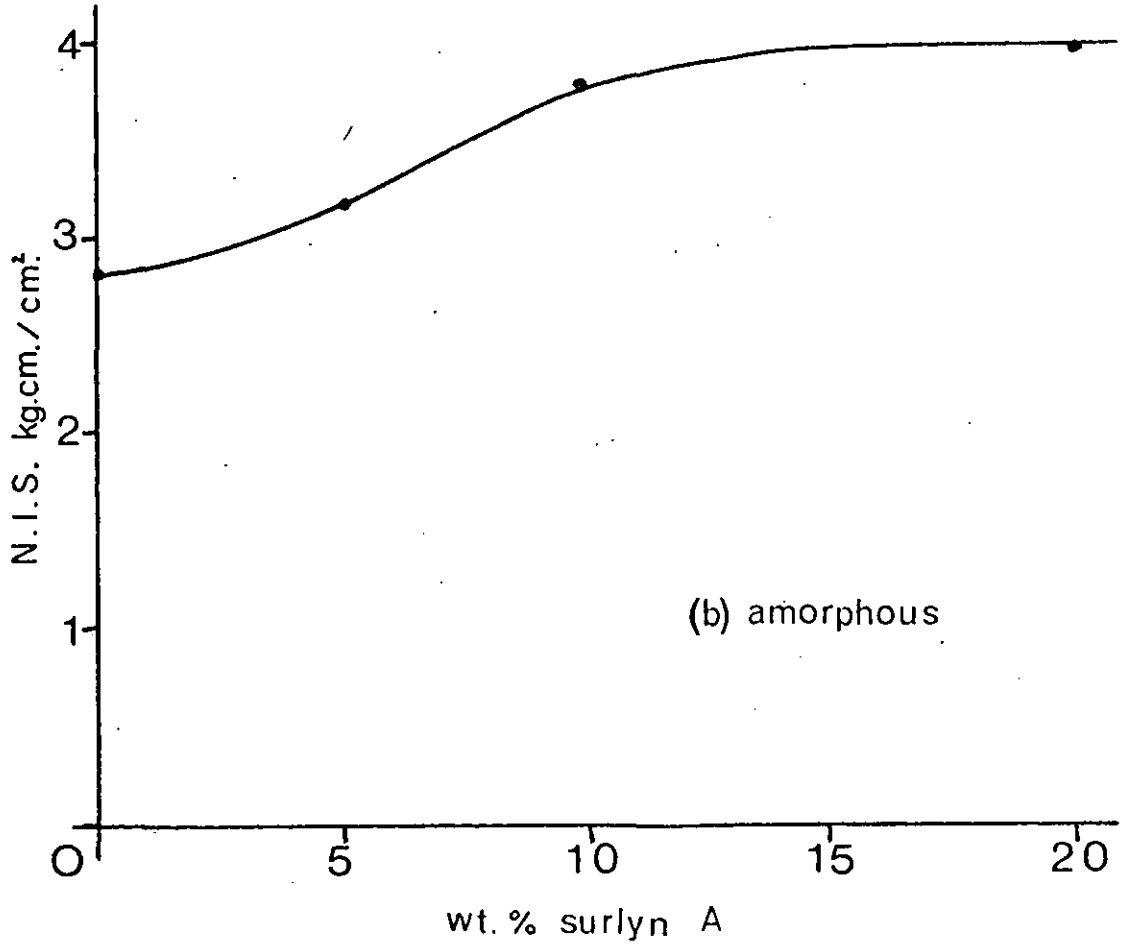
4
3
2
1
N.I.S. kg.cm./cm²
(b) amorphous
0
5
10
15
20
wt. % surlyn A

FIG 3-9

3.4.5. Phase Separation

Phase separation of PET/Surlyn A blends proved to be more difficult than with the PET/E-VA blends. After dissolving the PET in o-chlorophenol and filtering off the undissolved Surlyn A, the remaining solution was found to contain a fine suspension of rubber particles of $\sim 1\mu$ in diameter. Attempts were made to separate out this suspension by centrifuging and subsequent filtration through a microporous filter. After this treatment the PET was reprecipitated in acidic benzene, and the precipitate repeatedly extracted with benzene to remove any remaining Surlyn A. Subsequent IR investigation did not give evidence of a graft reaction having taken place.

3.4.6. Discussion of Physical Properties

PET blends containing Surlyn A ionomer showed slightly improved impact characteristics compared with the E-VA blends. However, Surlyn A proved to be more easily dispersed than the E-VA, and higher quality mouldings were produced, particularly at the higher loadings.

The marginally improved impact characteristics were achieved at the expense of the modulus and yield stress, making the blend uninteresting from a commercial viewpoint. Examination of the fracture surfaces of impact specimens did not reveal any large scale plastic deformation processes to have taken place during the fracture, as is observed in ABS polymer blends.

There would appear to be little or no grafting between the two phases, and experiments in which thin sections were stretched under a microscope showed that the matrix/rubber bond failed at low strains.

The results of the experiments on PET blended with ethylene copolymer were disappointing and this particular approach would have been abandoned but for some unexpected observations concerning the melt viscosity of the Surlyn A/PET blends.

3.4.7. Melt Rheology of PET/Surlyn A Blends

During the course of melt extrusion blending of Surlyn A with PET using a die with a large hold-up volume, the die became blocked. This indicated that the viscosity of the blend held in the die head had increased dramatically eventually blocking the extruder and this effect was investigated in detail using a Weissenberg Rheogoniometer.

a. Parameters Measured

When a linear viscoelastic body is subjected to a stress varying sinusoidally with time, its mechanical behaviour at a single frequency must be specified by two independent quantities. These may be chosen in various ways.

The stress, which for viscoelastic materials is out of phase with the strain, may be separated into two components, one in phase and the other 90° out of phase with the strain. For deformation in shear the component in phase divided by the strain is the real part of the complex modulus of rigidity G'; the out of phase stress component divided by the strain is the imaginary part G". The moduli G' and G" may be added vectorially on a complex plane to give $G^* = G' + iG''$. The absolute modulus $|G^*| = \sqrt{(G')^2 + (G'')^2}$ is the ratio of the peak stress to peak strain. The phase angle between the strain and the stress is defined as χ. The two independant quantities used to specify the dynamic behaviour may be chosen as $|G^*|$ and χ instead of G' and G". For a single cycle of deformation at a given

amplitude the energy stored and recovered (i.e. elastic part) in each cycle is proportional to G' and the energy dissipated (i.e. viscous part) is proportional to G".

An alternative analysis is to separate the stress into two components, one in phase and the other 90° out of phase with the rate of strain. These stress components each divided by the rate of strain give the real and imaginary parts of a complex viscosity $\eta^* = \eta' - i\eta''$.

These quantities are related by the equations

$G'' = \omega \eta'$ and $G' = \omega \eta''$ where ω is the frequency.

The Weissenberg Rheogoniometer provides the means of measuring the peak stress and strain together with the phase angle as a function of temperature and frequency.

Therefore, from these parameters G' and G", η' and η'' may be calculated as follows

$$G' = |G^*| \cos \chi \qquad G'' = |G^*| \sin \chi$$

$$\eta' = G''/\omega \qquad \eta'' = G'/\omega$$

The parameters chosen to characterise the PET/SA blends in this study were G' and G".

b. Variation of Melt Viscosity with Time

The investigations were carried out on blends made by a single melt extrusion of a mixture prepared by tumble blending ~~dry~~ of dry PET and Surlyn A.

The extrudate was dried, granulated and then hot pressed at 270°C to obtain bubble free specimens suitable for investigation in the Weissenberg instrument. During sample preparation care was taken to ensure that the polymers were in the melt state for a minimum period of time consistant with reasonable dispersion of the two components. It was estimated that the blend had been 2 - 4 minutes in the melt at a temperature not greater than 270°C.

The Weissenberg Rheogoniometer was used in the oscillatory mode. With this mode of operation the real and imaginary parts of the complex shear modulus can be obtained. The real part G', is the in phase component associated with the elastic (reversibly stored) work. The imaginary part G" is the 90^{o} out of phase component associated with the viscous (irreversibly dissipated) work.

Before investigation of the blends the viscosity versus time behaviour of the two separate components, Surlyn A and PET was obtained. The results are shown in Fig. 3/10 for a temperature of $270^{o}C$ and shear rate of 15.7 rads/sec. It is clear that the complex modulus is independent of time for both components. They behave as typical viscous fluids, G" being greater than G' (i.e. phase angle $>45^{o}$)..

A 20 wt% blend of Surlyn A with PET exhibits very different behaviour Fig. 3/10. Both G' and G" increase in magnitude whilst the blend is in its molten state, the value of G' and G" attaining their maximum value after $\sim$50 minutes. It is also clear that G' has increased at a greater rate than G" and consequently during the experiment the phase angle ($\tan^{-1}\frac{G"}{G'}$) has decreased indicating that the melt has become more elastic in its nature.

c. Effect of Surlyn A Concentration

Runs were performed using blends containing 10, 20 and 30 wt% of Surlyn A. Care was taken to ensure that each blend had the same thermal history and mechanical work prior to the investigation. The results are shown in Fig. 3/11. The graphs show that the maximum obtainable value G' and G" is a function of the Surlyn A content but has little effect upon the rate of increase. Consequently a longer time is required to reach equilibrium for the higher Surlyn A loadings.

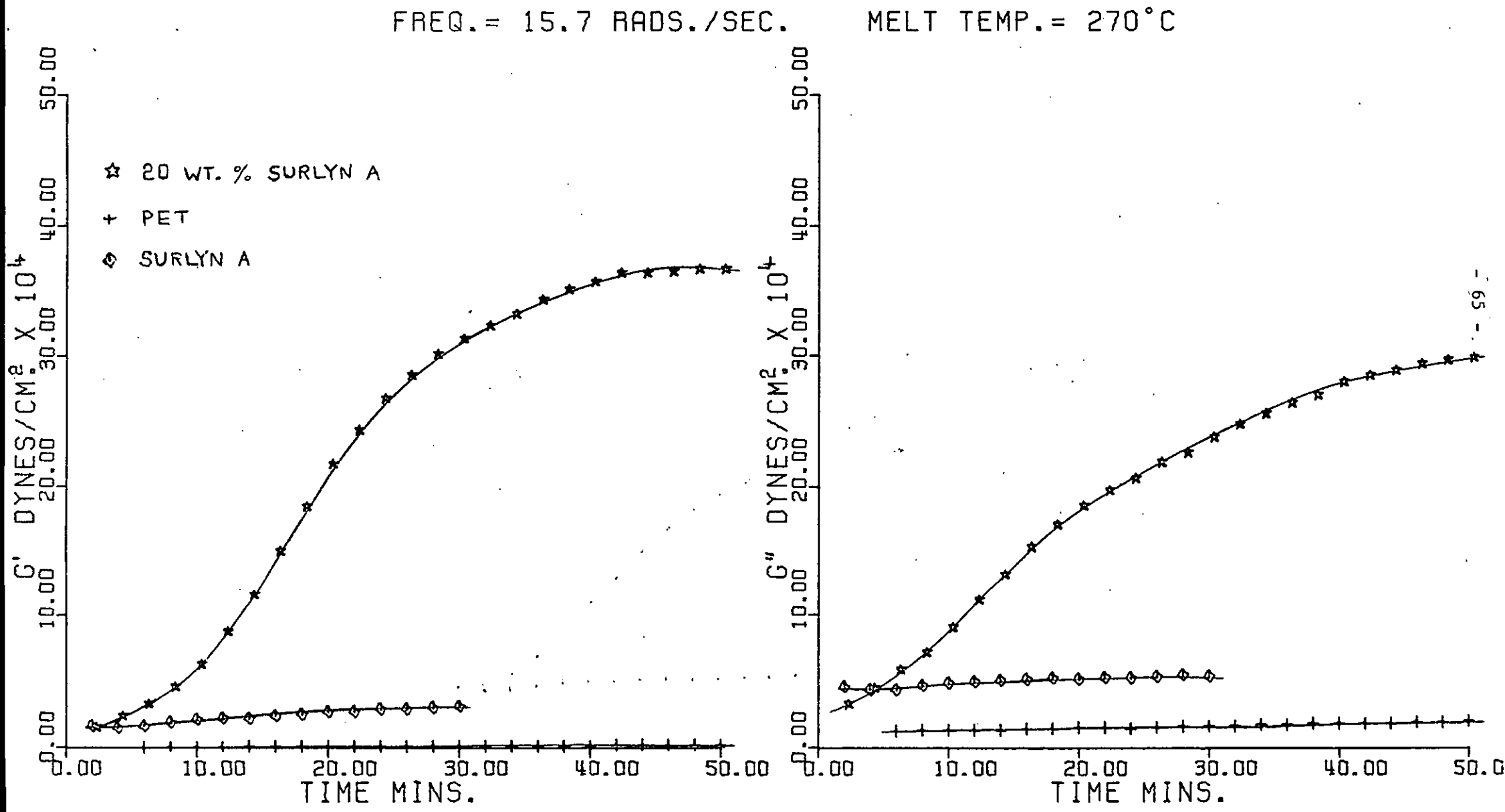
FREQ.= 15.7 RADS./SEC.
MELT TEMP.= 270°C
20 WT. % SURLYN A
PET
SURLYN A
G' DYNES/CM.² X 10⁴
G'' DYNES/CM.² X 10⁴
0.00
10.00
20.00
30.00
40.00
50.00
TIME MINS.

FIG 3-10

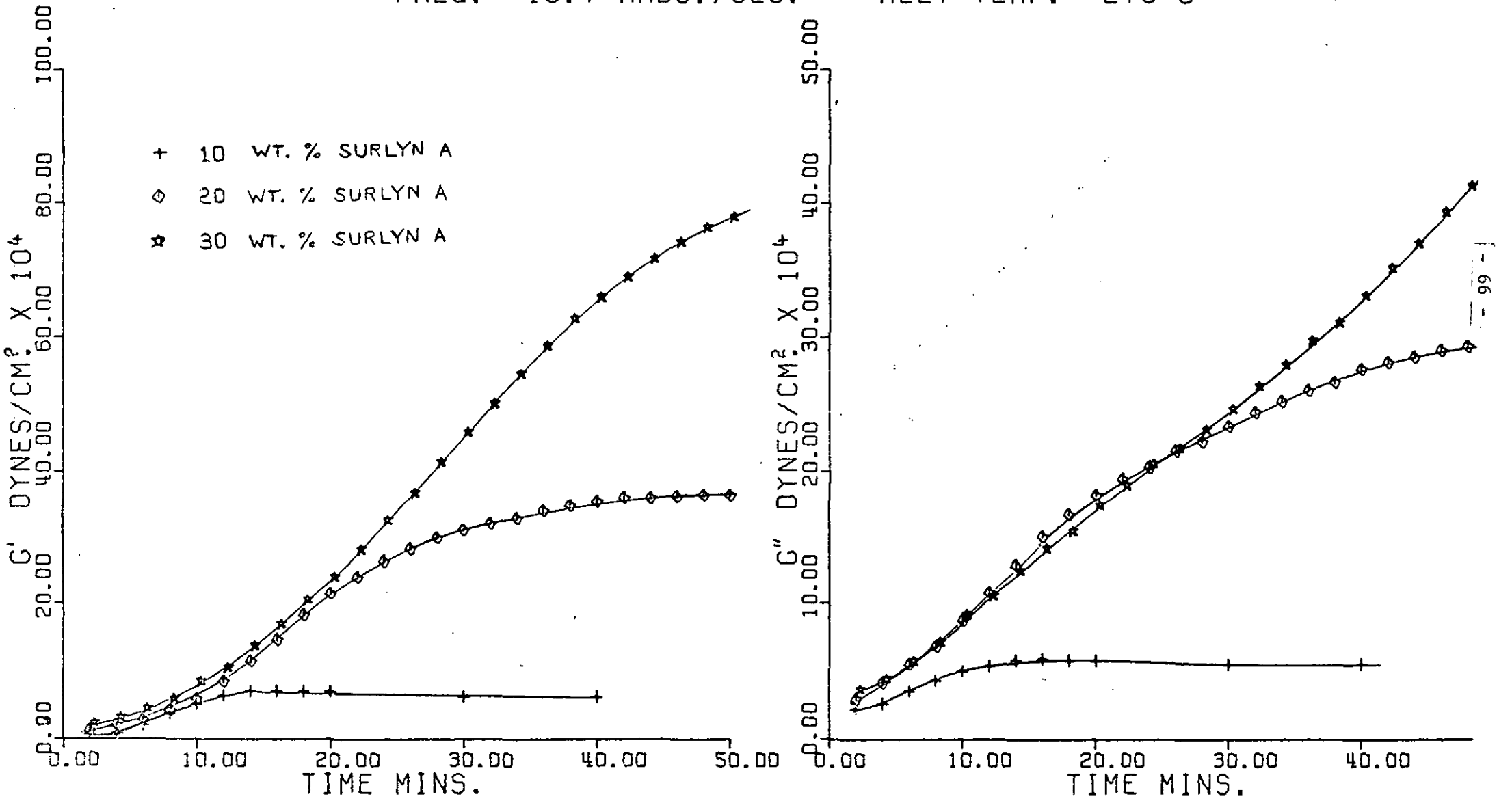
FREQ.= 15.7 RADS./SEC.
MELT TEMP.= 270°C
+ 10 WT. % SURLYN A
◇ 20 WT. % SURLYN A
☆ 30 WT. % SURLYN A
G' DYNES/CM.² X 10⁴
G'' DYNES/CM.² X 10⁴
TIME MINS.
TIME MINS.
0.00
10.00
20.00
30.00
40.00
50.00
60.00
80.00
100.00

FIG 3-11

d. Shear Rate Dependence

The separate components Surlyn A and PET exhibit behaviour deviating little from that of a classical Newtonian fluid, over the range of shear rates used (0.5→157 rads/sec). The shear rate dependence of a blend after reaching equilibrium is however highly non Newtonian. It exhibits thixotropic (shear thinning) behaviour Fig. 3/12. Increasing the shear rate also increases the phase angle indicating that the elastic property of the melt is reduced under the action of shear.

e. Effect of Melt Temperature

The viscosity/time plot for a 30 wt% Surlyn A blend at three melt temperatures is shown in Fig. 3/13. The effect of increasing the melt temperature is to increase the rate of the reaction, in the latter stages G' and G" are observed to decrease, particularly at 290°. This is almost certainly due to the thermal degradation of the PET which becomes important at temperatures in excess of 280°C[10]. The observed rate at 290°C is therefore likely to have an appreciable negative contribution from the degradation.

f. Effect of Sodium Ion on Melt Properties

The importance of the sodium ion on the melt rheology behaviour was investigated by making a blend of PET with poly(ethylene/methacrylic acid) which had been prepared by acidification of Surlyn A.

Preparation of the poly/ethylene/methacrylic acid) from Surlyn A

5g of Surlyn A were refluxed in 250 mls of Benzene containing 10 mls of 1N ethanolic HCl until all the polymer was in solution.

FIG 3-12

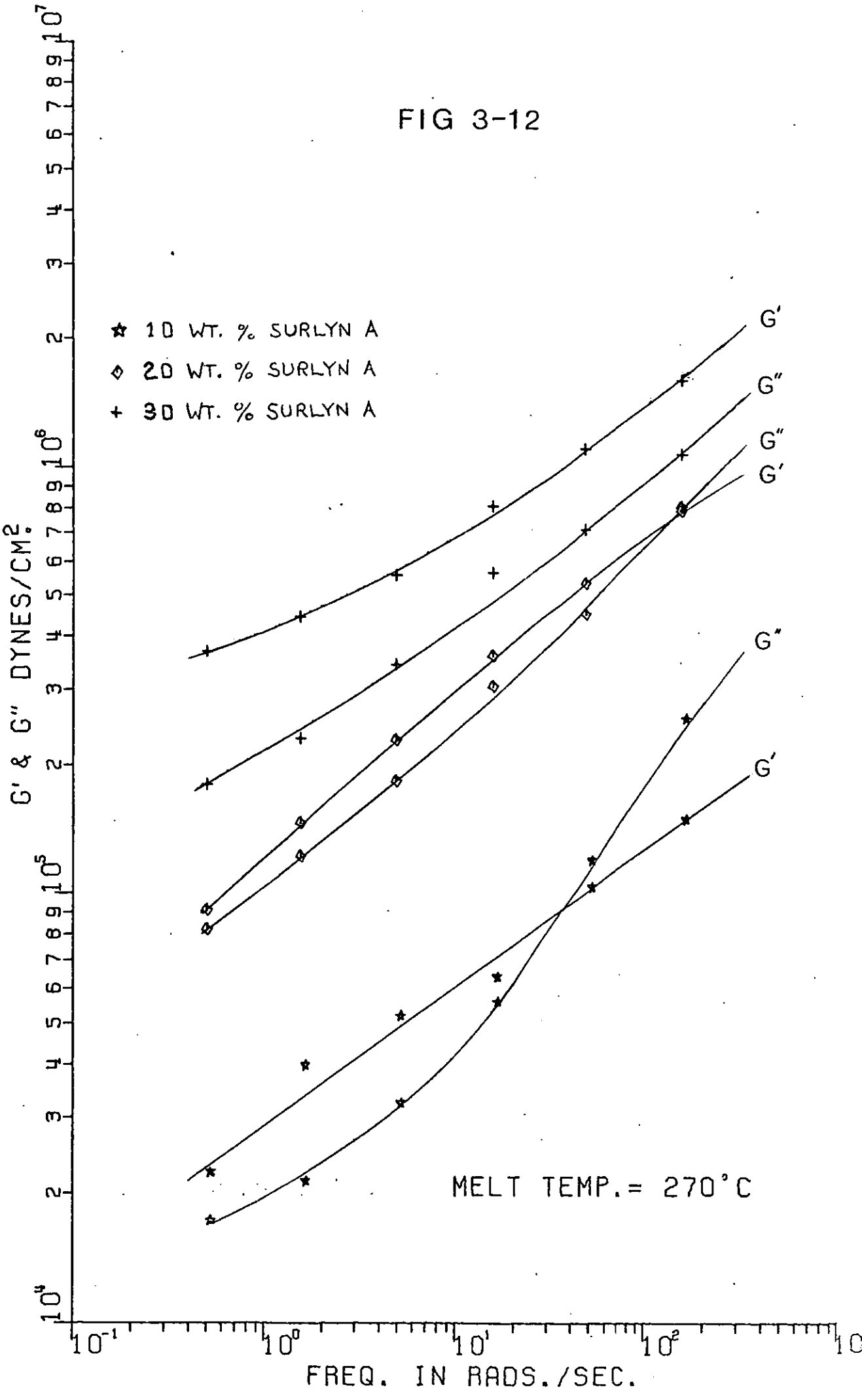
★ 10 WT. % SURLYN A
◇ 20 WT. % SURLYN A
+ 30 WT. % SURLYN A
G'
G"
G"
G'
G"
G'
MELT TEMP.= 270°C
G' & G" DYNES/CM²
FREQ. IN RADS./SEC.

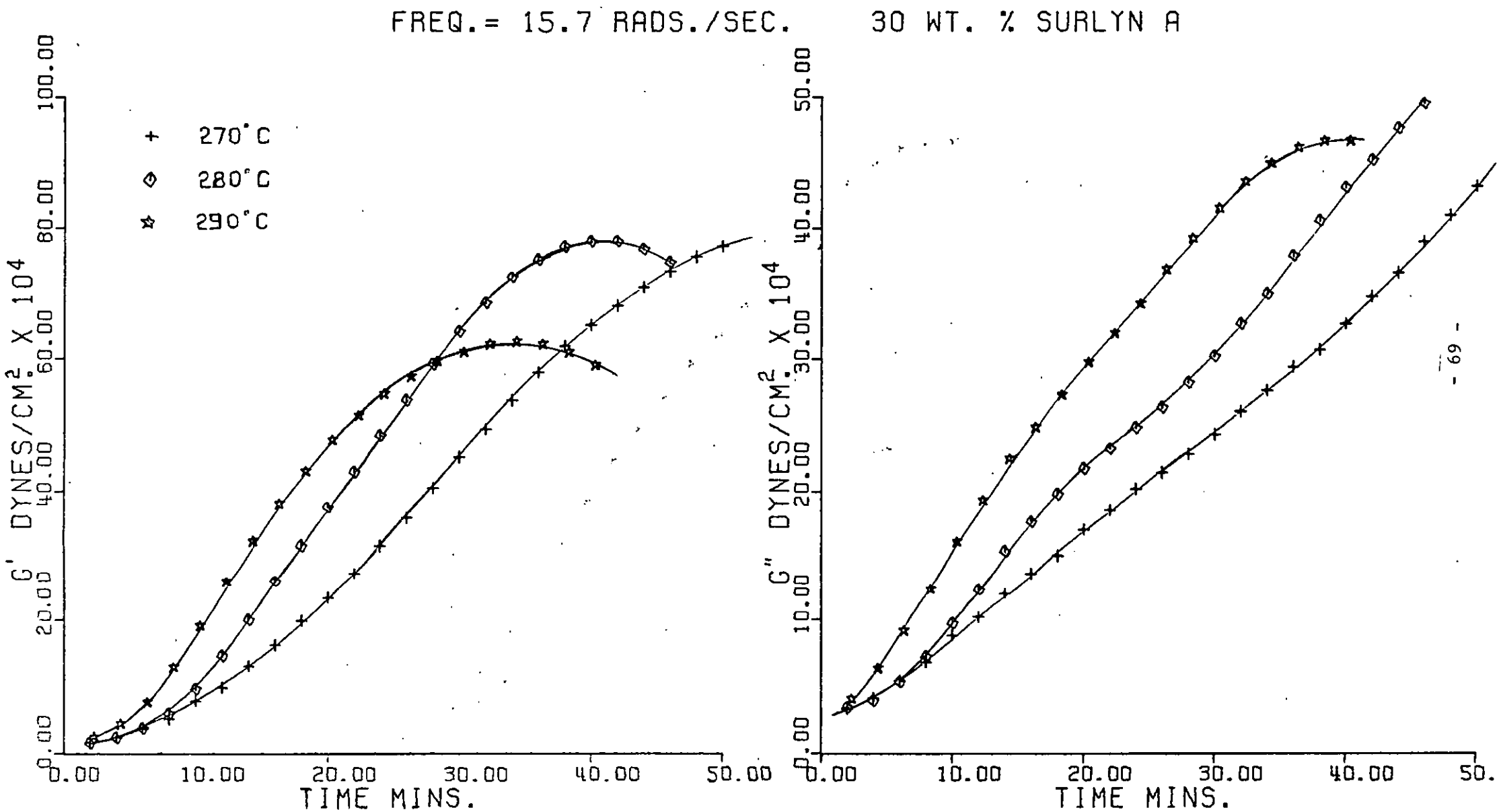
FREQ.= 15.7 RADS./SEC.
30 WT. % SURLYN A
270°C
280°C
290°C
G' DYNES/CM.² X 10⁴
G'' DYNES/CM.² X 10⁴
TIME MINS.
TIME MINS.
0.00
10.00
20.00
30.00
40.00
50.00
60.00
80.00
100.00

FIG 3-13

The polymer was then precipitated into $\frac{1}{10}$ N ethanolic HCl with brisk stirring. The precipitate was thoroughly washed in ethanol and dried under vacuum. The reaction was shown to have gone to completion by the disappearance of the carboxylate carbonyl absorption at 1550 cm^{-1} in the IR spectrum.

Melt Rheology

A blend containing 70 wt% PET and 30 wt% of ethylene methacrylic acid was prepared by melt mixing at 270°C. It was found that η' of the melt gave a value of 3000 poise at a shear rate of 15.7 rads/sec and melt temperature of 270°C. Both G' and η', were found to be independent of melt residence time.

The fact that the anomalous viscosity behaviour is only seen when the neutralised copolymer is used suggests that either the sodium cation or the carboxylate anion is the active species.

If the active species was the sodium cation the sodium salt of PET should show anomalous viscosity behaviour. To test this possibility the sodium salt of PET was prepared.

Preparation of the Sodium Salt of PET

The sodium salt of PET was prepared by addition of a measured excess of ethanolic sodium hydroxide to a solution of the polyester in o-cresol/chloroform, and potentiometric titration of the excess with standard ethanolic hydrochloric acid.

The titration shows two end points corresponding to the points of inflection A and B.

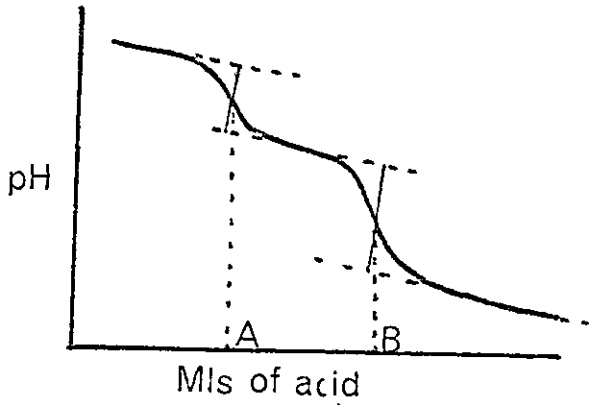

Therefore, by stopping the addition of acid at any point between A and B and precipitating the polymer by adding its solution to methanol/water an entire range of samples may be obtained from 100% neutralised (all the sodium salt) to 0% Neutralised (unreacted PET).

Samples were prepared that were 100%, 60%, 30% neutralised and the cresol extracted with chloroform, the samples then being held at 100°C under vac for 3 - 4 days and their rheological properties studied.

In all cases the sample was found to behave in the same way as fibre grade PET.

It was clear from this experiment that the abnormal behaviour seen in the blends was not due to the presence of sodium ions in the PET acting as ionic linking agents.

g. Infra-red Spectra Before and After Viscosity Change

Infra-red spectra of samples before and after investigation in the Wiessenberg were compared. No striking differences were seen between the two spectra, particular attention was paid to the absorbance at 1550 cm^{-1} associated with the carboxyl group - COO^{-}. This band was found to have the same optical density in both spectra. It would appear from the IR evidence that the viscosity change does not produce any noticeable effects of the infra-red spectra, and the reaction does not involve the production of an appreciable quantity of any new chemical species.

3.5. Results:- Surlyn A/PET Blends (Surlyn A Major Phase)

Blends containing 80 wt% of Surlyn A were prepared by melt extrusion at 270°C. These blends contain PET particles dispersed in the continuous Surlyn A matrix.

3.5.1. Melt Rheology

Fig. 3/14 shows the variation of G' and G" with time for a 80 wt% Surlyn A blend at two melt temperatures (270°C and 300°C). Both G' and G" increase with time in the melt in a similar fashion to that observed when PET was the major phase (cf. Fig. 3/11). Since in this case it is theproperties of the Surlyn A phase that are being measured, this being the continuous phase, presence of the dispersed PET particles is affecting the properties of the major Surlyn A phase. The reaction rate is again dependent on the melt temperature though in this case there is no evidence over the period of time measured to show any significant degradation reaction occurring.

3.5.2. Morphology of High Surlyn A Content Blends

Fig. 3/15a is a scanning electron micrograph of the low temperature fracture surface of an 80 wt% Surlyn A/PET blend obtained by melt extrusion (η' = 3000 poise). The PET can be seen to be present as approximately spherical particles in the region of 1μin diameter. It is clear from the photograph that there was very little adhesion between the two phases since the specimen has fracture preferentially at the interface between the two phases leaving holes where the PET particles were. After heating at 300°C for 30 minutes a very different type of low temperature fracture surface is obtained (Fig. 3/15b). In this case the adhesion between the two phases has been improved causing the crack to propagate through the dispersed phase in preference to separating at the interface. These photographs provide strong evidence that the higher thermal treatment has grafted the PET to the Surlyn A producing a strong bond at the interface.

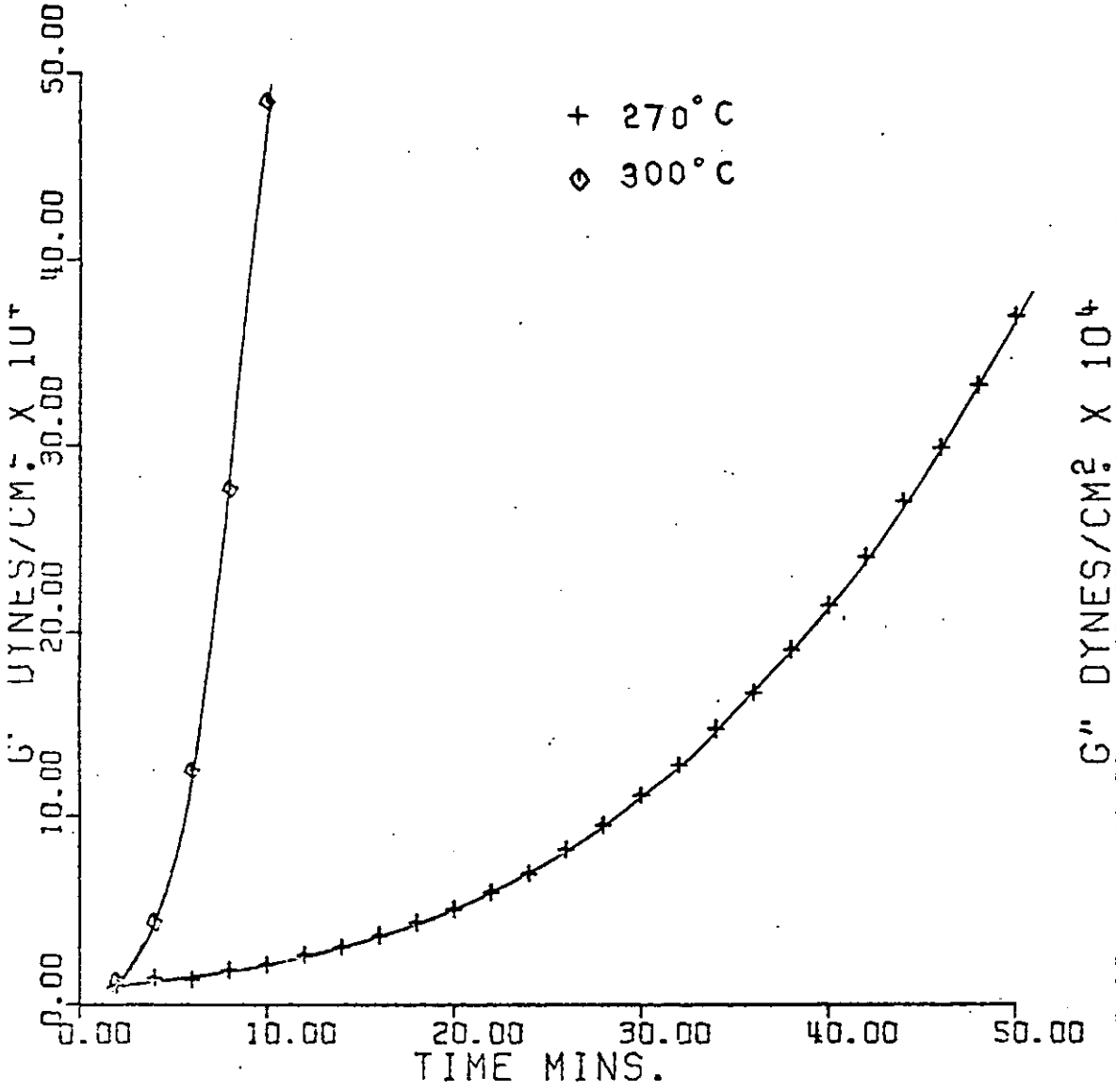
FREQ.= 15.7 RADS./SEC.
80 WT. % SURLYN A
+ 270°C
◇ 300°C
G' DYNES/CM². X 10⁴
50.00
40.00
30.00
20.00
10.00
0.00
0.00
10.00
20.00
30.00
40.00
50.00
TIME MINS.

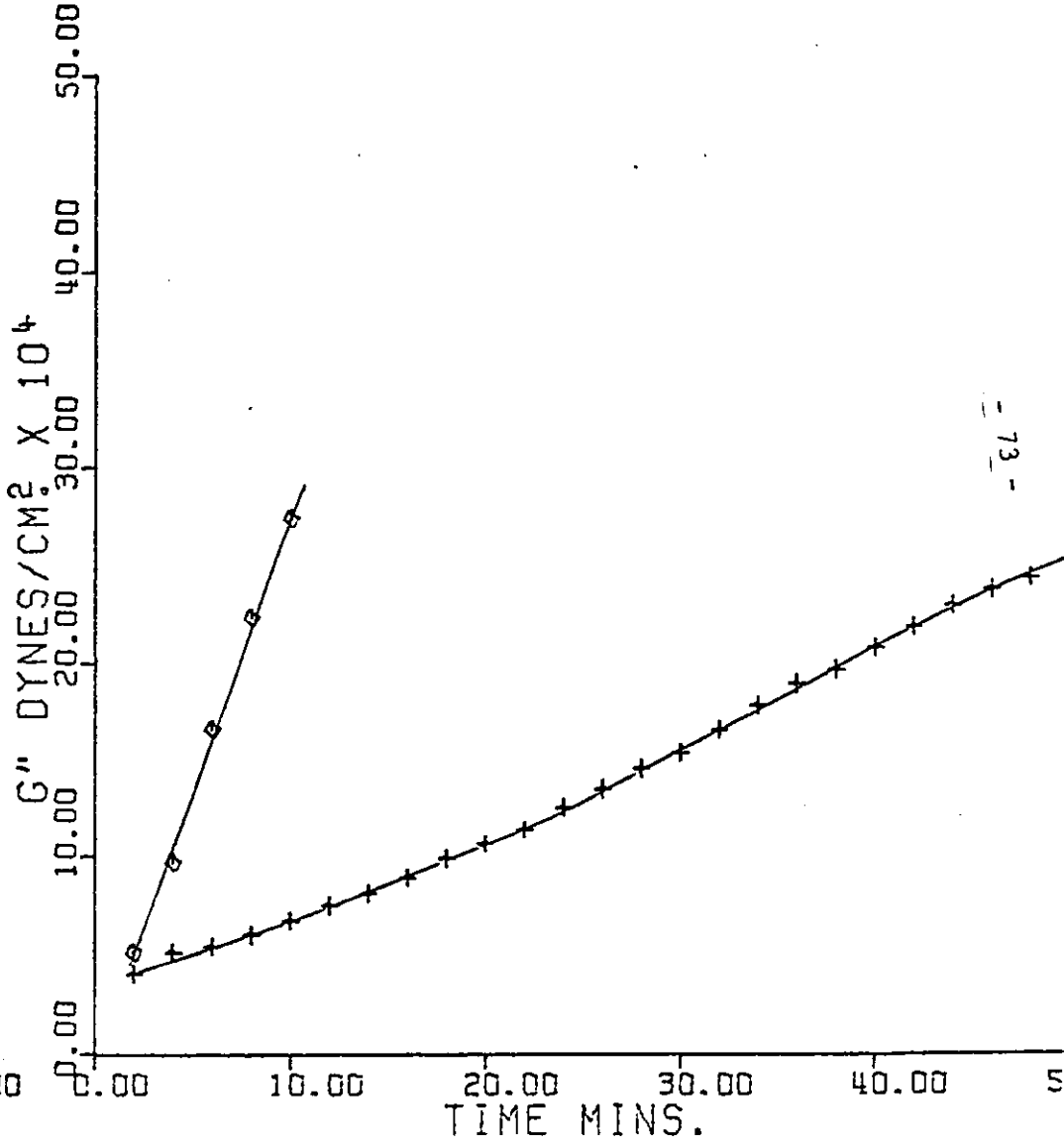
G'' DYNES/CM². X 10⁴
50.00
40.00
30.00
20.00
10.00
0.00
0.00
10.00
20.00
30.00
40.00
TIME MINS.

FIG 3-14

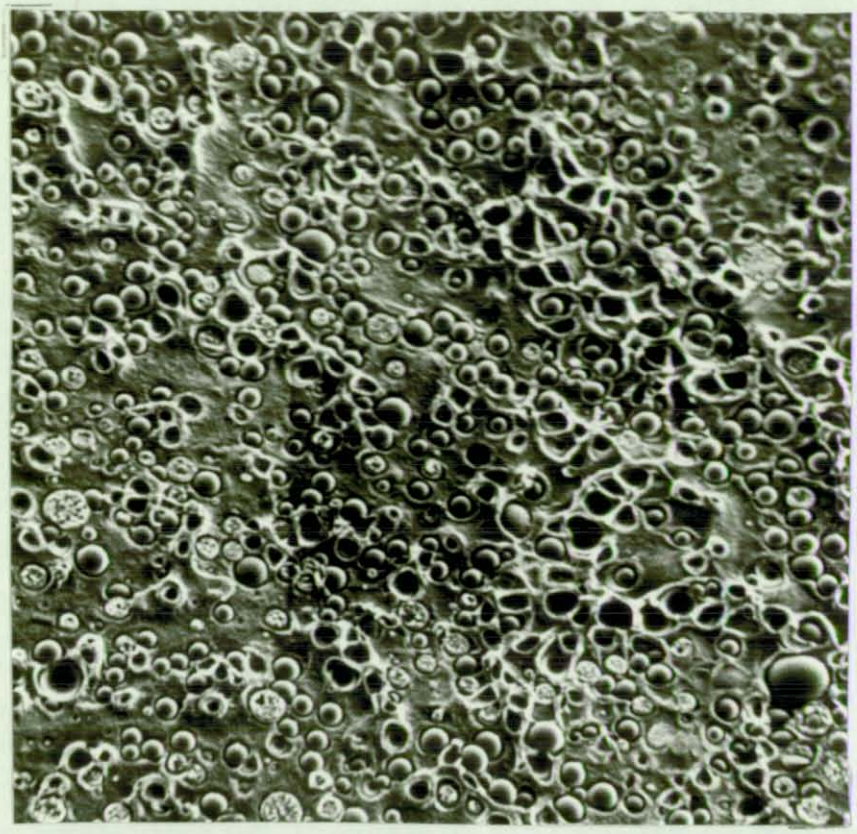

(a) Mag 1·6K

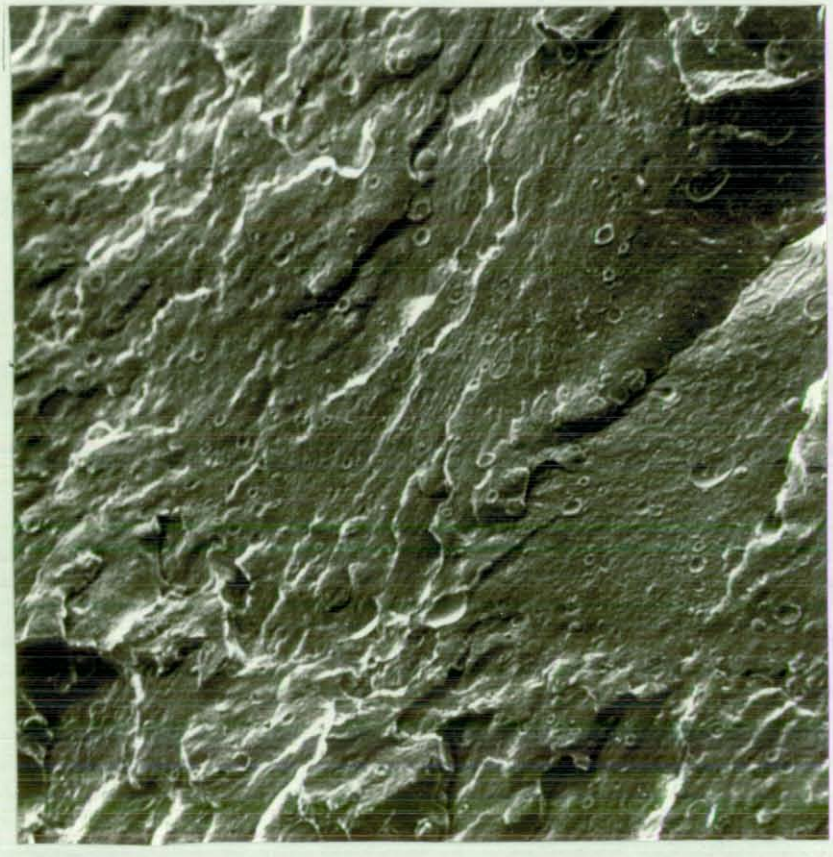

(b) Mag 1·5K

FIG 3-15

3.6. Discussion

3.6.1. Proposed Mechanism for Time Dependency of Melt Rheological Behaviour

In studies of two phase systems it is primarily the matrix phase that is under investigation. Changes in the disperse phase have only a second order effect on the shear modulus. The observed phenomena are therefore to be explained in terms of changes occurring in the major phase.

The observed increases in the elastic and viscous components of the dynamic shear modulus on maintaining the blend at melt temperatures (Fig. 3/10), and particularly the fact that the elastic component increases relative to the viscous component suggests a development of a cross-linked network. In melt rheology studies cross-linking tends to increase G' at a greater rate than G", whilst an increase in the molecular weight tends to increase G' and G" to approximately the same extent at low shear rates.

It has been shown that much of the elastic nature of the melt is decreased by increasing the shear rate (Fig. 3/12). This suggests that the gel network has a very low cross-link density. Any proposed mechanism must therefore be consistent with the following observed parameters.

i. A lightly cross-linked system is produced in the major phase.

ii. The reaction is specific to ionomers.

iii. The increase in G' and G" is a function of the Surlyn A loading.

iv. The final product is still a two phase system.

The mechanism proposed is that the PET and Surlyn A take part in an ester interchange reaction at the interface between the two phases in the melt. At high temperatures there is a normal interchange between ester groups in polyesters. It is proposed that Surlyn A chains at the interface take part in an ester interchange reaction with the PET via their pendant carboxylate groups.

This reaction may be expressed as

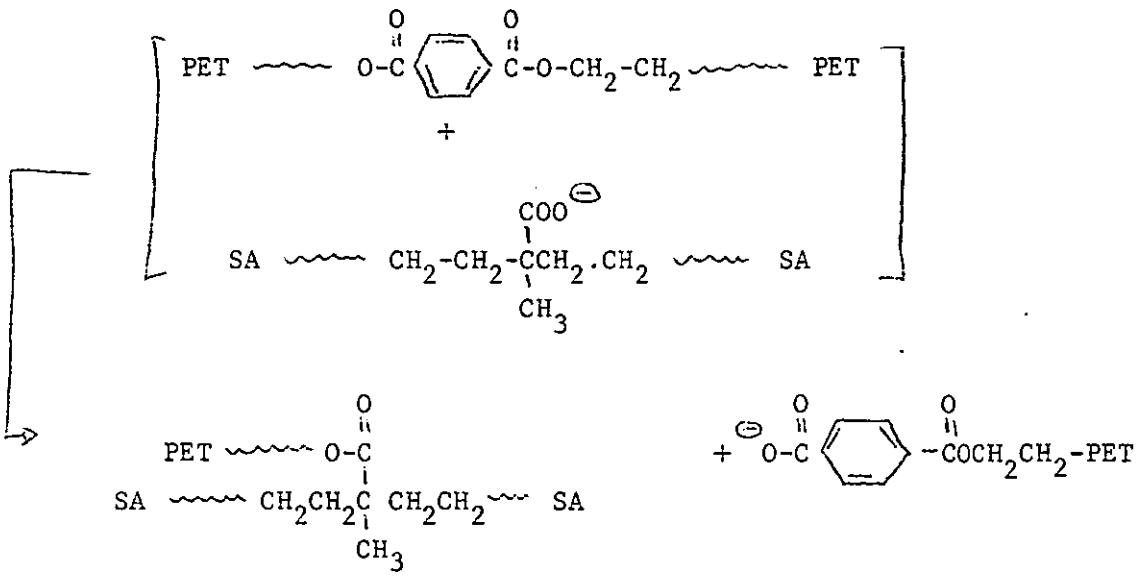

This type of reaction would produce a grafted chain at the interface which will be compatible with both phases. This grafted chain on diffusing into the PET matrix can undergo more ester interchange reactions involving PET chains and pendant carboxyl groups, and there is the possibility of a cross-linked structure developing, involving other Surlyn A chains due to their being several pendant carboxyls on each Surlyn A chain. The material surrounding each Surlyn A particle will therefore consist of a lightly cross-linked gel. A similar reaction will have taken place in the Surlyn A particle. In this case it is likely that the gel will have a higher cross-link density since there are more reactive carboxyl groups in the rubber phase. Therefore as the reaction proceeds its rate will decrease due to the formation of a highly cross-linked structure at the interface of the two phases. This gel will inhibit diffusion of one phase into the other and the reaction will terminate (Fig. 3/17).

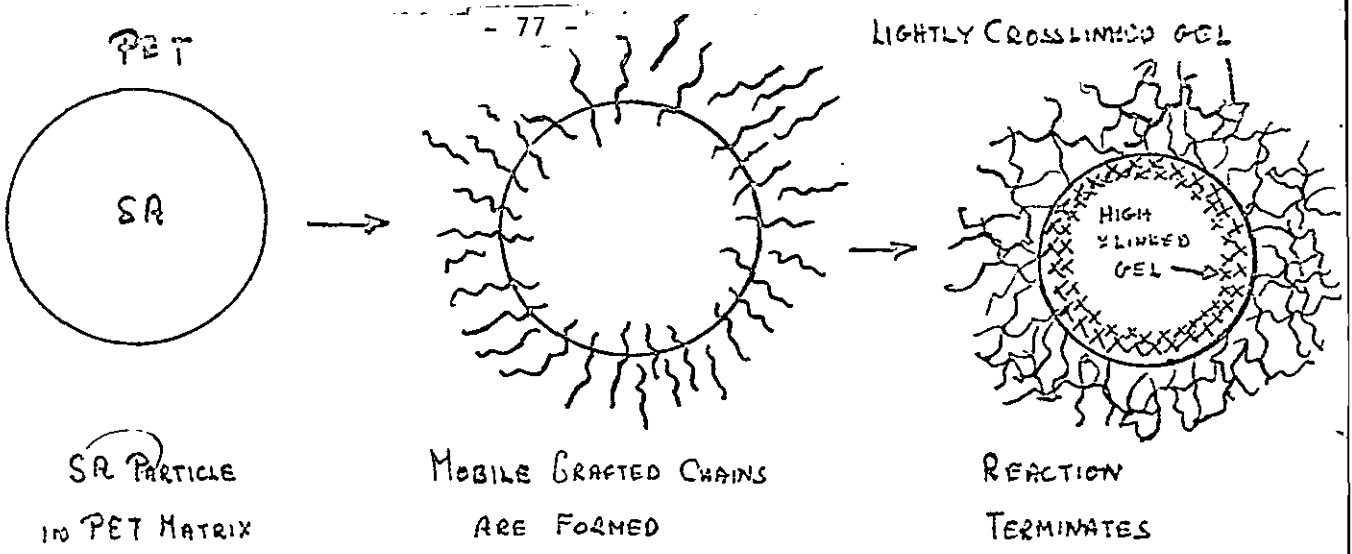

FIG 3-17.

The amount of gel in the PET will therefore be a function of the surface area of the Surlyn A (i.e. vol% of Surlyn A if the particle size distribution is identical for each blend) as is indicated in Fig. 3/11. The melt temperature can be expected to have an effect upon the reaction rate since the formation of the cross-linked network is controlled by the rate of diffusion of polymer chains across the interface.

3.7. PET/Grafted Surlyn A Blends

The studies on the melt rheology of PET/Surlyn A blends strongly suggests that an ester interchange reaction can occur between the two components when the blend is held at melt temperatures. It would therefore seem desirable to allow this ester interchange (graft) reaction to occur in order to improve the adhesion between the rubber particles and the PET matrix. A convenient way of accomplishing this is to increase the residence time in the melt of a blend by altering the total cycle time during injection moulding, or alternatively to increase the melt temperature.

3.7.1. Effect of Increasing the Melt Residence Time

The blends produced in the normal fashion by melt extrusion blending. This process was performed at the lowest melt temperatures (220 - 265°C) and the shortest time (~ 3 - 4 mins) consistent with obtaining a reasonable dispersion (particle size ~ 5μ).

The number of moulding cycles necessary to clear the barrel on the injection moulding machine fitted with the mould was then determined. This was achieved by changing the feed stock from a colourless polymer to a pigmented polymer, moulding and determining how many moulding cycles elapsed before the pigmented material appeared in on of the samples. Using this technique it was found that for the mould 10 cycles were required to transfer polymer from one end of the barrel to the other. The melt residence time can be found by multiplying the total cycle time by 10.

Table 3-4 shows the range of cycle times and consequent melt residence times used for a 10 wt% blend of Surlyn A in PET.

Table 3-4

Sample No.	Injection sec	Cool sec	Interval sec	Melt residence time (min)
1	5	5	5	2.5
2	5	5	20	5
3	5	5	35	7.5
4	5	5	50	10
5	5	5	65	12.5
6	5	5	80	15
7	5	5	95	17.5
8	5	5	110	20

The plot of notched impact strength versus melt residence time (Fig. 3/18a) shows that there is an increase in impact strength over the first 7 to 8 minutes and thereafter the impact strength drops progressively.

I.V. measurements on the phase separated PET shows that the I.V. drops progressively with melt residence time and it would therefore appear that any increase in impact properties as a result of the grafting reaction is being nullified by the normal thermal degradation processes that take place in the melt under process conditions.

3.7.2. Effect of Increase of Melt Temperature for Constant Melt Residence Times

The machine barrel temperature was varied in the range 270° - 300°C for a total cycle time of 40 secs which corresponds to a melt residence time of 6.7 minutes. Once again there was an increase in impact strength for temperatures of 270 and 275°C but at the higher temperatures the impact strength fell progressively.

Fig. 3/18b shows the I.V. of the PET versus the melt temperature. Thermal degradation again is found to have affected the PET and resulted in the observed fall in impact strength.

It is clear from these results that by holding the blend in the melt in order to allow time for the graft reaction to take place, there is also time for the PET to degrade. This effect is not observed to the same extent when performing experiments in the Weissenberg Rheogoniometer since the melt is then in an atmosphere of dry nitrogen when hydrolytic degradation is reduced to a minimum.

One answer to this problem would be to heat the blend in a reactor under nitrogen. However, there are problems associated with this technique, namely

i. The blend will increase in viscosity and will consequently be difficult to remove from the reactor.

ii. If the reacted blend were to be allowed to solidify the material would have to be removed from the reactor and granulated prior to moulding.

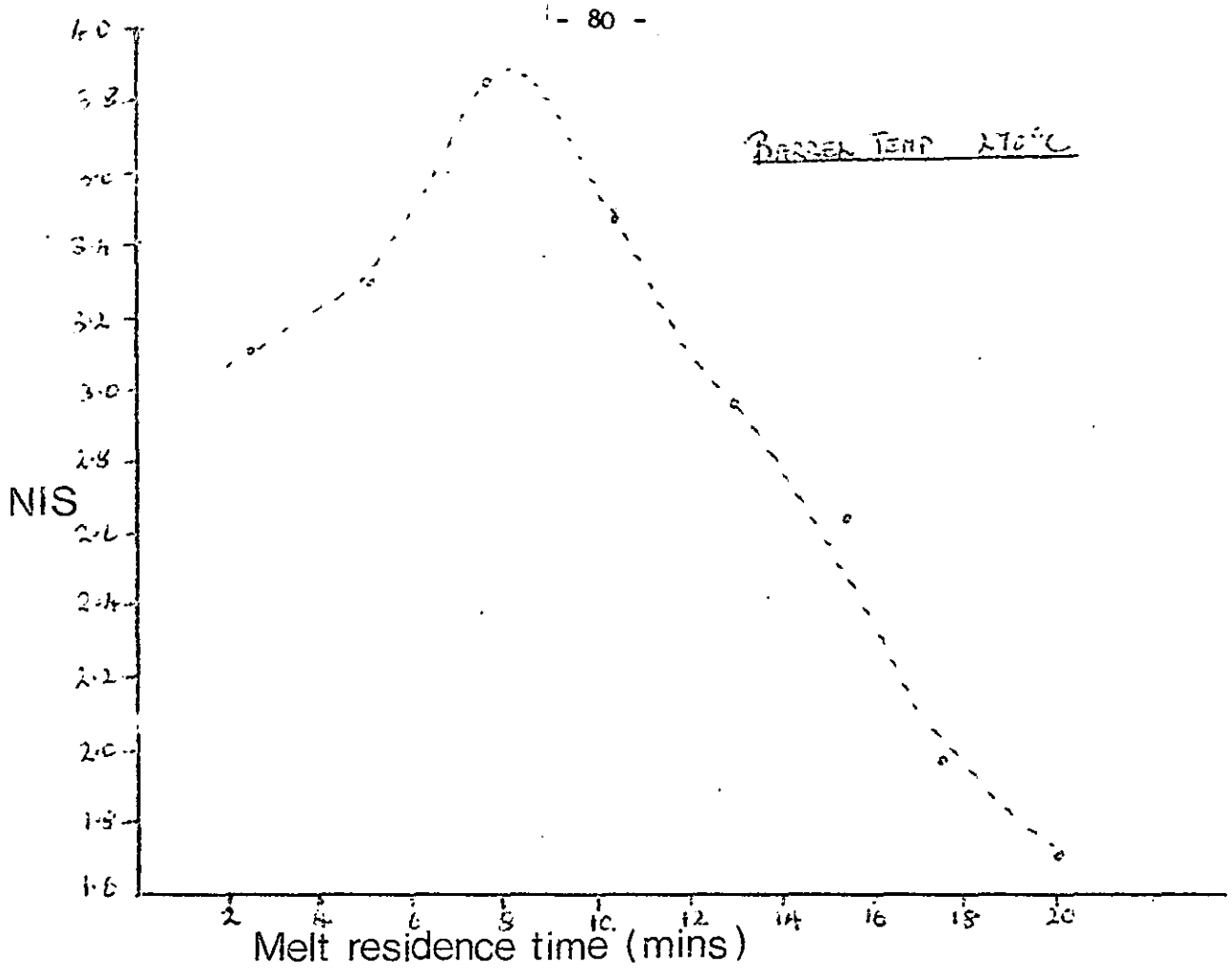

FIG3/18a

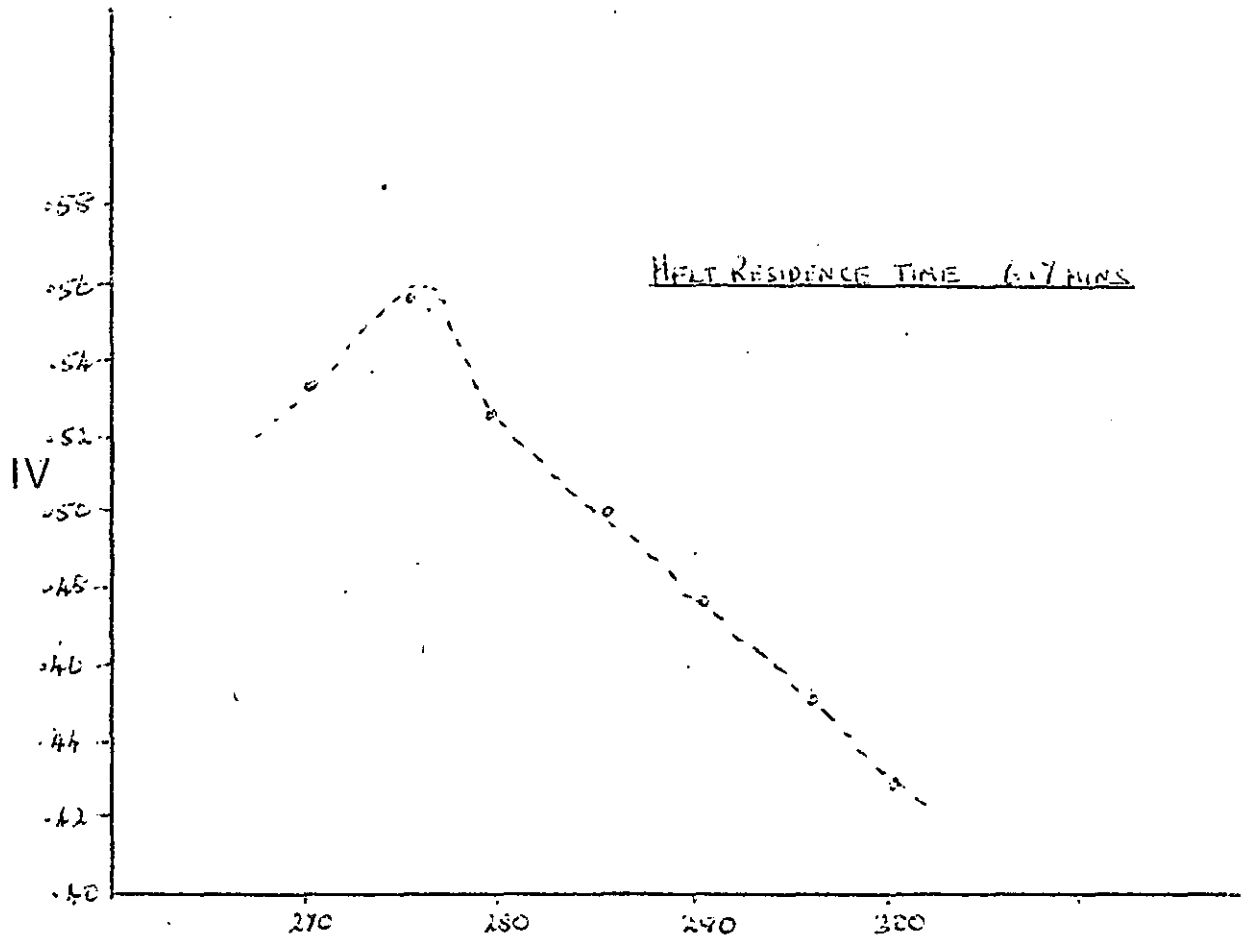

FIG3/18b

iii. The economics of batch processes are not as attractive as a continuous process and are best avoided if possible.

3.7.3. Preparation of Grafted Surlyn A

The approach eventually adopted to overcome the problem of degradation of the PET matrix was to produce a grafted Surlyn A prior to melt blending with the PET using a "masterbatch technique".

The grafted Surlyn A was prepared by first producing a blend containing 90 wt% of Surlyn A and 10 wt% of PET, by melt extrusion. This blend was then reacted in the injection moulder such that the melt residence time was 12.5 min at a melt temperature of 280°C. This gave a blend with a melt viscosity of 10,000 poise. The longer the reaction was allowed to proceed the higher was the final viscosity obtained. It was necessary to compromise on the extent of the reaction since the Surlyn A must subsequently be dispersed into PET, and the greater its viscosity the more difficult would this process become.

3.7.4. Blends Using Grafted Surlyn A

The reacted ionomer was granulated and mixed with PET chip such that the final blend contained 20 wt% of rubber. Blends were produced by melt extrusion using the Iddon 1½" extruder but the results were disappointing. The mixing efficiency of the extruder was not sufficient to produce adequate dispersions of the Surlyn A which now had a viscosity of 10,000 poise. Optical microscopy showed that there were large irregular particles of the rubbery phase in the PET.

It was found that adequate dispersion of the grafted Surlyn A could be obtained if a static mixer was used. Fig. 3/19a and b are scanning electron micrographs of fracture surfaces of the blend, obtained by fracturing at liquid nitrogen temperatures. The particle size range is 1 - 10 and it is interesting to note that the particles are themselves two phase systems. It can be seen that they contain PET particles. It was hoped that the PET grafts

produced in the Surlyn A during the first processing stage would aid adhesion between the two phases in the final blend.

The impact strength results for these blends are shown in a slightly different form to previous data Fig. 3/20. Experiments in the laboratory had shown that the impact strength of PET mouldings varies with the sample number, an effect believed to be due to the feed stock picking up water whilst in the hopper of the machine. The effect of moisture uptake is found to significantly effect the impact strength after the PET has been exposed to the atmosphere for greater than 30 minutes.

Fortunately the impact data reported so far are for samples moulded within 30 minutes of being removed from the vacuum oven, and therefore the results are believed to be valid. This view is supported in that where I.V. measurements had been made on samples, the observed drop in I.V. was from 0.62 - 0.55 which is normal for a dry feed stock.

Fig. 3/20 is a plot of notched impact strength versus sample number for amorphous specimens as obtained from the injection moulding machine operating on an automatic cycle of 20 secs injection, 10 sec cooling, 10 secs interval.

The injection moulder was initially purged with PET and sample No. 1 is that obtained when the blend was first fed into the hopper. The first ten samples are PET containing no rubber; the blended material begins to be moulded from sample number eleven and onwards. When the blend comes through the impact strength is seen to increase dramatically from 2 to 7 kg cm/cm^2 but from then on decreases steadily as the sample number increases. This is caused by the molecular weights of the PET matrix decreasing due to the feed stock picking up moisture. Fig. 3/21 is a graph of the yield stress obtained for amorphous specimens and shows the expected decrease in the yield stress for sample numbers greater than ten i.e. those which contain the Surlyn A.

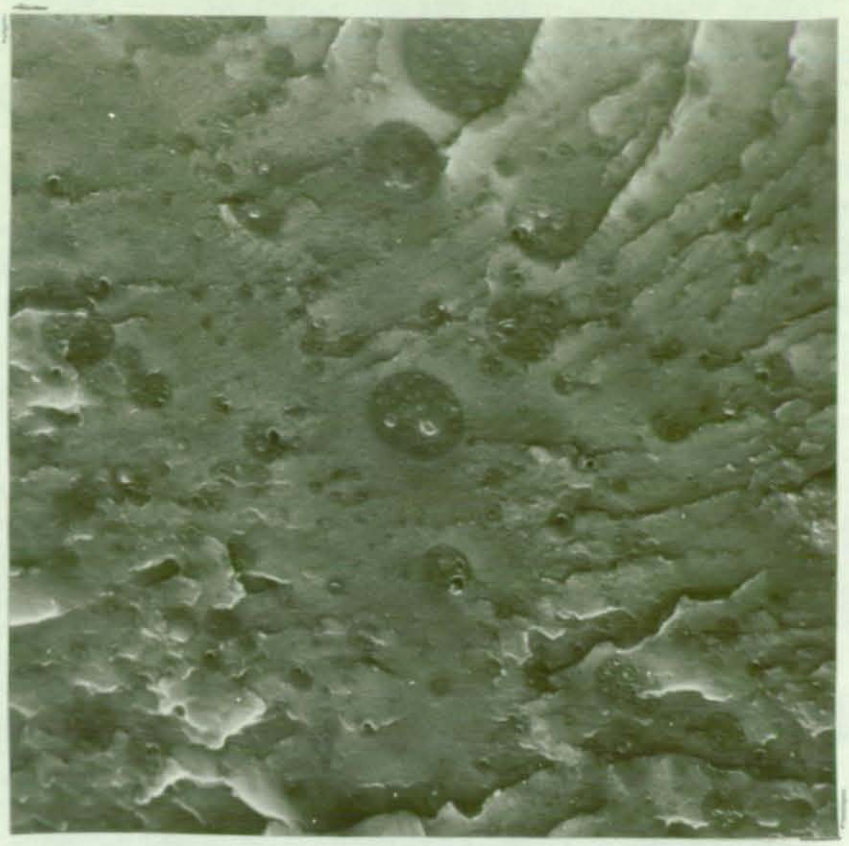

a Mag. 1·5K

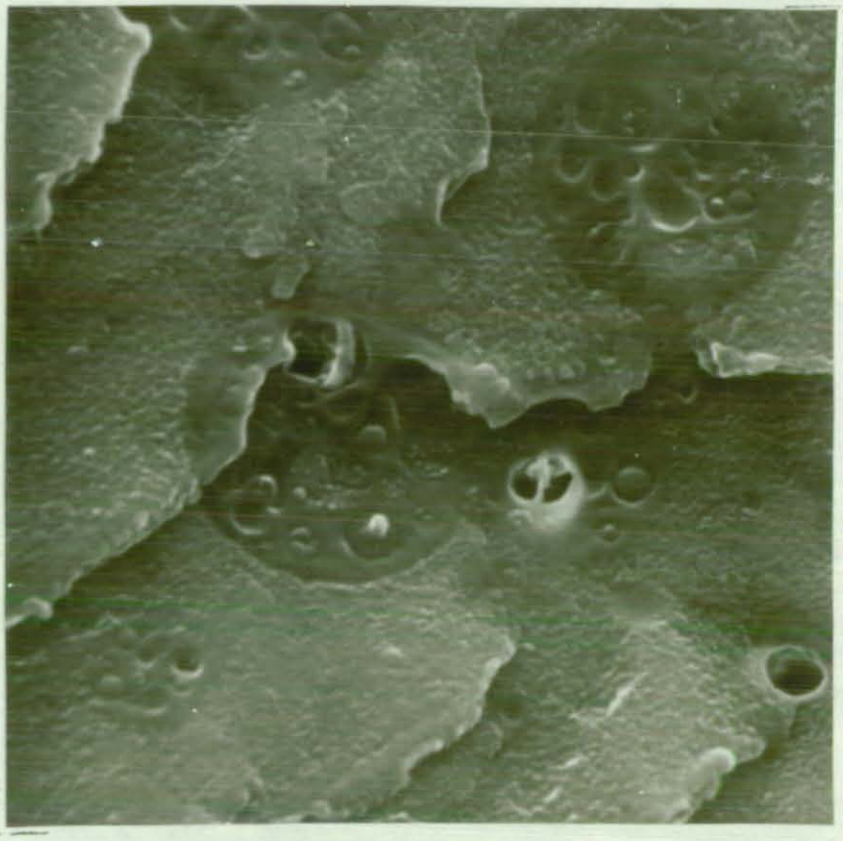

b Mag. 4·5K

FIG. 3-19

FIG 3-20

20 WT. % GRAFTED SURLYN A / PET
(AMORPHOUS)

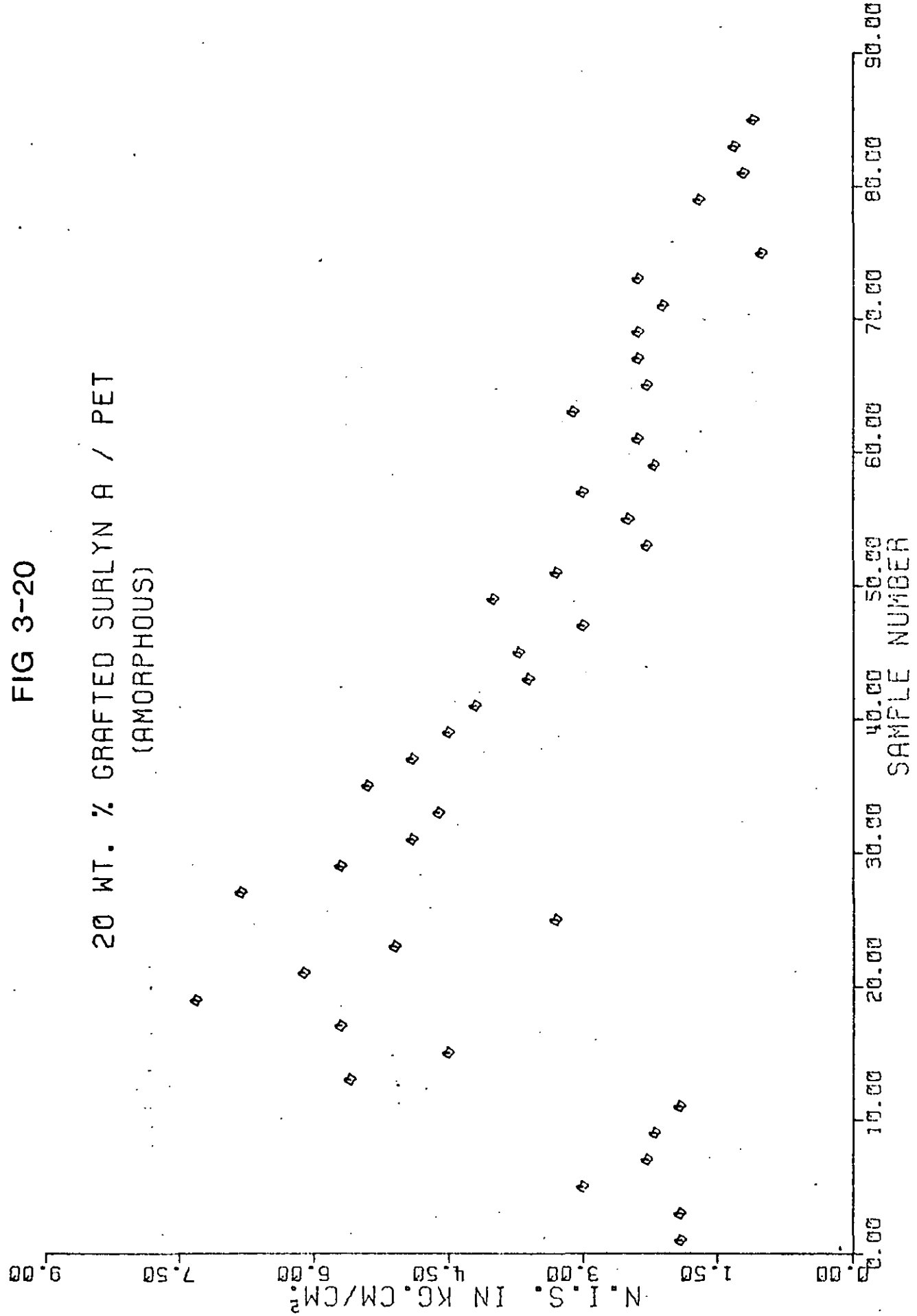

FIG 3-21

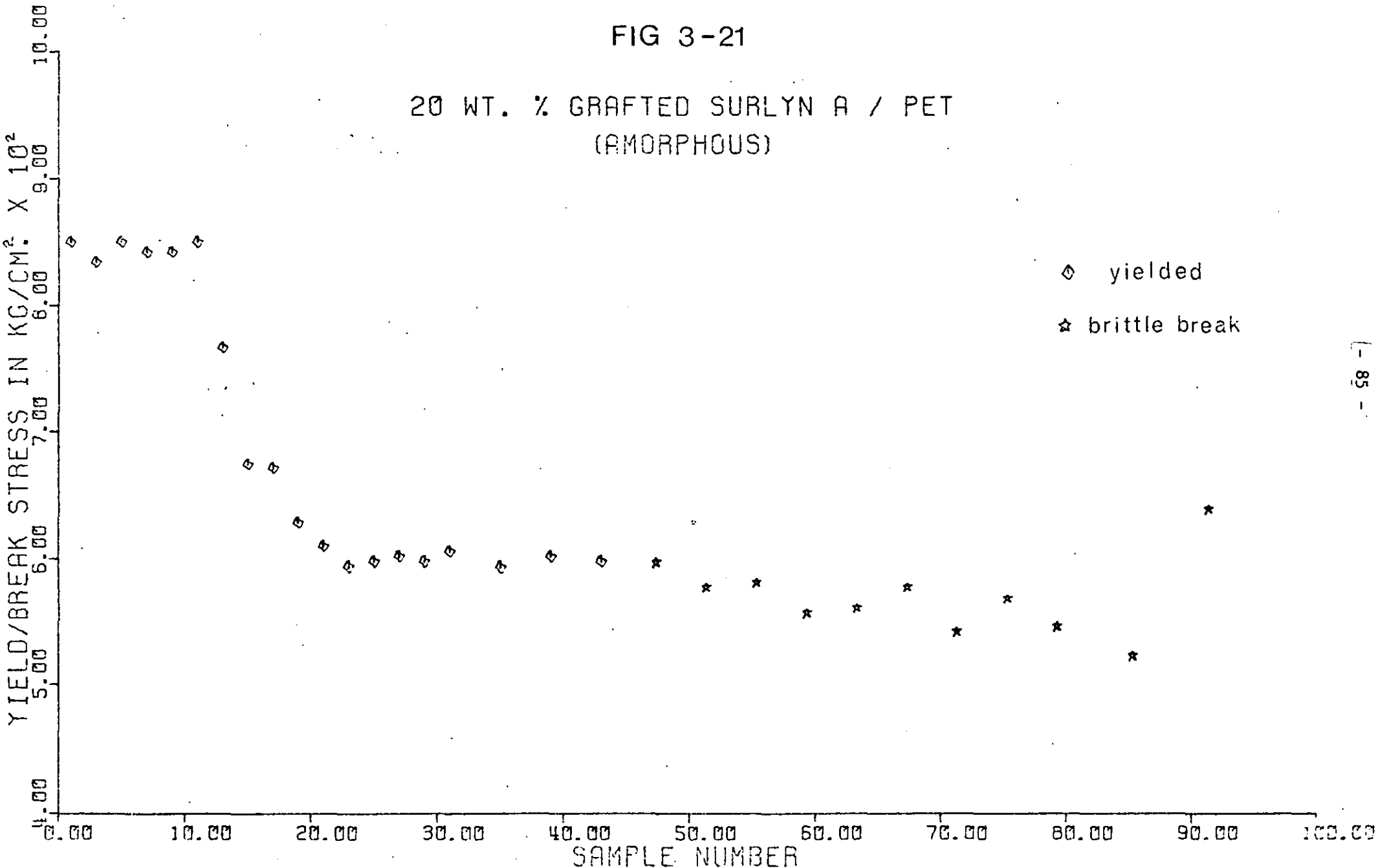
20 WT. % GRAFTED SURLYN A / PET
(AMORPHOUS)
YIELD/BREAK STRESS IN KG/CM.² X 10²
10.00
9.00
8.00
7.00
6.00
5.00
4.00
0.00
10.00
20.00
30.00
40.00
50.00
60.00
70.00
80.00
90.00
100.00
SAMPLE NUMBER
yielded
brittle break

3.8. Discussion

Throughout the study quenched amorphous samples were prepared since it was thought that any improvements in impact properties due to the inclusion of a minor rubbery phase would be more evident when the matrix had the greatest facility for cold flow. This would be the case when the PET was in the amorphous state as opposed to the more ordered crystalline condition. Also variables such as the degree of crystallinity and crystalline morphology are difficult to control during sample preparation and were therefore best avoided during the initial study. In the event of obtaining an amorphous blend showing improved impact strength it was intended to extend the experiments to include crystalline materials since it is in the highly crystalline form that the exceptional properties of PET occur and the material then becomes an economic proposition.
PET/Surlyn A blends when prepared by melt extrusion mixing and subsequent injection moulding do not show spectacular increases in impact strength. Fig. 3/9. However, it has been demonstrated that PET and Surlyn A interact when in the melt state. This interaction is most easily followed by investigation of the rheological behaviour as a function of time in the molten form. It is then seen that both the elastic and viscous components of their shear modulus increase with time and the evidence would suggest that a lightly cross-linked structure was formed

Attempts to study the effects of this interaction on the physical properties of the blend were hampered by the fact that under real processing conditions degradation of the PET masked the effects of the interaction between the two polymers. Hence any improvements due to the expected increase in interphase adhesion were not observed.

In an attempt to overcome this problem, the Surlyn A was pre-reacted with minor amounts of PET and subsequently diluted with more PET during melt blending to bring about phase inversion when the Surlyn A became the minor disperse phase. By following this procedure the impact strength for a 20 wt% Surlyn A in PET blend was increased from 2 Kg cm/cm^2 to 6 Kg cm/cm^2.

The blend produced would appear to incorporate many of the properties thought to be necessary in successful rubber modified systems.

i. It is a two phase system, a rubbery phase being dispersed within the brittle glassy phase.

ii. The particle size of the disperse phase is in the region of 1 μ.

iii. The adhesion between the two phases has been improved by graft reactions.

iv. The disperse phase has excellent low temperature characteristics.

v. The rubber particles are lightly cross-linked (in this case by ionic forces).

As this is the case one might have expected a substantial improvement in impact strength due to the formation of large numbers of craze structures during and prior to fracture, a similar mechanism to that operating in rubber modified polystyrenes. Some proposals as to why a craze mechanism of impact reinforcement does not operate in the case of PET/Surlyn A blends will be formulated in the following chapter.

REFERENCES

Chapter Three

1. U.S. Patent No. 3,286,992
2. Chemical Engineering, May 19, (1969) p. 94-96
3. Private Communication, Roberts T.A., ICI, P and P Laboratory
4. Alexander R.L. et al, Polymer Eng. and Sci., May (1966) p 5
5. Mahling, D., Kunstoffe, 57, p. 321 (1967)
6. Private Communication, Jones M.E.B., ICI, P and P Laboratory
7. Ward T.C., Tobolsky A.V., J. Appl. Poly. Sci., 11, p. 2403 (1967)
8. Longworth R., Vaughn, D.J., (A.C.S. Polymer Reprints, 9, (1) p.525 (1968)
9. Du Pont B.P. 1,034,268 (1966)
10. Polyesters. I. Goodman and J.A. Rhys, Iliffe Book Ltd., London (1965)

CHAPTER FOUR

4. Fracture Surface Topography and its Relationship to Crack Velocity in Amorphous Poly(ethylene terephthalate)

4.1. Introduction

Impact strength is a measure of the energy absorbed under impact conditions. This energy is either absorbed by the specimen without explosive fracture, or a crack propagates explosively producing catastrophic failure. An important proportion of the total energy to failure in high impact materials is the energy required to produce new surface as the crack grows. A powerful technique in the study of mechanisms taking place during crack propagation is the observation of fracture surfaces.

The following experiments were designed to elucidate the mechanisms of crack propagation in amorphous PET which hopefully would aid the design of impact improved polymers.

4.1.1. General Theory of Brittle Fracture

Brittle fracture can be considered as occurring in two main stages, initiation and propagation.

In the initiation stage stress is applied and energy is absorbed as the strain develops until the stress reaches some critical value at a flaw which then becomes unstable and develops into a growing crack.

In the propagation stage, for perfectly elastic materials, under constant stress conditions the crack will accelerate and explosive fracture occurs.

Initiation has been theoretically treated by Griffith[1,2] and Irwin[3], using related but somewhat different approaches to arrive at the critical stress required to produce instability in a flaw of known size.

The body of the work described in this chapter concerns events after initiation of a crack and therefore relevant to the propagation stage of fracture. By an extension of the Griffith treatment to include the contribution of the kinetic energy associated with the moving crack it is possible to describe the behaviour of the dynamic system in terms of the equation of motion of the crack. This approach developed by Mott[4], starts with the assumption that for a moving crack in a perfectly elastic solid conservation of energy requires that

$$K + S + F = \text{constant} \qquad \text{Eq (1)}$$

where K = the kinetic energy of the time varying displacement field associated with the moving crack.

S = the elastic energy in the material due to the presence of the crack, minus the elastic energy in the material without the crack.

F = the total surface energy associated with the new surface created by the crack.

This energy balance has been evaluated for the following system: A uniform stress, applied at infinity normal to the long axis of a static crack in the interior of a thin plate, is increased to a critical value σc at which the crack grown in the direction of its long axis. The applied stress (σc) must remain constant during propagation. Under these conditions equation (1) can be evaluated to give equation (2) for the variation of crack velocity with crack length.

$$dc/dt = (2\pi E/k\rho)^{\frac{1}{2}} (1 - Co/C)^{\frac{1}{2}} \qquad \text{Eq (2)}$$

where dc/dt = crack velocity

Co = half initial crack length as in the Griffith theory of Fracture

C = half crack length

E = Young's modulus of the material

ρ = Density of the material

k = a numerical constant whose value depends the stress and displacement fields surrounding the moving crack.

Roberts and Wells[5] using static crack expressions for stress and displacement fields in a material of Poisson's ratio 0.25 obtained a value for k that gives

$$dc/dt = 0.38 \sqrt{E/\rho}\ (1 - Co/C)^{\frac{1}{2}} \qquad \text{Eq (3)}$$

Therefore, at large crack lengths $(1 - Co/C) \rightarrow 1$, the crack velocity approaches a terminal value V_T where

$$V_T = 0.38\ (E/\rho)^{\frac{1}{2}} \qquad \text{Eq (4)}$$

A refinement due to Dulaney and Brace[6] allowed a theoretical production of the crack velocity in the acceleration stage of crack growth, the equation obtained being

$$dc/dt = V_T\ (1 - Co/C) \qquad \text{Eq (5)}$$

giving the predicted velocity profile shown in Fig. 4/1.

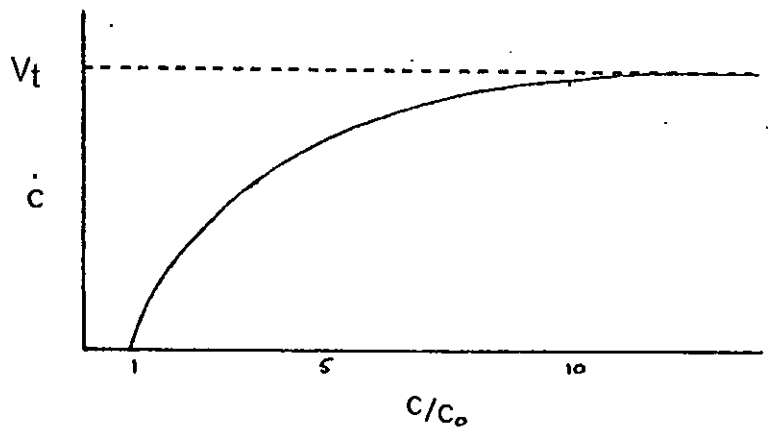

FIG 4/1

Various attempts have been made to extend the theory of brittle fracture to viscoelastic materials by including a small ductile region in front of the crack tip. This has the effect of blunting the crack and thus modifying the stress and displacement fields around the crack. An energy balance is then obtained using these modified stress fields and taking account of the strain energy in the yielded zone.

Experiments on inorganic glasses[17] confirm the general validity of the predictions of elastic theory. The terminal velocity was found to be independent of the bulk stress at fracture, and an approximate relation between the terminal velocity and $\sqrt{E/\rho}$ was seen to exist. However, it has been shown that fracture speed does depend to some extent on the chemical composition of inorganic glasses.

Polymeric materials do not give such reproducible results for maximum fracture velocities as the inorganic glasses. 'Steady' maximum velocities varying between 400 - 700 ms^{-1} have been observed for example in PMMA[17]. The value is apparently related to the stress level in the specimen at the moment of fracture, an effect that is not found in more brittle solids. A similar dependence has been found in bursting tests on cellulose acetate films[18]. It is likely that the propagation behaviour in polymers results from the small amount of local plastic deformation that accompanies 'brittle' crack propagation in polymeric glasses.

4.1.2. Fracture Surface Topography

Studies of fracture surfaces have been used to throw light on the mechanisms taking place during fracture[7,8]. However, due to the multiplicity of features seen on the fracture surfaces of polymeric solids the literature is confused and abounds with specially coined terms to describe the features observed.

Below are described some of the more general features observed on the fracture surfaces of 'brittle' polymeric materials when fractured in tension.

The fracture initiates at a flaw which is usually at or near the edge of the specimen, and progresses slowly until the flaw reaches a size which is critical for the applied stress. At this point it becomes unstable and propagates rapidly. The area over which slow growth occurred contains the origin of failure. It is smooth and of high specular reflectivity. This is known as the mirror area and appears to be featureless under low magnifications but on close examination can exhibit much detail characteristic of the conditions of test[9,10]. The size of the mirror zone is a function of many variables, e.g. in PMMA, studies have shown that loading rate, molecular weight and temperature all effect the area of the mirror region.

Beyond the mirror or slow growth area, there is a transition region which is recognised as an area of increasing roughness, leading on to a much rougher region the surface of which is usually referred to as 'hackle'. It is on this region that many geometric figures may be observed, resembling primarily parabolas and hyperbolae. Since the stress level and crack velocity are higher in this region, the stress is sufficient to actuate flaws well in advance of the main crack front[11]. The geometric markings are produced by the intersection of the main crack front with secondary cracks propagating radially from the numerous local flaws which had been activated by the advance stress wave. The two cracks form a conic section at their juncture. If the velocities are equal, a parabola is formed. If the secondary front is slower, the primary front will completely enclose it and an

eclipse will result. Many other more complex markings have been observed, such as "scallops", "chevrons" and river systems[12]. The majority of surface roughness is therefore explained by the existence of heterogeneity in the material and its interaction with the fracture process. One type of characteristic surface marking not explained by this process and usually observed in the mirror region is "Wallner Lines". This phenomenon was first described by Wallner[13] and has been extensively studied in inorganic glasses. Its cause has been established by experiments in which a specimen was irradiated by ultrasonic waves[14] generated externally throughout the duration of fracture; an evenly rippled surface resulted. True Wallner phenomena are believed to rely on self generated stress waves from the relaxation of material behind the crack tip to produce the periodicity on the fracture surface. Wallner lines have been observed in polymers, though in the cases so far reported they do not take the form of smooth undulations as in inorganic glasses, but rather of periodic variations in surface roughness[15]. This is possibly because polymeric solids are less homogeneous than glass and the momentarily increased local stress, caused by the passage of a stress pulse, results in more widespread secondary fracture rather than deviation of a single fracture plane.

A distinctive feature of the Wallner phenomenon is the appearance of several systems of Wallner lines. These arise from interaction of the main fracture front with stress pulses that have undergone reflections at the specimen boundary. By assuming the stress pulses to emanate at a small distance behind the crack tip, and that the stress pulses have a higher velocity than the main fracture front, it is possible to calculate the intersection loci of the fracture front with reflected stress pulses (Fig. 4/2).

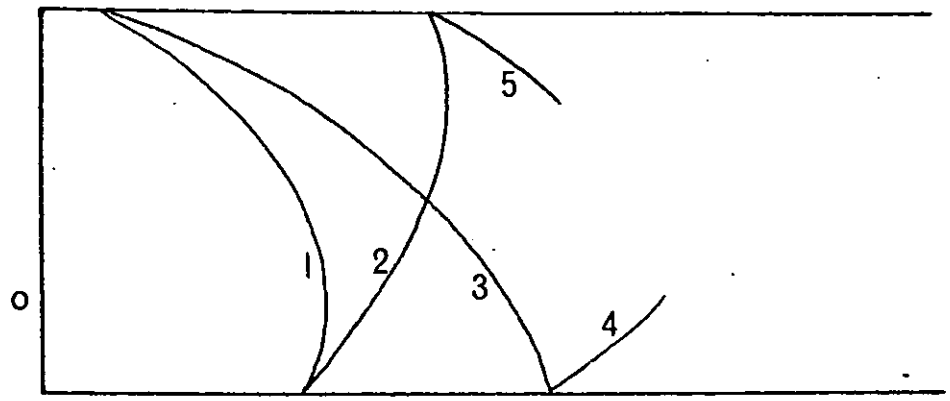

FIG 4/2

1) circle centre O due to interaction of fracture front with stress pulses generated immediately behind the fracture front.

2) Arising from first stress reflection at lower edge

3) Arising from first stress reflection at upper edge

4) Arising from second stress reflection at lower edge

5) Arising from second stress reflection at upper edge.

From analysis of the Wallner Lines Andrews[15] determined that the ratio of the stress pulse velocity to the velocity of the fracture front was $\sim$ 2 in carbon filled rubbers.

4.2. Experimental

The polymer used throughout this work was "Fibre grade PET (code B43)". All samples used were melt quenched into the amorphous state.

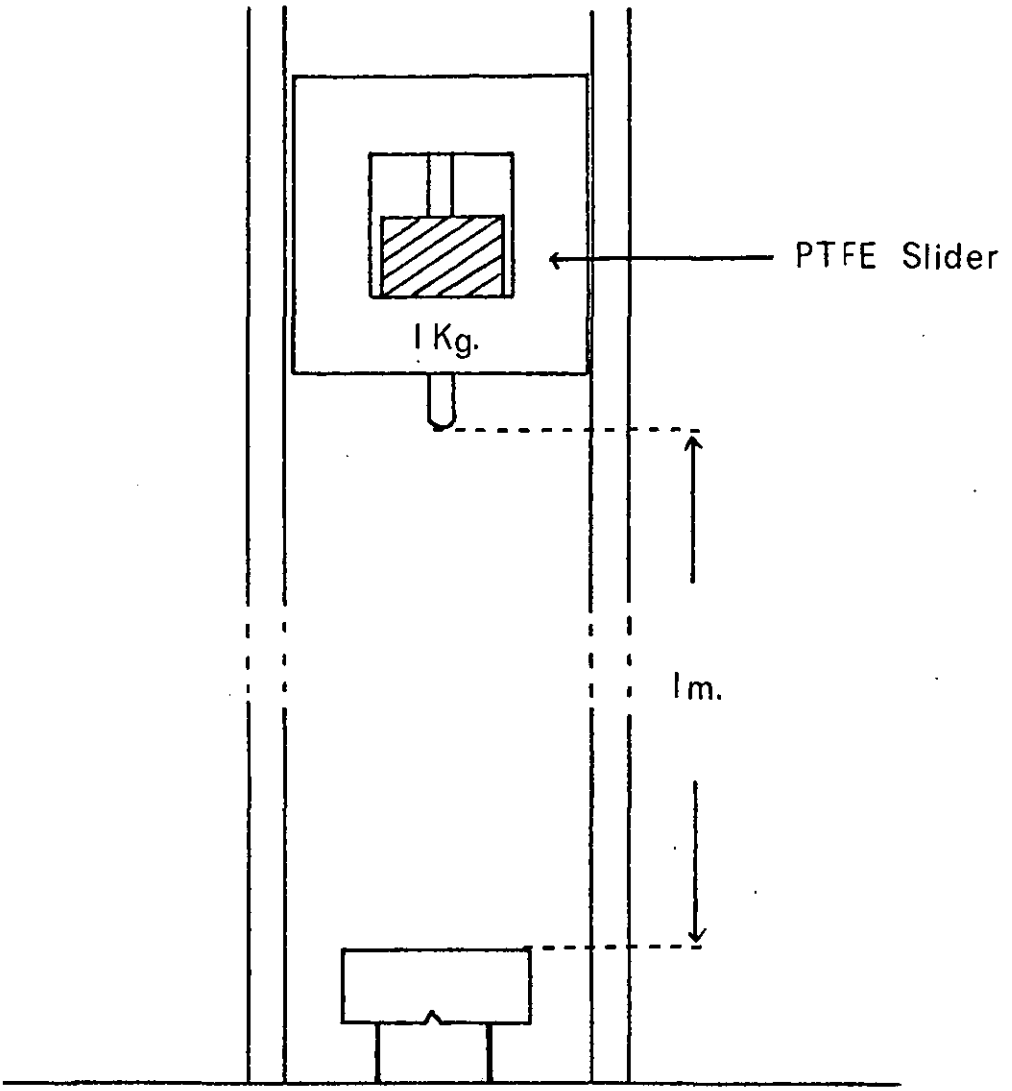

FIG 4/4

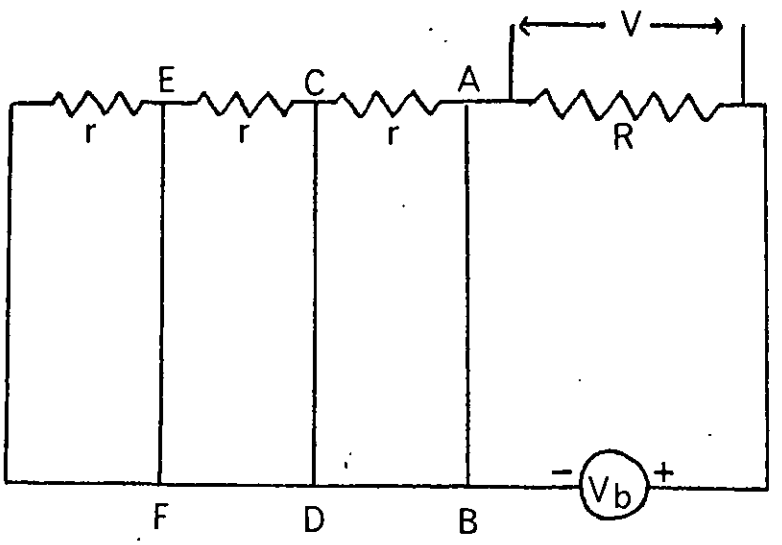

FIG 4/5

4.2.3. Technique for Determination of Crack Velocity

In order to correlate the surface topography and the crack velocity, it was necessary to obtain data on the crack velocity as a function of the crack length. Since the theoretrical terminal crack velocity is given by $0.38\sqrt{E/\rho}$ this means that velocities of up to 600 m/s have to be measured several times over a total crack length of 2.5 cm. To do this type of measurement photographically, in order to obtain twenty values during the time required to fracture it would be necessary to expose at the rate of 4×10^5 frames per second. Because of the expense of the type of equipment required to give this frame speed, the velocities were measured indirectly using a modified broken strip technique.

a. General Principle

Consider the circuit diagram (Fig. 4/5). AB, CD and EF represent low resistance strips, they are joined by resistances r , and current is passed through the circuit via an external resistance R by a DC power source of voltage V_b.

In the circuit initially, the voltage drop across the external resistance R is $V = V_b$. If strip AB is broken, the voltage drop across R becomes $V_1 = RV_b/(R + r)$, if strip CD is also broken the voltage drop across R becomes $V_2 = RV_b/(R + 2r)$. For n consecutive broken strips the voltage drop across R is $V_n = RV_b(R + nr)$. Therefore if this type of circuit is laminated onto the sample such that the running crack breaks the strips as it propagates, the breaking of each strip will be marked by a decrease in the voltage across the external resistance, and consequently a voltage jump at A. The time interval between these voltage jumps can be equated to the time required for the crack to travel the distance between the strips, enabling the average crack velocity between these two points to be calculated.

b. Sample Preparation

The technique developed for sample instrumentation involved the production of a precision metal mask, through which metal could be evaporated to produce the desired circuit design. The mask was manufactured using a photo-resist technique outlined below:

1. A drawing of the required design was made on card and reduced photographically to the required size on line film. Fig. 4/6.
2. A sheet of 0.003" copper was cleaned by immersion in carbon tetrachloride, followed by a 2 minute dip in a saturated aqueous solution of ferric chloride.
3. Under the specified safelight conditions, equal volumes of "Kodak Ortho Resist" (K.O.R.) and "K.O.R. Thinner" were mixed together. The cleaned foil was dip coated with the solution and drained carefully to obtain a thin, even coating Fig. 4/7a.
4. The coated foil was dried at room temperature for 30 minutes and subsequently baked at 60°C for 30 minutes.
5. The photographic line negative of the required design was placed in intimate contact with one face of the coated foil and both sides exposed to ultra violet light for a period previously determined by use of test strips Fig. 4/7b.
6. The exposed foil was dipped in "KOR Developer" for 5 minutes, spray washed in water, and dried for 15 minutes at 60°C Fig. 4/7c.
7. The bared parts of the copper foil were etched away in a ferric chloride solution to finish with a mask of the original design Fig. 4/7d
8. Finally the remaining photoresist was removed by washing in KOR thinner Fig. 4/7e.

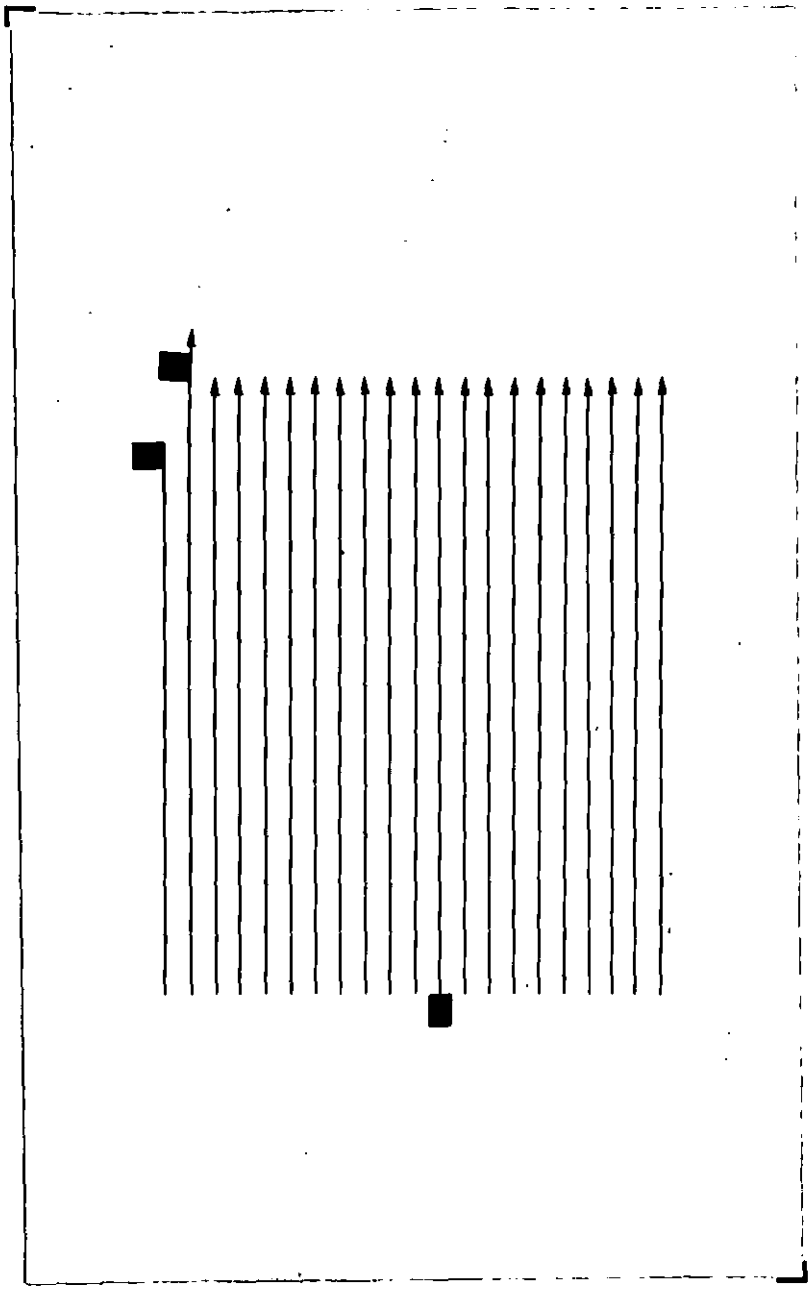

FIG 4/6

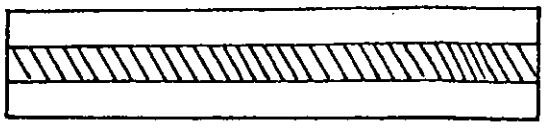

a

Copper foil coated with unexposed photoresist

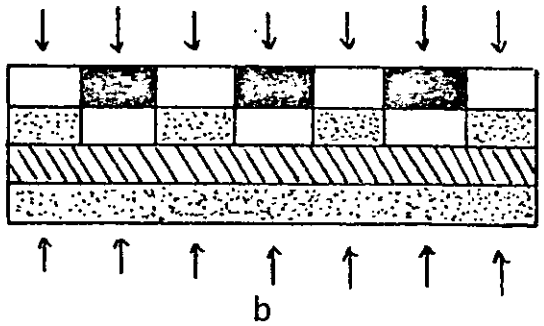

b

Exposure to U.V. light through the photographic negative.

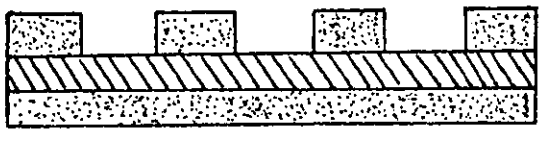

c

The unexposed areas of the photo resist are dissolved.

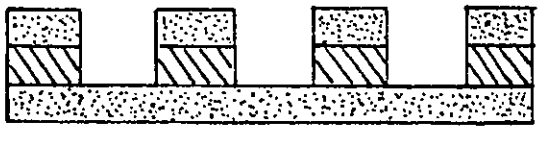

d

The bared areas of foil are etched away.

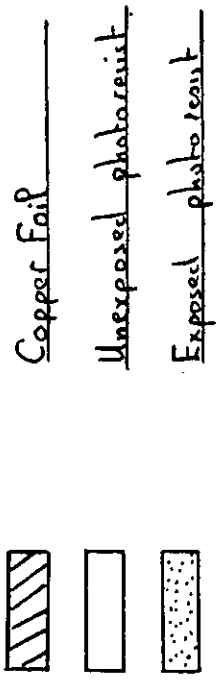

FIG 4/7

With the copper mask in contact, a silver grid was evaporated onto the sample using a 'Birvac' vacuum coating unit. The evaporation conditions were adjusted to give a good conducting layer, consistant with the necessity of avoiding overheating of the sample. The inter-strip resistances (r) were incorporated into the circuit by evaporating a thin strip of Bismuth at right angles to the silver grid. Figure 4/8. Since bismuth has a high resistivity (120 ohm.cm.), it is possible by controlling the evaporation time to obtain a resistance of 100 Ω between each strip.

Electrical contact was made with the sample at points A, B and C by melting wires into the polymer; making contact by means of silver paint. The thin film circuit on the sample was then joined to themain circuit as shown in Fig. 4/9.

c. Data Acquisition

On fracturing the sample the crack propagates from the notch across the sample, breaking the strips in order as it proceeds. On breaking strip 1 the voltage at A increases from 0 to 10 volts. This voltage jump serves to trigger the oscilloscope time base. At this juncture the voltage on the oscilloscope Y plate is 0 volts.

On breaking strip 2, an extra 100 Ω resistance is brought into the circuit in series with the 20kΩ external resistance, and the voltage at the scope Y plates increases to 0.05V. On breaking strip 3 a further 100 Ω is brought into the circuit and the voltage on the Y plates of the oscilloscope increases to 0.1 volts. Therefore, there is an increase of 0.05V for each strip broken, until strip 21 when the voltage jumps to 10 volts.

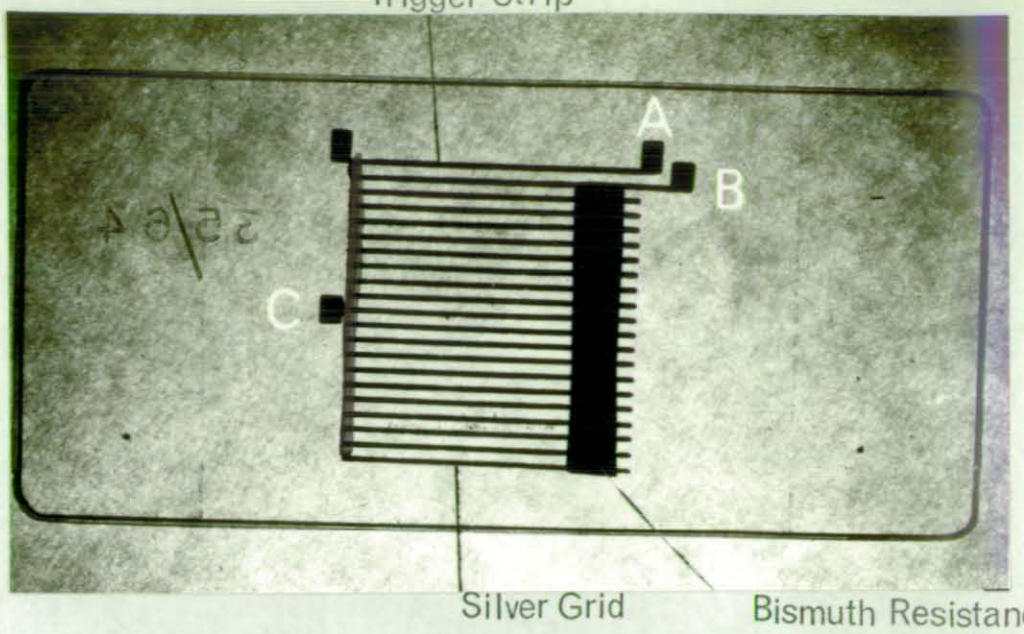

FIG 4/8

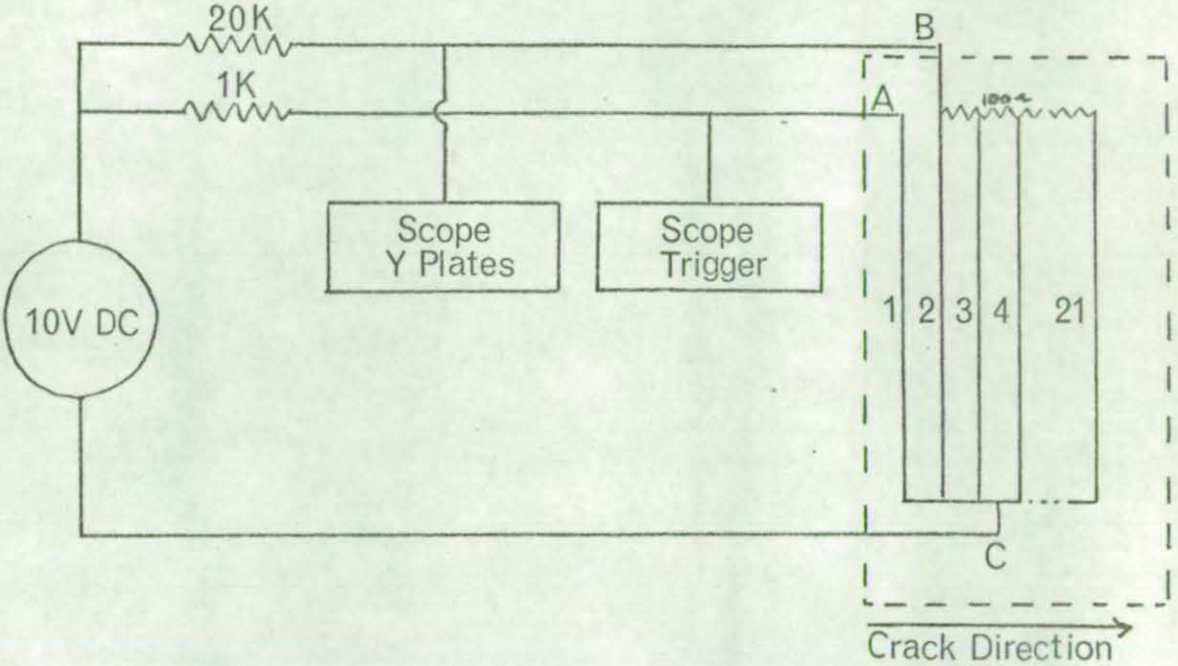

FIG 4/9

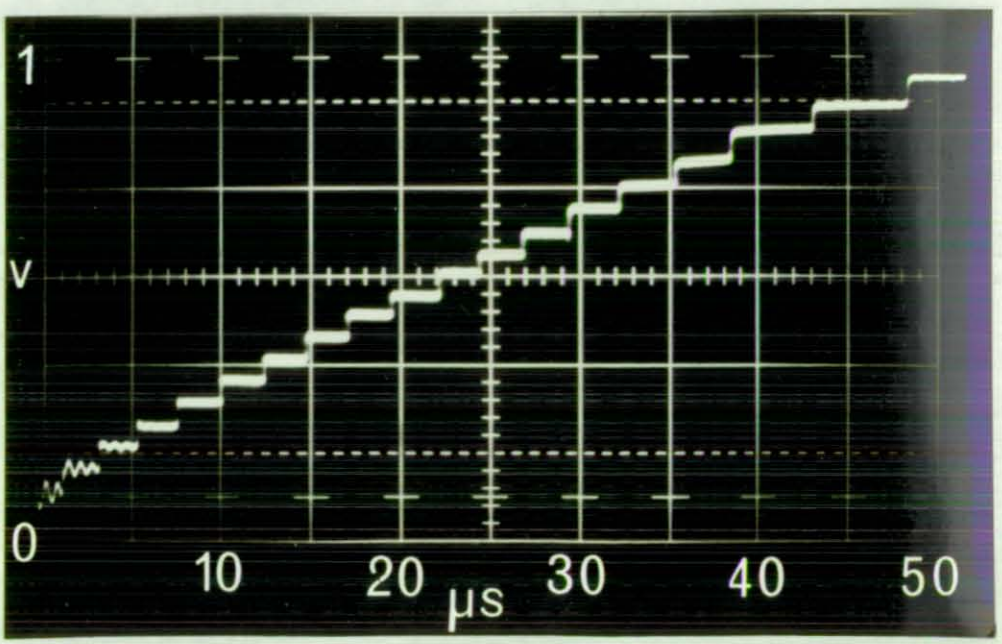

FIG 4/10

Figure 4/10 shows the trace obtained from a typical PET fracture. By calibration of the oscilloscope time base against a crystal oscillator the time taken for the crack to reach and break each strip can be calculated by measuring the distance to each vertical jump on the photograph (OA, OB etc) and multiplying by the time base. Then by measuring the crack length when each strip was broken, one can make a plot of time as a function of crack length, which on differentiation gives crack velocity as a function of crack length.

With PET samples the crack velocity was found to decrease during propagation. The apparatus was therefore modified to include two oscilloscopes. One used a fast time base (5 μs/cm) to measure the high crack velocity at the start of the fracture; the other using a slower time base (10 μs/cm) to measure the lower crack velocity near the end of fracture. This enabled accurate trace measurements to be made during the entire course of the fracture.

The oscilloscopes used in these experiments were 'Textronix' Type 547 exposures being made on 'Polaroid' Type 47 High speed film.

4.2.4. Fracture Surface Topography

The fracture surfaces were observed using three experimental techniques, a brief outline of which is given below.

a. Optical Microscopy

The instrument used was a "Carl Zeiss Photomicroscope" set up for operation in the reflected light mode. The illumination was either darkground or common light, depending on the type of features to be observed. Generally samples were untreated, however in some cases where the features were particularly non-reflective the surface was vacuum coated with a thin layer of aluminium prior to observation.

Figures 4/16 and 4/17 are examples of composite phtotgraphs of the entire fracture surface. It was found that in order to obtain a photograph of the complete fracture surface showing all the relevant topographical features, it was necessary to take many high magnification photographs in an orderly sequence and subsequently build up a composite photograph using the resulting prints. Figures 4/16 and 4/17 are photographs built up of 80 separate prints.

b. Transmission Electron Microscopy

For investigation of fine surface detail a two stage replication technique was used to obtain a suitable sample for examination in a 'Phillips' E.M. 300 transmission electron microscope.

The main sequence of events in the preparation of a two stage replica of PET fracture surfaces were as follows.

a. A few drops of a concentrated solution of nitrocellulose in amyl acetate were placed on the surface to be replicated and allowed to dry at room temperature overnight (Fig. 4/11a).

b. The nitrocellulose layer was carefully stripped off and coated with a thin layer of carbon. The first stage replica being rotated during evaporation in order to obtain an even coating (Fig. 4/11b).

c. The replica was 'shadowed' at an angle of 60° with a gold/palladium alloy to show up the surface relief.

d. The replica was then placed on a fine copper grid and the nitrocellulose dissolved away using acetone.

e. Finally, the two stage replica was allowed to dry and placed into the microscope for observation .

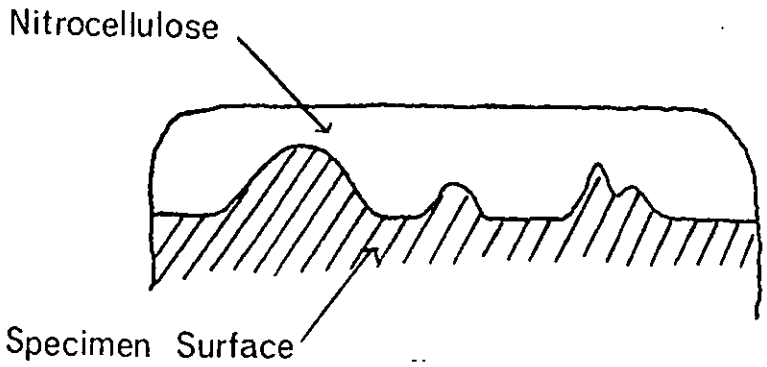
Nitrocellulose
Specimen Surface

a

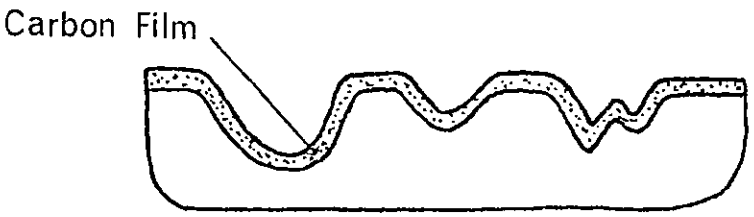
Carbon Film

b

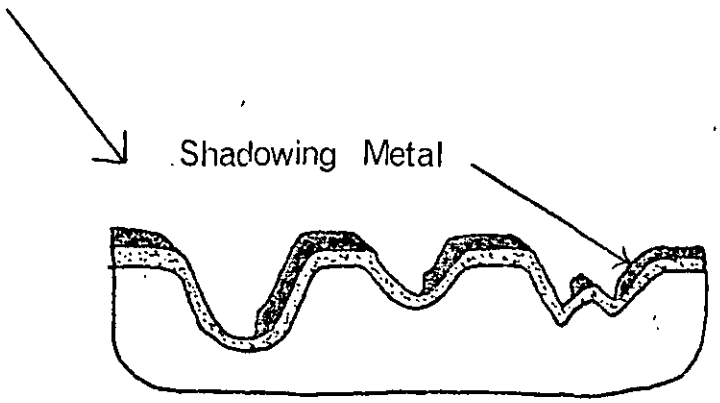
Shadowing Metal

c

c. Scanning Electron Microscopy

The fracture surface was evenly coated with a thin layer of aluminium prior to investigation in a 'Cambridge Stereoscan' scanning electron microscope. The metal coating is necessary to provide a conducting layer to enable charge, built up on the specimen by the electron beam, to be dissipated to earth. The accelerating voltage and specimen tilt were adjusted to give adequate contrast. (e.g. 5KV and 45° tilt).

4.3. Results and Discussion

4.3.1. Crack Velocity Profiles

Specimens of fibre grade PET with silver grids on their surface were fractured as described in the experimental section. The data obtained were used to determine the crack propagation time to each of the twenty strips on the specimen.

This time versus crack length data was fitted by a progressive polynomial curve fitting procedure using a 'Hewlett Packard' 200A digital computer. Fig. 4/12 is a plot of the experimentally obtained data points and the corresponding fitted curve. In this, as in most cases, a polynomial of degree five was considered to give a sufficiently good fit. The fitted curves were computed assuming the measured crack lengths to be the independent variable, that is the form of the equation of the fitted curve is:

$$t = Ac^5 + Bc^4 + Cc^3 + Dc^2 + Ec + F$$

where t = crack propagation time from the notch

c = crack length measured from the notch

and A, B, C, D, E and F are numerical constants.

It must be noted that the equation obtained is not unique but represents the best smoothed curve. That is, no further reduction in the sums of squares is obtained in the equation of the next higher degree.

FIG 4/12

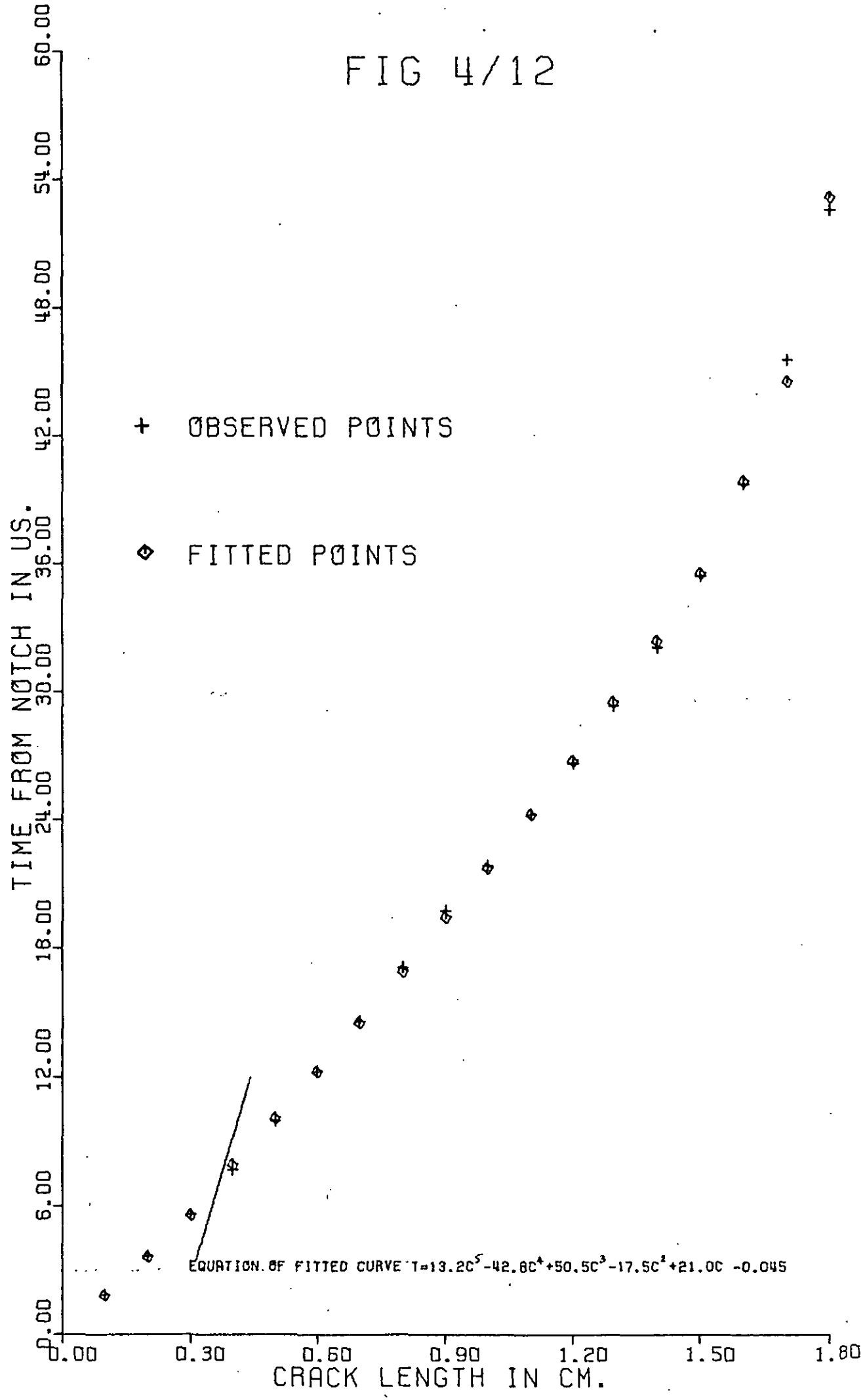
+ OBSERVED POINTS
FITTED POINTS
TIME FROM NOTCH IN US.
0.00
6.00
12.00
18.00
24.00
30.00
36.00
42.00
48.00
54.00
60.00
0.00
0.30
0.60
0.90
1.20
1.50
1.80
CRACK LENGTH IN CM.
EQUATION OF FITTED CURVE T=13.2C^5-42.8C^4+50.5C^3-17.5C^2+21.0C -0.045

Differentiation of the smoothed curve with respect to the crack length (c) gives

$$dt/dc = 5Ac^4 + 4Bc^3 + 3Cc^2 + 2Dc + E$$

Therefore, the crack velocity $C = dc/dt =$

$$1/(5Ac^4 + 4Bc^3 + 3Cc^2 + 2Dc + E)$$

Knowing the values of the coefficients a plot of the crack velocity versus crack length was obtained.

Figure 4/13 is a plot of the crack velocity versus crack length for three specimens fractured at room temperature. The shape of the velocity profiles of the three specimens is similar, though the actual value of the velocity at a specific crack length in each specimen is seen to be different.

From the velocity profiles the crack may be considered to propagate in four main stages.

In stage one the crack accelerates rapidly after initiation. No experimental points are obtained during this stage since it occurs prior to breaking of the trigger strip. In stage two the crack velocity falls to ~ 400 m/s. In stage three the crack propagates at an approximately constant velocity of 400 m/s. Stage four is marked by the onset of a drop in the crack velocity which continues until the specimen is broken, or in some exceptional cases until the crack stops.

The explanation of the observed velocity profile is thought to be found in an appreciation of the type of stress fields prevailing in a bent beam, and in the viscoelastic nature of the polymer. In a bent bar the maximum tensile stress is at the outer surface. The tensile stress then decreases to zero at a point halfway through the bar (neutral zone) and then is compressive to the inner surface where the compression is greatest.

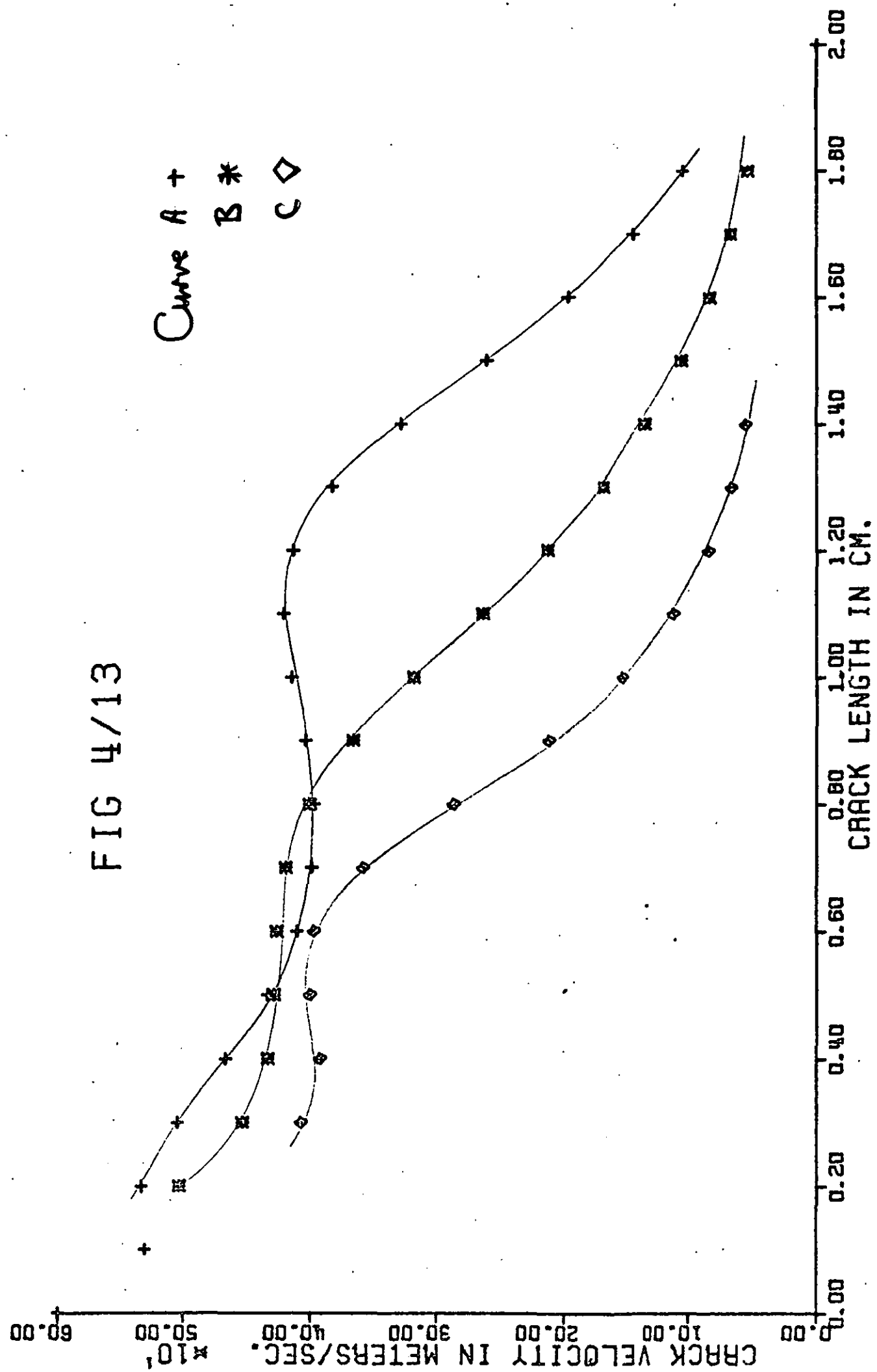
Curve A +
B *
C ◇
CRACK VELOCITY IN METERS/SEC. ×10¹
0.00
10.00
20.00
30.00
40.00
50.00
60.00
0.00
0.20
0.40
0.60
0.80
1.00
1.20
1.40
1.60
1.80
2.00
CRACK LENGTH IN CM.

FIG 4/13

Schardin[16] in work on inorganic glasses assumes this to be the form of the stress field encountered by the crack tip as it propagates through a bent bar. He noted that the crack ran at terminal velocity even in the compression zone of the specimen. The apparent anomaly of fracture proceeding in a compression zone may be explained by maintaining that the movement of the material behind the crack tip provides the energy to deform the zone in front of the crack producing the tensile stress necessary for fracture. The magnitude of this tensile stress will decrease as the crack moves through the compression zone.

In viscoelastic materials the crack velocity is thought to be dependant upon the bulk stress as has been shown in tensile tests on PMMA[17] and in bursting tests on cellulose acetate film[18]. If this is the case, in PET one would expect the crack velocity to decrease during a bending test since the bulk stress level decreases through the specimen.

It has been previously noted that although each specimen shows similar velocity regions, they occur at different values of crack length from specimen to specimen. It is proposed that the crack velocity is directly related to the bulk stress and that the onset of stage four (Fig. 4/13) occurs at some specific value of the bulk stress. This point of view is supported by the fact that the curves in Fig. 4/13 come into good register on bringing into coincidence the point of onset of stage four by shifting the velocity/crack length curve parallel to the X axis. Figure 4/15 is the master curve obtained on using the above procedure with data from fifteen separate fractures.

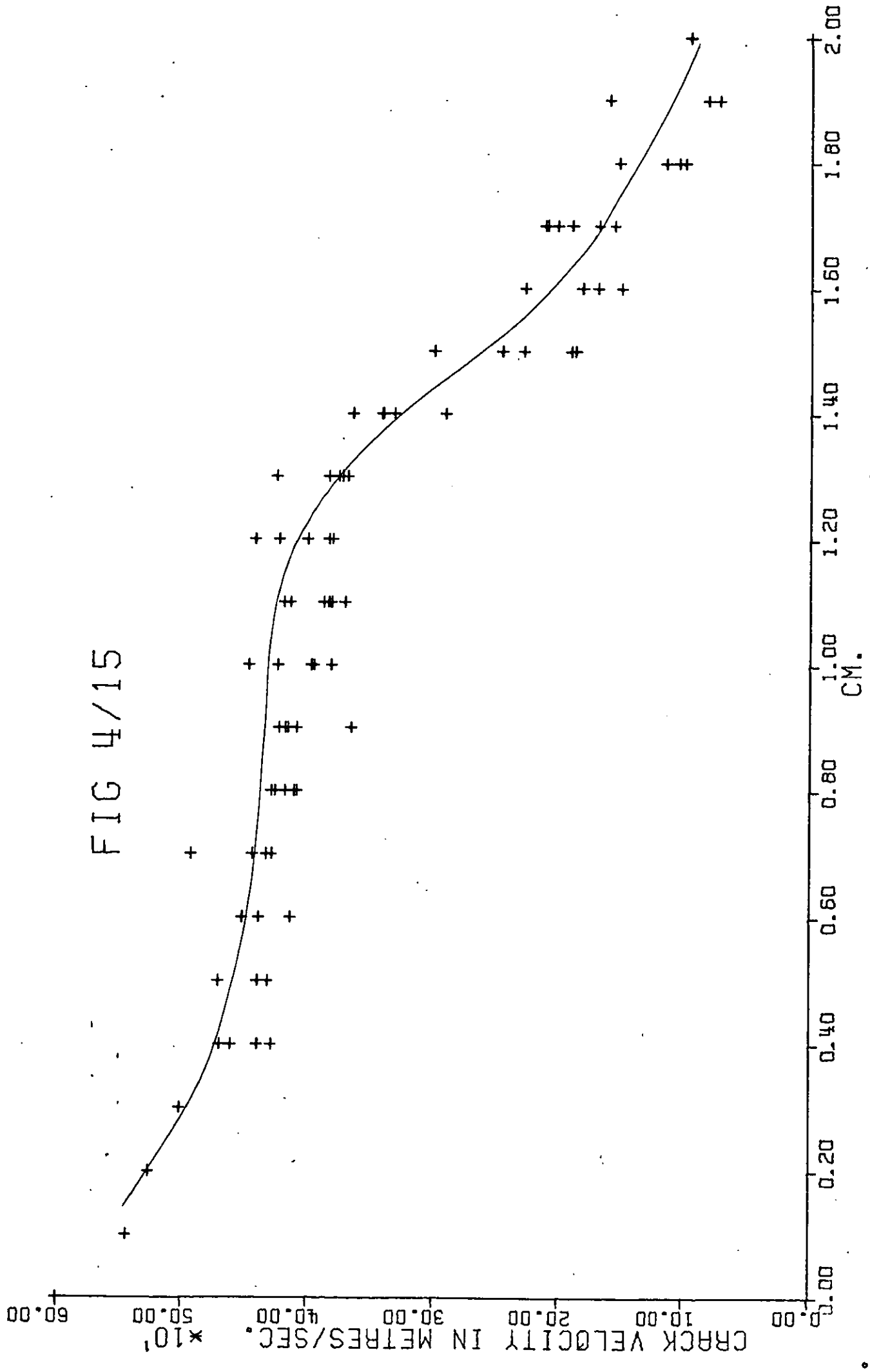
CRACK VELOCITY IN METRES/SEC. *10'
0.00
10.00
20.00
30.00
40.00
50.00
60.00
0.00
0.20
0.40
0.60
0.80
1.00
1.20
1.40
1.60
1.80
2.00
CM.

FIG 4/15

The variation of bulk stress with distance from sample to sample could be a consequence of a scatter in the initiation stress. In tensile tests on PET there is a large variation in breaking stress unless great care is taken in standardising notch geometry, and removing all foreign matter that could act as stress raisers[19]. The specimens used in these experiments were not impurity free since commercial polymer was used and they were fabricated by injection moulding. As a consequence it is likely that the fracture initiated at a different stress level in each test, and therefore the running crack would experience the same stress level at different penetrations from sample to sample.

Using this model, in Fig. 4/13 curve A corresponds to a fracture initiated at high stress, whilst curves B and C correspond to fractures initiated at progressively lower stresses.

4.3.2. Fracture Surface Topography and its Relationship to Fracture Velocity

The large range of crack velocities (600 to 50 m/s) obtained in the bent beam impact test provide an opportunity of relating topographical features on the fracture surface with the velocity of crack propagation. A study was therefore made of the fracture surfaces used in the velocity measurements.

Figure 4/16 is a composite photograph of the fracture surface of a typical specimen. The illumination used was darkground reflected light.

The crack initiation centre is identified by a mirror region (A) which corresponds to a slow growth area. Two mirror regions can be observed in Fig. 4/16 which indicates that there were two centres of crack initiation. The mirror region is followed by an area of increasing roughness (B) in which there are signs of regular banded structures. Following region B the surface roughness

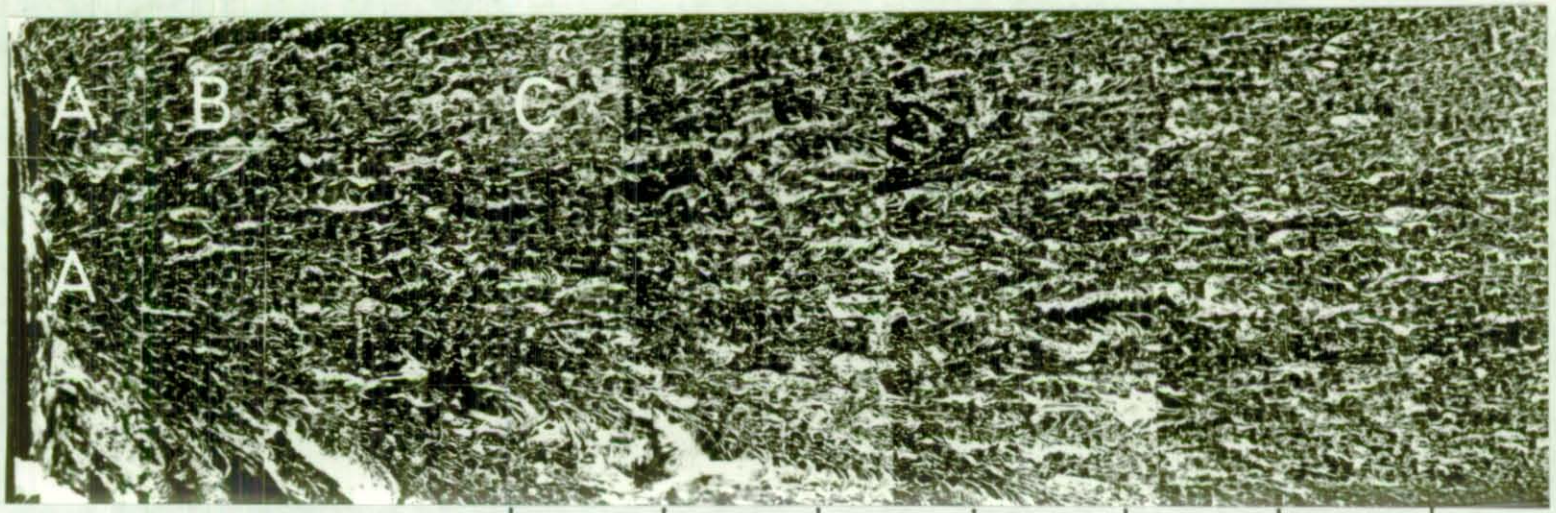

crack vel. 490 470 450 440 425 420 420 m/s

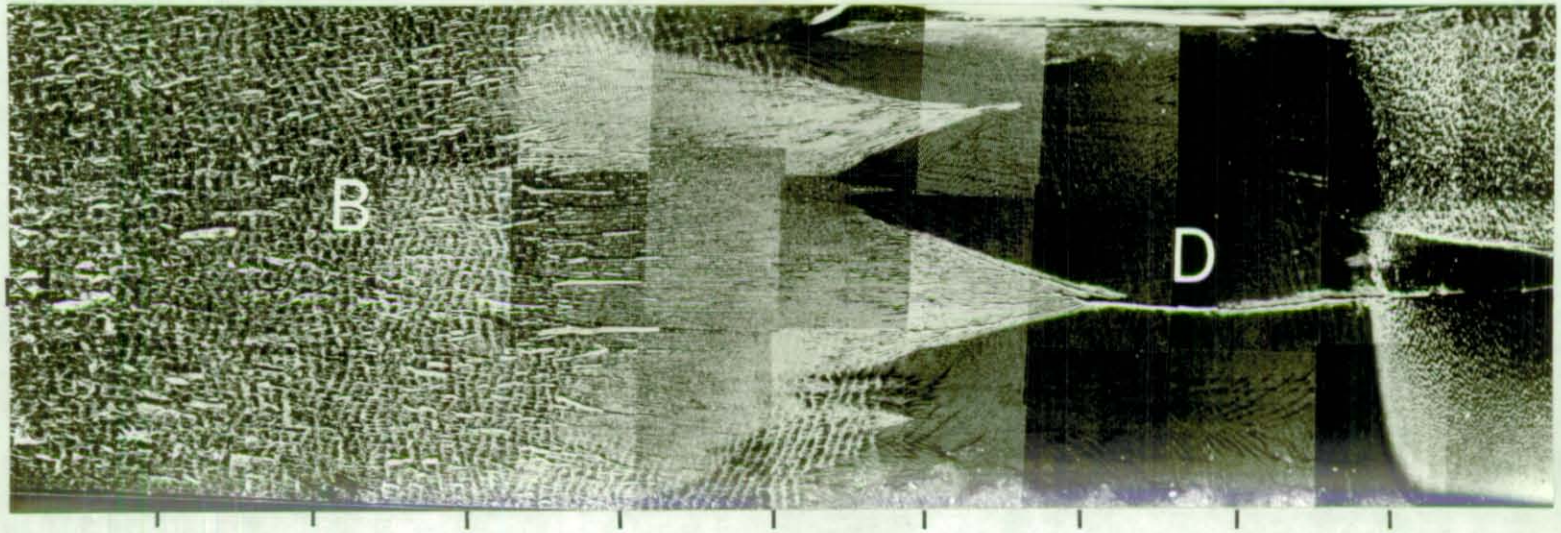

crack vel. 410 380 370 320 180 170 160 100 70 m/s

mag. 20X

FIG 4/16

increases (C) where no regular structures can be seen. This type of surface is usually associated with fast crack growth. The banded markings then reappear (B), however in this region there is evidence of two types of regular markings at different line spacings. Finally the markings with the larger line spacing disappears and one is left with a smooth surface covered with a system of regular lines (D).

From the crack velocity profiles associated with the specimens typical values for the crack velocity were assigned to the regions B, C and D.

Region C is associated with a crack velocity greater than

420 metres/sec.

Region B is associated with a crack velocity of between

420 and 300 metres/sec.

Region D is associated with a crack velocity of between

300 and 50 metres/sec.

The change from region B to region D was found in all fractures to correspond approximately to the onset of stage four observed in the velocity profile. It will be shown later that the drop in crack velocity at this point is associated with the appearance of the regular periodic markings typical of Region D.

More detailed studies of regions B and D were made with particular reference to the periodic nature for the fracture surface markings observed.

Region B

Figure 4/17 is a composite photograph of a fracture surface taken using common reflected light. This specimen was not typical in that it fractured with a much slower crack velocity. It is however, useful in discussing the slower velocity regions B and D. The two types of regular markings are clearly seen on this sample.

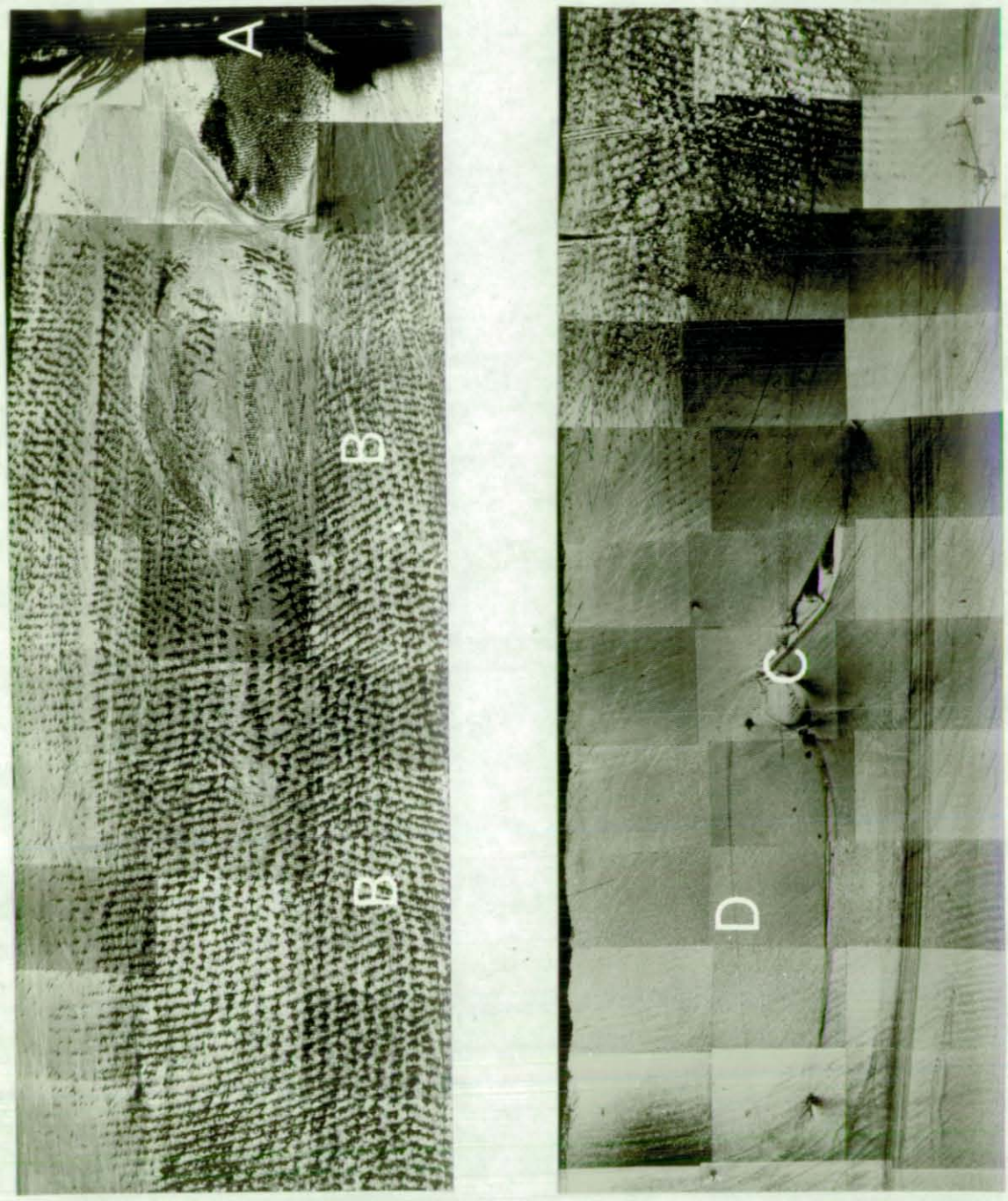

MAG 20X

FIG 4/17

Closely spaced lines can be seen over the entire fracture surface. The wider spaced lines are also in evidence over the first half of the fracture surface; these can be seen to be the result of lines of 'hackle'. They have the appearance of Wallner lines, being very similar to those observed by Andrews[15] in the low temperature fracture of filled rubbers. A distinctive feature of the lines in region B, and of Wallner lines is that they intersect. This feature immediately shows that they do not represent periodic (i.e. stick-slip) behaviour of the fracture front, since separate fracture fronts can only intersect along a single line.

Closer examination of region B (4/17) shows that these lines are made up of areas of 'hackle'. As has been noted in the introduction the higher the local stress in an inhomogeneous material, the rougher will be the resulting surface. It seems clear, therefore, that the surface markings described represent periodic variations in the state of stress in the body prior to the passage of the fracture front. They are from Wallner phenomena arising from the interaction of the fracture front with stress waves within the body. These stress waves are believed to be generated by oscillation of material behind the moving crack.

The closer spaced lines exhibit different characteristics from the Wallner lines.

1. Their line spacing is smaller
2. They do not intersect each other
3. They are a result of much smaller variations in surface texture.

As can be seen in Fig. 4/17 this fine surface detail is independent of the Wallner lines in that it subtends a different angle to the crack direction. Its source is, therefore, unlikely to be the same as that producing the Wallner pattern.

There are two possible ways in which periodic surface texture can be produced. One way is the result of periodic stress variations in the sample, due either to a Wallner type disturbance or natural sample resonances. The other way is the result of periodic stick-slip behaviour of the fracture front.

The closely spaced markings under discussion are unlikely to be Wallner phenomena since no evidence of intersection of the lines is observed. Also since the closely spaced lines are present together with the typical Wallner pattern, two frequencies of stress wave would need to be generated behind the crack tip to give the different line spacings for the two phenomena.

From the knowledge of the crack velocity, the frequency of a periodic stress disturbance necessary to produce lines of the spacing observed would be 20 MHz. This is well outside the range of any natural resonance of the sample.

The fracture surface markings typified by region D seem most likely to be produced by a 'stick-slip' mechanism which would indicate that the fracture front proceeds in a series of jumps. The spacing between the lines representing the distance travelled during each jump of the fracture front. It is to proposed that stick-slip behaviour is responsible for the closely spaced lines and that their production is intimately associated with the crazing behaviour of the material in front of the crack tip.

4.3.3. Detailed Examination of Low Velocity Region D

a. Surface Topography

The features observed are believed to be a consequence of variation in topography of a craze layer on the surface. This view is supported by the appearance of the fracture surface at C (Fig. 4/17). An enlarged view of this area is shown in Fig. 4/20.

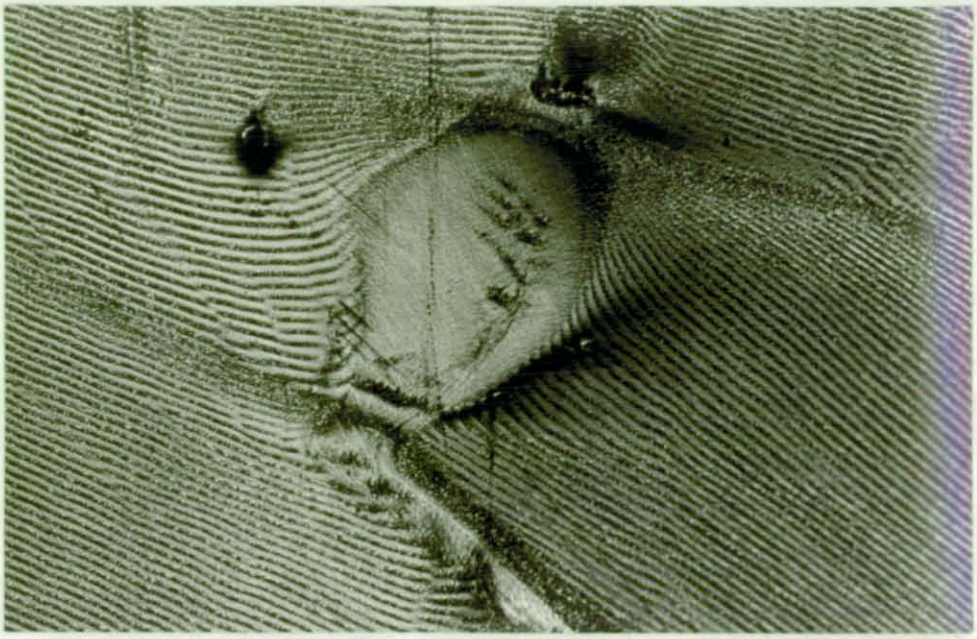

MAG 100X

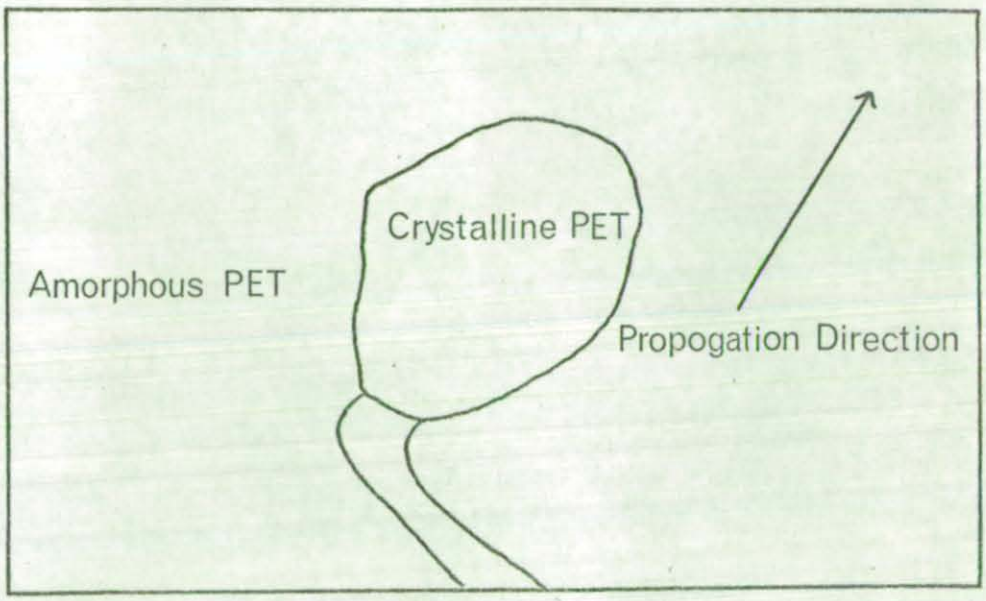

FIG 4/20

The periodic line pattern is not formed over part of the photograph. This area free of lines was found to be a region of crystalline material within the specimen that was formed during its moulding. That the line pattern is produced preferentially in the amorphous PET suggests that its formation requires a degree of viscoelastic flow. The crystalline material is less likely to draw plastically due to the lower mobility of the polymer chains in the more ordered crystalline regions.

If, as will be suggested, the markings are a consequence of craze formation during the crack propagation, their occurence on crystalline PET fracture surfaces is unlikely due to the difficulty of producing crazes requiring large amounts of ductile flow in crystalline material.

Optical microscopy proved to be inadequate in determining the fine detail responsible for the observed line pattern. Electron microscopy was therefore employed in further investigations of their structure. Figures 4/18 and 4/19 are electron micrographs of small areas of region D.

Figures 18a and 18b are transmission electron micrographs of two stage replicas made of matching areas of opposing fracture surfaces, one of the photographs having been reversed at the printing stage to aid comparison of the matching features.

Figures 19a and 19b are scanning electron micrographs of matching areas of opposing fracture surfaces.

With the detail available in these micrographs, the lines can be seen to consist of strips where the craze layer is discontinuous and is present as regular shaped patches (M), separated by strips where the craze layer is continuous (N).

a

mag. 2K

b

FIG 4/18

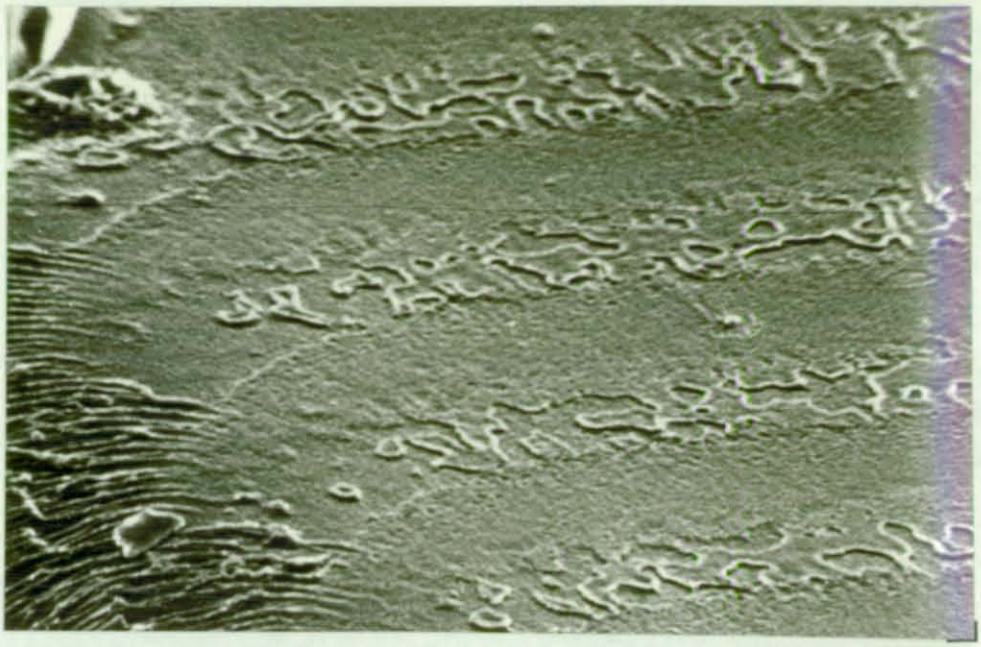

a

Mag. 2·5 K

b

FIG 4/19

By comparison of opposing fracture surfaces it can be seen that in strip M, areas where the craze is attached to one surface correspond in the opposite surface to areas where the craze layer has been stripped off. In strip N however, the craze layer is present on both surfaces shown most clearly in Fig. 4/19. By analysis of shadowing detail (N.B. the shadows in Fig. 4/18 are produced by heavy metal of high density and therefore appear white, it can be shown that the craze layer on the surface is thinner in strip N than in the craze islands of strip M.

b. The Relationship between Line Spacing on Measured Crack Velocity

For the purposes of this investigation the line spacing is defined as the distance between successive, abrupt changes of surface from 'smooth' to 'rough' i.e. aa' in Fig. 4/18a.

The relationship between the line spacing and the measured velocity was obtained by measuring the number of lines on the surface over the distance that the mean average velocity was measured using an optical microscope. The average line spacing was then computed and a plot of the average line spacing versus the measured average velocity over the same part of the crack propagation was obtained (Fig. 4/24). The spacing is seen to decrease in an approximately linear fashion with decreasing crack velocity. The best line drawn through the points does not pass through the origin. Above 420 m/s the lines could not be seen. They were either not produced above this crack velocity, or they were obscured by the increased roughness of the surface. Below 70 m/s the fracture surface showed evidence of a very ductile fracture with much plastic flow, on this type of surface there was no evidence of periodic lines.

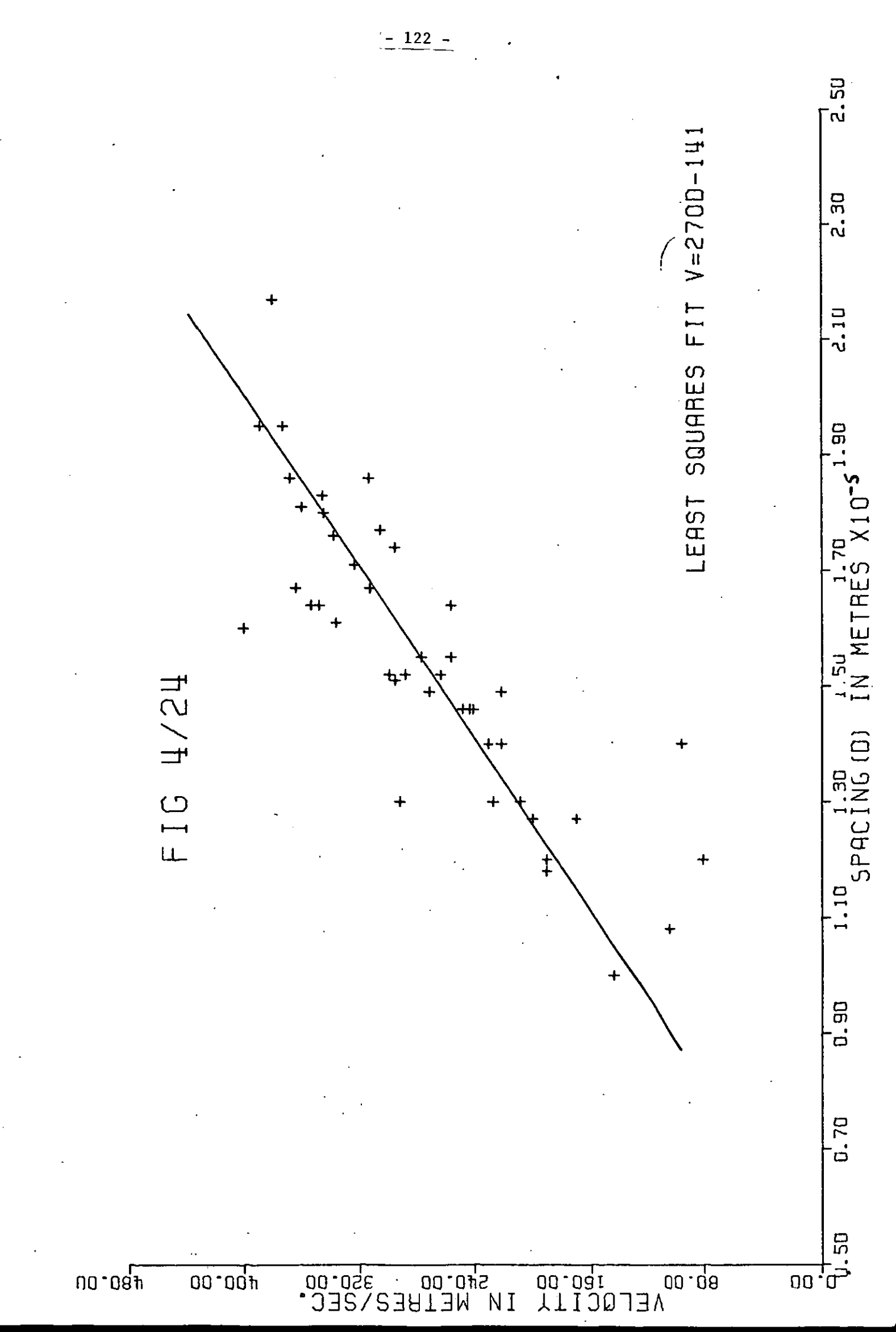
LEAST SQUARES FIT V=2700-141
VELOCITY IN METRES/SEC.
0.00
80.00
160.00
240.00
320.00
400.00
480.00
0.50
0.70
0.90
1.10
1.30
1.50
1.70
1.90
2.10
2.30
2.50
SPACING (D) IN METRES X10⁻⁵

FIG 4/24

It is interesting to note that the line spacing increases in the high velocity region by an expansion of the smooth region N, whilst the rough region M remains approximately the same width.

4.3.4. Proposed Model for the Production of the Periodic Surface Markings Typical of Low Velocity Region D

Hull has shown good evidence for the development of crazes during high speed crack propagation in Polystyrene[9,10,20]. The crack is seen to grow by the rupture of crazes formed by transitory stresses in front of the propagating crack.

From his experiments he concludes that fracture of a craze can occur in two ways:

a. In slow moving cracks, or cracks propagating in thick preformed crazes, the crack grows through the centre of the crazed material, leaving approximately equal depths of craze on each fracture surface Fig. 4/21B.

b. Fast moving cracks growing in thin crazes propagate by splitting of the material along the interface between the craze and bulk polymer. The resultant fracture surface consists of islands of craze layer attached to one or other of the fracture surfaces (Fig. 4/21B). This type of fracture in polystyrene produces the surface, shown in Fig. 4/22.

By analogy with the polystyrene fracture surfaces, the regions M in Figures 4/18 and 4/19 are produced by 'rapid' fracture of a craze whilst regions N are produced by 'slow' fracture of the craze. This immediately suggests a stick-slip mechanism of crack propagation, the periodicity observed being a consequence of the crack front moving in a series of jumps from a to a' (Fig. 4/18a) and so on.

A. Fast

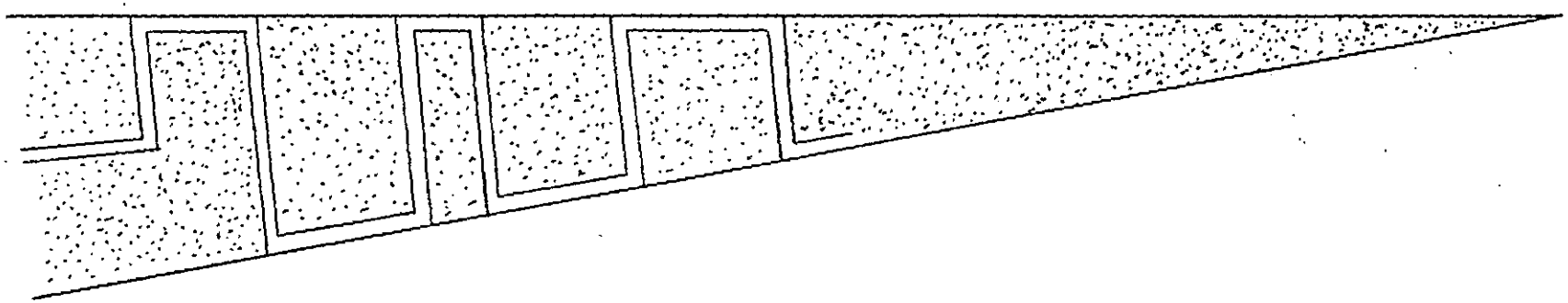

Schematic representation of mechanisms of crack propagation in a craze.

B. Slow

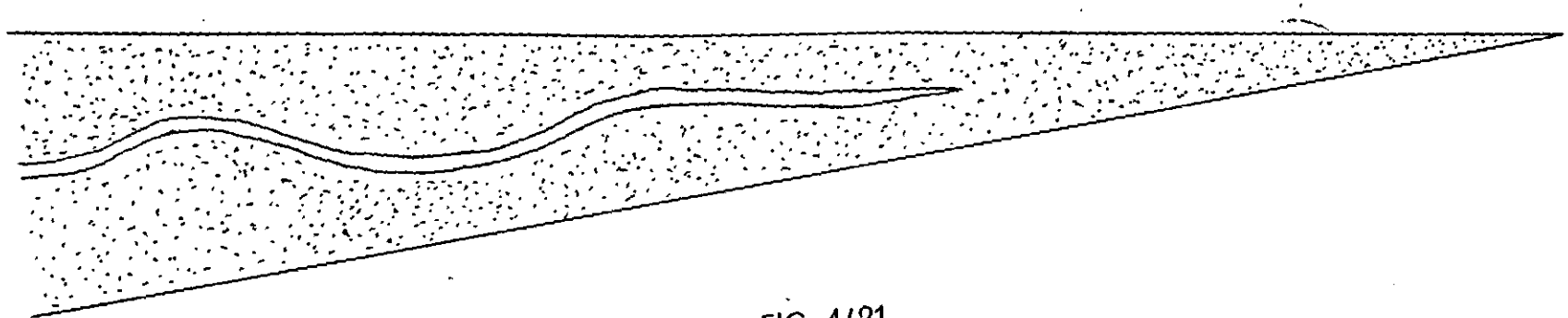

FIG. 4/21

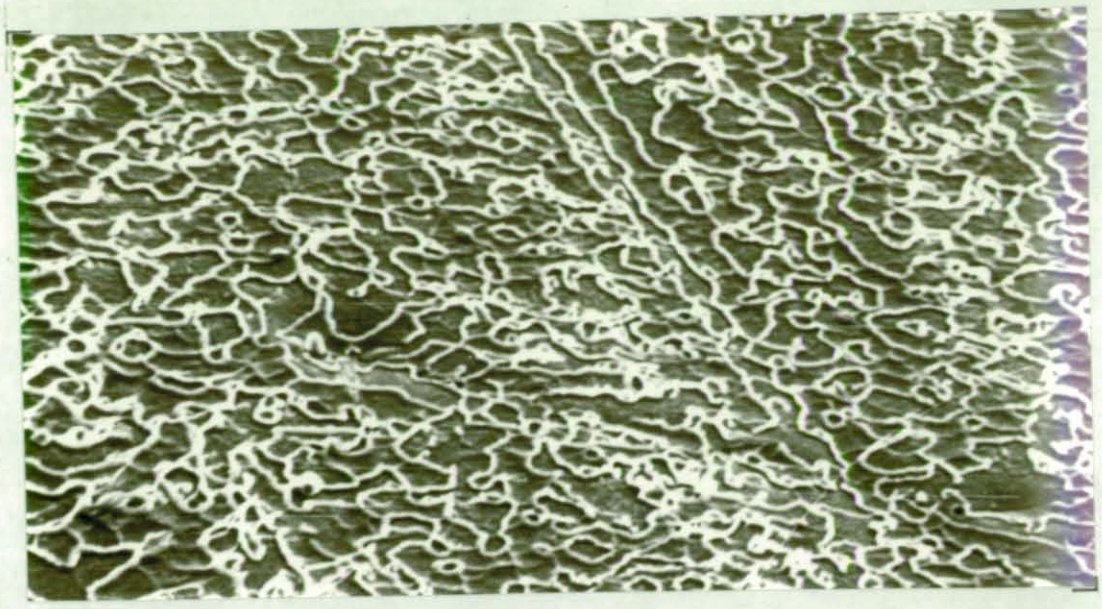

FIG 4/22

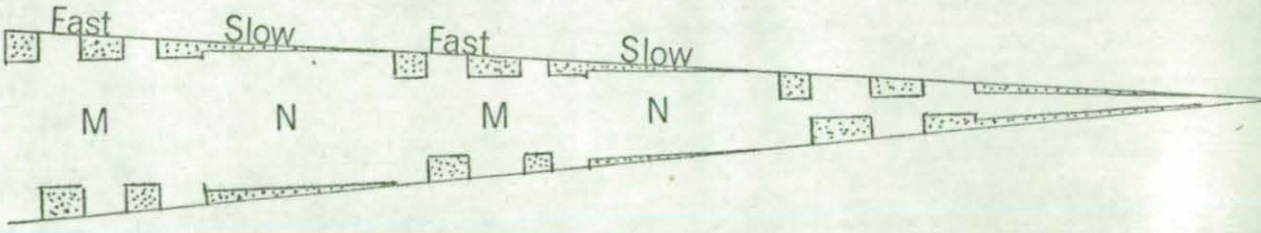

FIG 4/23

The jump distance as determined by the line spacing has been shown to have a linear relationship with the measured average velocity. This behaviour could be explained by proposing that the crack front encountered an oscillating stress field as it propagated through the specimen, the periodic nature of the stress being the cause of the periodic fast/slow nature of the crack growth. The origin of the varying stress field could be the oscillating material behind the crack tip similar to that producing Wallner phenomena. However, since one can distinguish Wallner lines and these fine periodic lines on the same surface (Fig. 4/17) it is easy to show that they have important differences. In order to avoid the anomaly of two different types of surface marking having the same origin, it is proposed that the varying stress field is caused by the stress at the crack tip being relieved due to the fracture of the craze material itself.

The proposed mechanism for the production of the surface marks is outlined below:

The crack front bursts through the craze at its tip at high velocity. Separation of the material during this stage is at the craze/matrix interface leaving islands of craze matter on the fracture surface. As a consequence of the fracture of the craze the stress in the near vicinity of the crack tip is relaxed, slowing down the crack and eventually causing it to propagate through the centre of the craze leaving a continuous layer of craze on both fracture surfaces.

On reaching the end of the craze the crack stops and the local stress increases again allowing time for a new craze to grow at the crack tip. When the stress has increased to the craze fracture stress the crack front once again bursts through the new craze at a high velocity. The repetition of this cycle would produce the type of

periodic markings observed on the fracture surfaces. This mechanism is illustrated schematically in Figure 4/23 with a transmission electron micrograph as a comparison.

As has been noted the line spacing increases in the higher velocity region by an expansion of the smooth, or 'slow' growth portion of the line. This at first would appear to be contradictory with the higher measured velocity. However since the model involves the crack stopping whilst the craze grows, the higher measured velocity is a consequence of fewer stops per unit distance. The line spacing on this model is dependent on the craze growth kinetics under the stress conditions prevailing since the jump length of the crack front depends on the length of craze formed during the time the crack is stopped. The jump length is also necessarily an important parameter in the actual measured velocity and therefore the velocity, line spacing, and craze kinetics are all functions of the stress. Having stated this it is not inconsistent to explain the measured velocity in terms of the bulk stress conditions or the fracture surface markings.

As has been noted previously the occurrence of regular periodic markings on the fracture surface corresponds to a dramatic decrease in the measured velocity. It is proposed that the stick-slip mechanism for the propagation of the crack, occurs below some critical value of the bulk stress. At this point the crack propagation mode changes from rapid continuous fracture to a stick-slip fracture that will necessarily make the average measured velocity decrease markedly.

4.4. Summary and Conclusions

1. The crack velocity is dependent upon the stress in the vicinity of the crack tip. That is the crack velocity decreases with decreasing stress.

2. As the crack propagates from the outer surface of a bent beam it encounters a decreasing tensile stress.

3. The stress profile in each test is similar, but the magnitude of the stress depends upon the value of the bulk stress at initiation.

4. Two distinct types of periodic surface markings are observed on the fracture surfaces; one type occurring in the crack velocity region 420 - 150 m/s, has all the characteristics of Wallner phenomena. It is proposed that the other type observed in the 420 - 70 m/s range of crack velocity is produced during stick-slip behaviour of the fracture front.

5. The latter type of marking is explained in terms of fracture of crazes formed in front of the growing crack.

References

1. Griffith, A.A., Phil. Trans. Roy. Soc. A221, 163 (1921).
2. Griffith, A.A., Proc. Int. Congr. Appl. Mech. (Delft) (1924).
3. Irwin, G.R., J. Appl. Mech. 61, A49 (1939).
4. Mott, N.F., Engineering, 165, 16 (1948).
5. Roberts, D.K. and A.A. Wells, Engineering, 178, 820 (1954).
6. Dulaney, F.N. and W.F. Brace, J. Appl. Phys. 31, 2233 (1960).
7. Wolock, I. and S.B. Newman, Fracture Processes in Polymeric Solids, B. Rosen, Ed., Wiley, New York (1964) p. 237.
8. Andrews, E.H. Fracture in Polymers, Oliver and Boyd, London (1968) p. 177.
9. Murray, J. and D. Hull, Polymer (Lond.), 10, 451 (1969).
10. Murray, J. and D. Hull, J. Polym. Sci. A2, 8, 583 (1970).
11. Smekal, A. Ergeb. Exakt. Naturur, 15, 106 (1936).
12. Kies, J.A., A.M. Sullivan, and G.R. Irwin, J. Appl. Phys. 21, 716 (1950).
13. Wallner, H. Z. Physik, 114, 368 (1939).
14. Schardin, H. Fracture (ed. B.L. Averbach), p. 250, John Wiley and Sons Inc. (1959).
15. Andrews, E.H. J. Appl. Phys., 30, 740 (1959).
16. Schardin, H. Fracture (ed. B.L. Averbach), John Wiley and Sons Inc. (1959) p. 316.
17. Schardin, H. Fracture (ed. B.L. Averbach), John Wiley and Sons Inc. (1959) p. 297.
18. Reichenback, H. Actes de Zème Congrès Int. Phot. Cinem. Ultra Rapides, p. 333 Paris (1954).
19. Private Communication, T. Roberts, I.C.I., P. and P. Laboratory.

CHAPTER FIVE.

5. GENERAL CONCLUSIONS AND RECOMMENDATIONS.

Arising from the work described, the following conclusions can be drawn.

5.1 General Conclusions.

i) Crazed structures can be produced in amorphous polyethylene terephthalate. This may be accomplished by stressing oriented specimens perpendicular to the direction of orientation in an air environment. Alternatively unoriented specimens may be crazed by straining in a crazing environment. Suitable crazing agents have been found to be the lower aliphatic alcohols.

ii) The structures so formed were distinguished from cracks by investigations of their refractive index. The refractive index of methanol grown craze bands was found to be 1.40, corresponding to a void content of ~30% by volume. Electron microscopy of the craze internal structure showed detail of fibrillar structures similar to those observed in other polymer crazes.

iii) The blending of ethylene vinyl acetate copolymers with PET using melt mixing techniques did not give rise to appreciable increases in impact strength. Increased vinyl acetate content gave slightly improved mouldings with regard to the extent of phase separation during moulding.

iv) Similarly the blending of 'Surlyn A' with PET by melt extrusion mixing did not give rise to any appreciable increase in impact strength of the composite over that of amorphous PET.

v) The rheological properties of Surlyn A/PET melts were found to be time dependant, the most noticeable aspect being a substantial increase in viscosity of the melt with time. A mechanism has been put forward to explain the observed phenomenon. This involves the chemical interaction of the pendant carboxyl groups of the Surlyn A chain with the ester linkages of the PET. Because one ionomer chain contains a number of active pendant groups, the net effect is the production of a crosslinked species in the vicinity of the phase interfaces. This is thought to give rise to the anomalous behaviour observed.

vi) The activity of the ionomer to the PET was used to graft PET units onto the Surlyn A chains. The grafted polymer was subsequently melt blended into virgin PET using a static mixer. The resultant blend was shown to have an improved interfacial bond and this improvement showed up as a substantial increase in the impact strength of the blend over that of virgin amorphous PET.

vii) This blend was considered to incorporate many of the characteristics found in high impact polystyrene (HIPS) systems. However the increase in impact strength obtained was not as great as might have been anticipated. There was no evidence on the fracture surfaces of large scale stress whitening which tends to indicate that the observed increase in impact strength was not obtained by an energy absorbing mechanism involving the production of large numbers of micro-crazes. Below are some thoughts on the possible factors involved which will restrict the craze initiation and production in the rubber filled PET blends produced.

a) The Molecular Weight of PET.

The average molecular weights of condensation polymers are typically lower than those of additional polymers. It is proposed that craze structures will lose their tensile strength as the molecular weight of the bulk polymer decreases. Whilst there is no experimental evidence to support this view, the fibrils in crazes are very much larger than the chain lengths of the polymer molecules and hence must obtain their strength via such forces as chain entanglements to tie the molecules together. One piece of evidence to support these ideas is that PET will not form fibre at below an I.V. value of ~0.45.

Since after processing, the I.V. of the PET falls close to this limiting value it is reasonable to suppose that the crazes will become weak and will tend to fracture during formation, even in the presence of the stabilising influence of the rubber particles.

b) Rubber Phase Dilation.

Sternstein in unpublished work has shown that in rubber modified polystyrenes the rubber particles in their rest state are under the influence of a positive dilational stress. This fact he concludes from experiments using a Biaxial Torsion Pendulum to investigate the shift of the rubber peak in HIPS under the influence of a tensile stress. The dilation of the rubber particles is presumably a consequence of the thermal expansion mismatch of the rubber and glassy phases.

Evidence from the photographs shown on page (74) indicates that in PET/SA blends, the PET contracts more on cooling than does the Surlyn A. This being the case, the Surlyn A particles in the blend will be in a state of compression, i.e. opposite to that found in HIPS.

Since it is expected that chain segmental mobility (a requirement for large scale chain extension which occurs during crazing) would be enhanced by dilation, it follows that the craze initiation stress is reduced in HIPS due to the dilation of the rubber particles, and inversly in PET/SA blends the craze initiation stress will be increased due to the compression in the rubber. This concept may go some way to explaining why more crazing is not seen in the blends prepared from ethylene copolymers and PET. If the craze initiation stress is greater than the tensile strength of the bulk polymer no crazes can be expected to grow in the vicinity of the rubber particles before fracture takes place.

viii) Crack velocity measurements have indicated that in amorphous PET, the crack propagation velocity is a function of the tensile stress in the vicinity of the crack tip. In the particular technique of fracture chosen, a rapid decrease in velocity during the fracture is associated with the appearance of regular markings on the fracture surface. Investigation of these features on the fracture surfaces by electron microscopy revealed that they have similarities with some features found on polystyrene fracture surfaces which have been shown to be formed from remnants of craze material. A mechanism of crack propagation in PET has been proposed therefore which involves craze growth and fracture to explain the observed markings.

5.2 Recommendations.

If further study is to be carried out the following points should be considered.

i) The chemistry of the reactions taking place in the melt between Surlyn A and PET should be further investigated. The unusual activity of carboxylate ions in chain scission reactions in PET could give rise to interesting copolymers if polymers terminated with carboxylate ions are reacted with PET in the melt.

ii) Further investigations on the grafted PET/Ionomer blends should be initiated to determine their physical characteristics other than impact strength, e.g. crystallisation rate, thermal stability, moulding properties. Also the characteristics of crystalline blends and fibre properties should be investigated.

iii) The spacing of the line markings on the low velocity areas of the fracture surfaces of PET have been shown to be a function of the crack velocity. This information could be used to investigate the effect on crack growth of, for example, fibres or bundles of fibres in a composite. By moulding a single fibre or bundles of fibres into a specimen and subsequently fracturing the sample, a study of the surface markings would give information on the way in which the crack front is perturbed in the vicinity of the fibre inclusions.

If, as has been proposed, the velocity of the crack is a function of the stress in the vicinity of the crack tip, a study of the surface line markings in the vicinity of an inclusion would give information on the stress fields in the bulk polymer produced as a result of the inclusion.

iv) The crack velocity technique was developed to be used with impact improved blends. It was thought that blends that absorbed fracture energy by flow process at the crack tip during propagation would have different velocity profiles to virgin polymer.

Time did not allow the final PET/SA blends that were prepared to be investigated by this technique. It would be of interest to determine if the measured impact strength could be associated in any way with the crack velocity characteristics.